POLITECNICO DI MILANO
Department of Aerospace Science and Technology
Master of Science in Space Engineering

Low-Thrust Trajectory Design and Attitude Strategies in Multi-Body Dynamical Regimes

Advisor:
Prof. Michèle Lavagna

Graduation Thesis of:
Stefano Crepaldi
838516

Academic Year 2017-2018

"The Night Has Long Hours"

Acknowledgements

In this section I would like to express my gratitude to all the people that supported me during the last years. Without them, this work would not have been possible.

First, I would like to thank my family. My mum and my brother have always supported and encouraged me, also when my decisions could seem unusual to them.

A great acknowledgement goes to my advisor, Prof. Michèle Lavagna. For me, it is sufficient to remember the first time when I asked her if it was possible to start the Master thesis under her supervision. I think she always valued my opinions and sent indelible signals of appreciation. I would like to thank her for her guide and help during the entire Master of Science period.

Special thanks to all the members of Hesperides Team: it has been very important to share a lot of moments with the best team-mates I could ever find. In general, if I think to the moment when I arrived in Milano, I really have to say that I have met fantastic people during this experience at Politecnico, it has been a pleasure to spend these years with them.

I am really grateful to all my friends from Adria. Sincere thanks to Enrico, my flatmate during the years in Milan, Jack, Bonny, Azz, Cipo, Toto, Fabio and Nikita, because they have been (and I know they will be) always there when needed.

Finally, particular thanks to all my friends and colleagues of the Èquipe Dynamique du Vol that I met during my internship at THALES Services in Toulouse. It has been a fantastic experience and I am really happy to rejoin you soon.

Contents

List of Figures

List of Tables

Abstract

The Restricted Two-Body Problem and the Circular Restricted Three-Body Problem represent two agile models that allow to perform trajectory design. The search for an increasing precision and accuracy in the problem pushes towards the development of more refined models. The addition of N gravity fields in the problem formulation defines new challenges for trajectory design and optimization. Besides, a constant technological progress opens to an increasing exploitation of low-thrust propulsion, making the framework even more challenging.

The adoption of Non-Keplerian orbits in the Earth-Moon system as a forthcoming achievement outlines unique scenarios. Attitude-orbital coupling represents one of these, encouraging to search for passive attitude control strategies.

In the first part of this work, dynamical models are presented. Particular attention is placed on the formulation of the N-body problem with respect to different coordinate systems. Attitude dynamics and kinematics treatment follows the orbital mechanics section. The coupled dynamics is the natural and reasonable conclusion.

Then, numerical methods for dynamical system analysis are introduced. The outlined tools steer towards the trajectory optimization problem. Two different methods (Sims-Flanagan Transcription method and an optimal control-based approach) are presented to face a trajectory optimization in a N-body framework. The described approaches are used and applied to real mission scenario.

Finally, coupled attitude-orbital dynamics is analysed along Non-Keplerian orbits of the Earth-Moon system, with particular focus on Near Retrograde Orbits (NROs) and Distant Retrograde Orbits (DROs).

Chapter 1

Introduction

Orbital mechanics and trajectory design are continuously improving. The simplest case of spacecraft dynamics can be described by the Restricted Two-Body Problem, characterized by an elegant formulation and a closed-form analytical solution. A further improvement, the Restricted Three-Body Problem, can be attained considering the dynamics of a man-made object under the simultaneous influence of two massive bodies. Yet, this formulation lacks accuracy when the outer space of system composed by the two primaries is explored. An increased level of accuracy becomes desirable. One of the most familiar environments, the Earth-Moon system, is, nowadays, characterized by an increasingly interest, in order to enhance human presence within and beyond its boundaries. As a matter of fact, a permanent human presence in the Earth-Moon regions and their exploitation as a gateway towards the interplanetary space are current and actual goals. In this sense, the above mentioned context involves exclusive and unique challenges, since higher-fidelity solution design must deal with a highly sensitive environment.

Besides, the recent success of missions employing low thrust propulsion can open even wider mission scenarios and challenges. Low thrust high specific impulses translates in high efficiencies, that can potentially reach strategical destinations with a reduced fuel consumption. These performances are counterbalanced by extended times of flight and thrusting activity. Hence, low thrust adds more complexity to the trajectory design and optimization phase.

In order to meet future mission requirements in multi-body regimes, efficient algorithms and an enhanced comprehension of the dynamical environments are required. In this sense, also the search for passive attitude control strategies in the Earth-Moon system can outline a new direction of study, so

that active control along multi-body trajectories can be minimized.

1.1 State of Art

The basis for the description of multi-body dynamical regimes were put by Isaac Newton in 1687, with his work *Philosophiae Naturalis Principia Mathematica* [35]. In 1772, Leonhard Euler developed the three body problem in a more detailed way: by using some simplifying assumptions he formalized the restricted version of the problem, introducing the description with respect to the synodic frame and identifying the collinear equilibrium points. Shortly after, Joseph-Louis Lagrange identified the two remaining equilibrium points. Carl Gustav Jacob Jacobi, George William Hill and Henri Poincaré offered further insight into the problem, by identifying,respectively, the Jacobi Constant, zero velocity surfaces and Poincaré maps [23, 41]. A global view of the 3-body problem is offered by Szbehely [51] and Koon [28].

The N-body formulation (in particular, in the synodic frame of two primaries) has been inspired by the work by Diogene Dei Tos [12]. Equally important, concerning multi-body regimes and correction schemes, it is important to cite the work by Pavlak [38]. The work by Pritchett [43] offers a general overview of low-thrust analysis.

Although optimal control originates with the calculus of variation and the intriguing brachistochrone problem posed by Johann Bernoulli, within this work particular focus is placed on direct methods. Direct optimization reformulates an optimal control problem and translates it in a Nonlinear Programming Problem. The discretization process of an optimal control is also called transcription, a term coined by Canon [8]. A superb treatment of trajectory optimization can be found in the work by Betts [4].

A detailed analysis of attitude-orbital coupling in the circular restricted 3-body problem and the study of periodic solution in Distant Retrograde Orbits is given by Lorenzo Bucci [6].

1.2 Structure of the Thesis

The main focus of this work is the development of a high-fidelity multi-body dynamical model, along with low-thrust trajectory design and optimization in N-body models. Besides, attitude-orbital coupling is analysed in Non-Keplerian orbits, with particular reference to NROs and DROs.

- **Chapter 2:** A fast overview of the circular restricted 3-body problem is given. Then, the description move towards high-fidelity multi-body

models. In particular, equations of motion of a spacecraft under the influence of N gravitational fields are described according to two different point of views: relative to a central mass with respect to an inertial frame and, then, relative to the barycentre of the system composed of two primaries with respect to their synodic frame.

- **Chapter 3:** A discussion on attitude dynamics is given. Acting external torques are also included in the treatment and particular attention is paid in modelling the gravity gradient perturbation. The knowledge of spacecraft angular velocities from dynamics allows to step into the attitude kinematics. Quaternions parametrization is, then, recalled. The conclusion of the chapter aims to a general treatment of attitude-orbital aspects.

- **Chapter 4:** Building blocks for the algorithms to be developed are summarized. Validation of the presented models is outlined, along with the assessment of their accuracy.

- **Chapter 5:** A general overview of numerical methods for dynamical models is given. Particular focus is placed for differential correction schemes. This anticipates the fundamentals of optimization problem. Differential correction schemes are, then, applied to the computation of periodic solution in multi-body regimes.

- **Chapter 6:** Trajectory optimization problem is introduced. With particular reference to low thrust trajectory design in N-body regimes, two optimization approaches are presented. The first one redesigns a Sims-Flanagan Transcription method. The second one is based on a shooting scheme for optimal control problems and it parametrizes control variables as Chebyshev interpolating polynomials.

- **Chapter 7:** The presented algorithms are applied to a real case scenario, offered by the Asteroid Redirect Mission (ARM) by NASA. This mission was supposed to exploit the Earth-Moon system before reaching a Near-Earth Asteroid. After the collection of a boulder from its surface, the spacecraft was supposed to re-enter the Earth-Moon region by using a NRO as a gateway and by leaving the collected material in a final, stable DRO.

- **Chapter 8:** Considerations about attitude-orbital coupling in NROs and DROs are explained. The main objective of this chapter aims to find interesting passive attitude control strategies to be applied in the above mentioned orbits.

- **Chapter 9:** A brief summary of the work is presented. Recommendation for future work are proposed.

Chapter 2

Orbital Mechanics Models

An appropriate dynamical model must be adopted in order to describe the motion of the spacecraft. The *restricted two-body* model is characterized by a closed-form solution, but it has the drawback of considering only one attractor. Including the gravitational fields of several bodies leads to more complex models that must be handled with a numerical approach. The *circular restricted three-body* problem takes into account the effects of two gravitational bodies and it can give useful insight of the problem, even though some simplifying assumptions are considered. In need of a more general and precise dynamics, a *N-body* model can be exploited.

2.1 The Circular Restricted Three-Body Problem

The restricted two-body problem cannot provide an accurate analytical solution in regions that are influenced by the gravitational effects of several bodies. Par excellence, this is the case of the Earth-Moon system, whose gravitational fields strongly and simultaneously affects the trajectory of a spacecraft. In this sense the circular restricted three-body problem represents viable model within the context of multi-body regimes.

In order to derive the equations of motions for restricted three-body problem, it should be remembered that the dynamics of a particle in a N-body system is given by

$$m_i \mathbf{r}_i'' = -G \sum_{\substack{j=1 \\ j \neq i}}^{N} \frac{m_i m_j}{r_{ji}^3} \mathbf{r}_{ji} \tag{2.1}$$

where $\mathbf{r}_i'' = \frac{d^2 \mathbf{r}_i}{dt^2}$ represents the second derivative of the position vector with respect to dimensional time and $\mathbf{r}_{ji} = \mathbf{r}_i - \mathbf{r}_j$. Equation 2.1 corresponds to

Newton's second law of motion. The particle under consideration is characterized by a concentrated mass m_i and its location is described by the position vector $\mathbf{r}_i$, expressed in an inertial reference frame $\hat{X}\hat{Y}\hat{Z}$. Analogously, the generic gravitating body has a mass m_j and its position is given by $\mathbf{r}_j$. Note that the position of the particle m_i relative to a body m_j is denoted by $\mathbf{r}_{ji}$, where $\mathbf{r}_{ji} = \mathbf{r}_i - \mathbf{r}_j$. In the case that $N = 3$, equation (2.1) can be adapted as follows:

$$m_3\mathbf{r}_3'' = -G\frac{m_3m_1}{r_{13}^3}\mathbf{r}_{13} - G\frac{m_3m_2}{r_{23}^3}\mathbf{r}_{23} \tag{2.2}$$

being the particle $i = 3$ the one of interest. The case $N = 3$ is sketched in Figure 2.1.

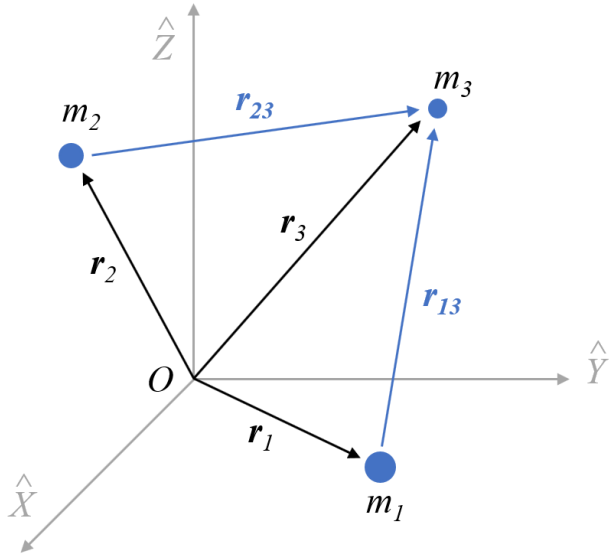

Figure 2.1: Three-Body Problem in the Inertial Frame

In the general case, the particle under consideration has a non-negligible mass, meaning that it can affects the motion of the other particles due to gravitational interactions. In order to move towards the circular restricted three-body problem (CRTBP), some simplifying assumptions must be assumed. First of all, the mass of the third body is negligible compared to the mass of the other two, that is $m_3 \ll m_1, m_2$. This assumption implies that the mass of interest (m_3) moves under the influence of the other two bodies, without affecting their motion. This is quite reasonable since the particle under consideration is usually a spacecraft. In addition, it is assumed that the two larger bodies (m_1 and m_2, also called *primaries*) revolve around

their center of mass in circular orbits.

For the sake of convenience, the motion of the smaller particle is described with reference to a non-inertial frame of reference $\hat{x}\hat{y}\hat{z}$ whose origin lies at the center of mass B of the two primaries. This frame co-rotates with the larger bodies according to their uniform circular motion around B. The $\hat{x}$-axis is parallel to the line connecting m_1 and m_2 and directed towards m_2 (let be $m_2 < m_1$). The $\hat{z}$-axis is perpendicular to the orbital plane of the primaries and directed as the their angular momentum. The $\hat{y}$-axis completes the right-handed triad. Figuring that the frame of reference $\hat{x}\hat{y}\hat{z}$ coincides with an inertial one $\hat{X}\hat{Y}\hat{Z}$ for some particular initial time t_0, any following angular mismatch between them is given by $\gamma = \Omega(t - t_0)$, where Ω is the constant angular velocity that characterizes the circular motion of the primaries. The geometry of the CRTBP is depicted in Figure 2.2. The frame of reference $\hat{x}\hat{y}\hat{z}$ is also called *synodic* frame.

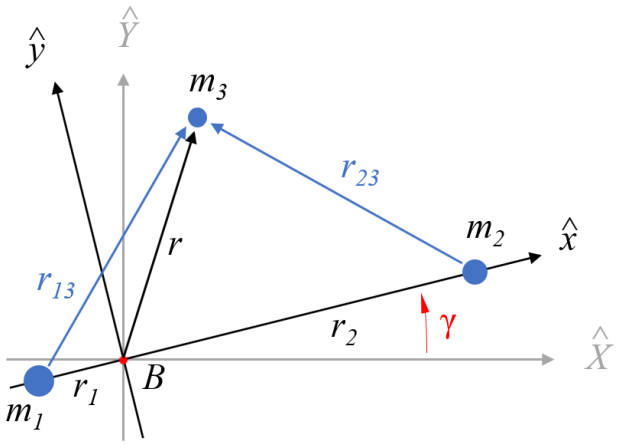

Figure 2.2: Geometry of the Circular Restricted Three-Body Problem

2.1.1 Equations of Motion

By simplifying equation (2.2), the acceleration of the body under examination is expressed as

$$\mathbf{r}'' = -G\frac{m_1}{r_{13}^3}\mathbf{r}_{13} - G\frac{m_2}{r_{23}^3}\mathbf{r}_{23} \tag{2.3}$$

The acceleration is relative to an inertial observer, but vectorial quantities can be resolved into components along the frame $\hat{x}\hat{y}\hat{z}$. So, in the synodic

frame the position vector $\mathbf{r}$ can be written, at any instant, as

$$\mathbf{r} = r_x\hat{\mathbf{i}} + r_y\hat{\mathbf{j}} + r_z\hat{\mathbf{k}} \tag{2.4}$$

where $\hat{\mathbf{i}}$, $\hat{\mathbf{j}}$ and $\hat{\mathbf{k}}$ are the unit vectors of the synodic frame. It is possible to obtain the acceleration by considering some kinematic expressions. The first time derivative of the position vector $\mathbf{r}$ yields

$$\mathbf{r}' = \frac{d\mathbf{r}}{dt} = \mathbf{r}'_{\text{rel}} + \boldsymbol{\Omega} \times \mathbf{r} \tag{2.5}$$

where $\mathbf{r}'_{\text{rel}} = \frac{dr_x}{dt}\hat{\mathbf{i}} + \frac{dr_y}{dt}\hat{\mathbf{j}} + \frac{dr_z}{dt}\hat{\mathbf{k}}$ is the velocity as seen from the synodic frame and $\boldsymbol{\Omega} = \Omega\hat{\mathbf{k}}$ is the angular velocity of the rotating frame. The acceleration is found by taking the time derivative of equation (2.5)

$$\mathbf{r}'' = \frac{d^2\mathbf{r}}{dt^2} = \mathbf{r}''_{\text{rel}} + \boldsymbol{\Omega} \times (\boldsymbol{\Omega} \times \mathbf{r}) + 2\boldsymbol{\Omega} \times \mathbf{r}'_{\text{rel}} \tag{2.6}$$

where $\mathbf{r}''_{\text{rel}} = \frac{d^2r_x}{dt^2}\hat{\mathbf{i}} + \frac{d^2r_y}{dt^2}\hat{\mathbf{j}} + \frac{d^2r_z}{dt^2}\hat{\mathbf{k}}$ is the acceleration as seen from the synodic frame. Expanding the terms in equation (2.6), it follows

$$\mathbf{r}'' = \left(r''_x - 2\Omega r'_y - \Omega^2 x\right)\hat{\mathbf{i}} + \left(r''_y + 2\Omega r'_x - \Omega^2 y\right)\hat{\mathbf{j}} + r''_z\hat{\mathbf{k}} \tag{2.7}$$

Comparing (2.3) and (2.7), the dimensional equation of motion for the CRTBP is derived

$$\left(r''_x - 2\Omega r'_y - \Omega^2 r_x\right)\hat{\mathbf{i}} + \left(r''_y + 2\Omega r'_x - \Omega^2 r_y\right)\hat{\mathbf{j}} + r''_z\hat{\mathbf{k}} = -G\frac{m_1}{r_{13}^3}\mathbf{r}_{13} - G\frac{m_2}{r_{23}^3}\mathbf{r}_{23} \tag{2.8}$$

Writing the equations in dimensionless form has several advantages from the numerical and practical point of view. For this purpose, some *characteristic quantities* are introduced. The characteristic length, L, is defined as the mean distance between the primaries

$$L = r_1 + r_2 \tag{2.9}$$

The characteristic mass, M, is given as the sum of the masses of the primaries

$$M = m_1 + m_2 \tag{2.10}$$

The characteristic time, T, is expressed as follows

$$T = \sqrt{\frac{L^3}{GM}} \tag{2.11}$$

Note that the inverse of the characteristic time represents the mean motion, Ω, of the primaries

$$\Omega = \sqrt{\frac{GM}{L^3}} \tag{2.12}$$

Parameter	Value	Units
L	384400	km
G	$6.67408 \cdot 10^{-20}$	$\mathrm{km}^3\ \mathrm{kg}^{-1}\ \mathrm{s}^{-2}$
m_1	$5.9722 \cdot 10^{24}$	kg
m_2	$7.3477 \cdot 10^{22}$	kg
M	$6.0457 \cdot 10^{24}$	kg
μ	0.0121535990	nondimensional
T	375194.88048	s

Table 2.1: Parameters in the Earth-Moon System

Characteristic quantities for the Earth-Moon system are reported in Table 2.1. At this point, quantities that appear in equation (2.8) can be nondimensionalized. The nondimensional mass, μ, and time, τ, are obtained by considering

$$\mu = \frac{m_2}{M} \tag{2.13}$$

$$\tau = \frac{t}{T} \tag{2.14}$$

The nondimensional positions of the two primaries are fixed with respect to the synodic frame and are expressed by $\boldsymbol{\rho}_1$ and $\boldsymbol{\rho}_2$. By exploiting the definition of center of mass, it follows

$$\boldsymbol{\rho}_1 = \frac{\mathbf{r}_1}{L} = -\mu\hat{\mathbf{i}} \tag{2.15}$$

$$\boldsymbol{\rho}_2 = \frac{\mathbf{r}_2}{L} = (1-\mu)\,\hat{\mathbf{i}} \tag{2.16}$$

Analogously, the position vectors of the spacecraft $\boldsymbol{\rho}$ (relative to the center of mass B), $\boldsymbol{\rho}_{13}$ and $\boldsymbol{\rho}_{23}$ (relative to the primaries) are given (in dimensionless coordinates) by

$$\boldsymbol{\rho} = \frac{\mathbf{r}}{L} = x\hat{\mathbf{i}} + y\hat{\mathbf{j}} + z\hat{\mathbf{k}} \tag{2.17}$$

$$\boldsymbol{\rho}_{13} = \frac{\mathbf{r}_{13}}{L} = (x+\mu)\,\hat{\mathbf{i}} + y\hat{\mathbf{j}} + z\hat{\mathbf{k}} \tag{2.18}$$

$$\boldsymbol{\rho}_{23} = \frac{\mathbf{r}_{23}}{L} = (x-1+\mu)\,\hat{\mathbf{i}} + y\hat{\mathbf{j}} + z\hat{\mathbf{k}} \tag{2.19}$$

So, the dimensionless form of equations (2.3) and (2.7) can be written, respectively, as

$$\ddot{\boldsymbol{\rho}} = -\frac{(1-\mu)}{\rho_{13}^3}\boldsymbol{\rho}_{13} - \frac{\mu}{\rho_{23}^3}\boldsymbol{\rho}_{23} \tag{2.20}$$

$$\ddot{\boldsymbol{\rho}} = (\ddot{x} - 2\dot{y} - x)\,\hat{\mathbf{i}} + (\ddot{y} + 2\dot{x} - y)\,\hat{\mathbf{j}} + \ddot{z}\hat{\mathbf{k}} \tag{2.21}$$

where dots represents the second derivative with respect to the nondimensional time. The comparison between (2.20) and (2.21) yields the three scalar, second-order differential equations of motion for the CRTBP in the dimensionless form

$$\ddot{x} - 2\dot{y} - x = -\frac{(1-\mu)(x+\mu)}{\rho_{13}^3} - \frac{\mu(x-1+\mu)}{\rho_{23}^3} \tag{2.22}$$

$$\ddot{y} + 2\dot{x} - y = -\frac{(1-\mu)y}{\rho_{13}^3} - \frac{\mu y}{\rho_{23}^3} \tag{2.23}$$

$$\ddot{z} = -\frac{(1-\mu)z}{\rho_{13}^3} - \frac{\mu z}{\rho_{23}^3} \tag{2.24}$$

Introducing a pseudo-potential function, U, defined as

$$U(x,y,z) = \frac{1-\mu}{\rho_{13}} + \frac{\mu}{\rho_{23}} + \frac{1}{2}\left(x^2+y^2\right) \tag{2.25}$$

the system of scalar equations (2.22)-(2.24) can be written as

$$\ddot{x} - 2\dot{y} = \frac{\partial U}{\partial x} \tag{2.26}$$

$$\ddot{y} + 2\dot{x} = \frac{\partial U}{\partial y} \tag{2.27}$$

$$\ddot{z} = \frac{\partial U}{\partial z} \tag{2.28}$$

2.1.2 Equilibrium Points

Studying the equations of motion for the CRTBP in the synodic frame, it is possible to find some equilibrium solutions. Equilibrium points are also called *libration* or *Lagrangian* points. Their locations are fixed and these points are characterized by null velocity and acceleration in the rotating frame. This is equivalent to find the solutions where the gradient of the pseudo-potenzial function is equal to zero

$$\nabla U = 0 \tag{2.29}$$

that means

$$\frac{\partial U}{\partial x} = -\frac{(1-\mu)(x_{eq}+\mu)}{\rho_{13,eq}^3} - \frac{\mu(x_{eq}-1+\mu)}{\rho_{23,eq}^3} + x_{eq} = 0 \tag{2.30}$$

$$\frac{\partial U}{\partial y} = -\frac{(1-\mu)y_{eq}}{\rho_{13,eq}^3} - \frac{\mu y_{eq}}{\rho_{23,eq}^3} + y_{eq} = 0 \tag{2.31}$$

$$\frac{\partial U}{\partial z} = -\frac{(1-\mu)z_{eq}}{\rho_{13,eq}^3} - \frac{\mu z_{eq}}{\rho_{23,eq}^3} = 0 \tag{2.32}$$

where x_{eq}, y_{eq} and z_{eq} are the coordinates of the equilibrium points in the synodic frame.

Equation (2.32) is satisfied if and only if $z_{eq} = 0$. This means that the equilibrium points lie in the xy-plane. An option to verify equation (2.31) is setting $y_{eq} = 0$ as well. The coordinates are found solving the remaining equation

$$-\frac{(1-\mu)(x_{eq}+\mu)}{|x_{eq}+\mu|^3} - \frac{\mu(x_{eq}-1+\mu)}{|x_{eq}-1+\mu|^3} + x_{eq} = 0 \tag{2.33}$$

Equation (2.33) has three real solutions, that identify three equilibrium points (L_1, L_2 and L_3). Since they lie on the x-axis, these solutions determine the so-called *collinear* points. The precise coordinates depend only on the system under consideration (so, on the mass ratio μ).

When $y_{eq} \neq 0$, equations (2.30) and (2.31) allow for other two solutions if and only if $\rho_{13} = \rho_{23} = 1$. This means that the remaining equilibrium points form equilateral triangles with the two primaries. This points (L_4 and L_5) are the so-called *equilateral* points. Libration points in the Earth-Moon system are depicted in Figure 2.3 (points are numbered according to the typical NASA convention) and their coordinates are reported in Table 2.2.

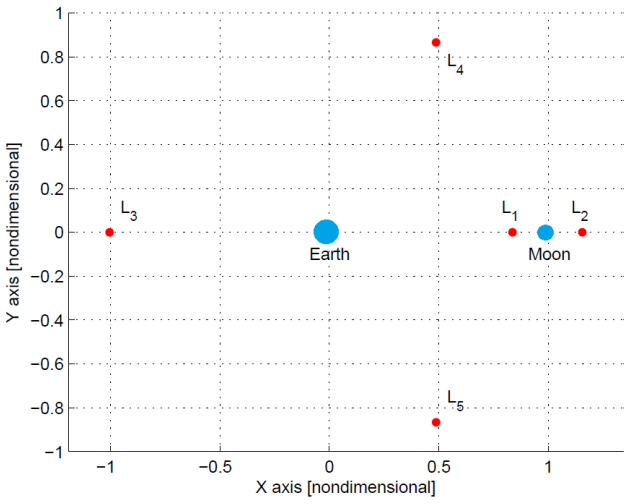

Figure 2.3: Lagrangian Points in the Earth-Moon System ($\mu = 0.012154$)

Lagrangian Point	Coordinates [nondimensional]		
	x_{eq}	y_{eq}	z_{eq}
L_1	0.836900	0	0
L_2	1.155693	0	0
L_3	-1.00506	0	0
L_4	0.487846	0.866025	0
L_5	0.487846	-0.866025	0

Table 2.2: Lagrangian Points in the Earth-Moon System ($\mu = 0.012154$)

2.2 N-Body Model

The dynamical model circular restricted three-body problem is relatively simple since only two gravitational fields are considered. In any case, it is suitable for a preliminary trajectory design in many systems. In presence of additional gravitational masses, the model of the CRTBP can be no more precise in terms of accuracy. A solution is proposed by the *N-body* model. In addition, this model takes into account the actual motion of the gravitational bodies, relaxing the assumptions of the CRTBP. Within the context of this thesis, accurate state vectors of celestial bodies are given Jet Propulsion Laboratory DE431 ephemerides. They are included in MATLAB® by exploiting the SPICE Toolkit [1]. First, equations of motion for the N-body model will be derived with reference to an inertial frame of reference and relative to a gravitational body. Then, they will be expressed with reference to a rotating frame.

2.2.1 Equations of Motion relative to a central mass

Equation (2.1) expresses the dynamics of a particle under the influence of other $N-1$ bodies and it is written with reference to an inertial frame of reference (as it can be the one centered on the Solar System barycenter). Usually, it is more convenient to write the equations of motion of a particle of interest (denoted with subscript i) relative to a central body (denoted with subscript q). The geometry of the considered problem is depicted in Figure 2.4. Particularizing equation (2.1) for the studied particle (for example, a spacecraft), it follows

$$m_i \mathbf{r}_i'' = -G\frac{m_i m_q}{r_{qi}^3}\mathbf{r}_{qi} - G\sum_{\substack{j=1 \\ j\neq i,q}}^{N} \frac{m_i m_j}{r_{ji}^3}\mathbf{r}_{ji} \tag{2.34}$$

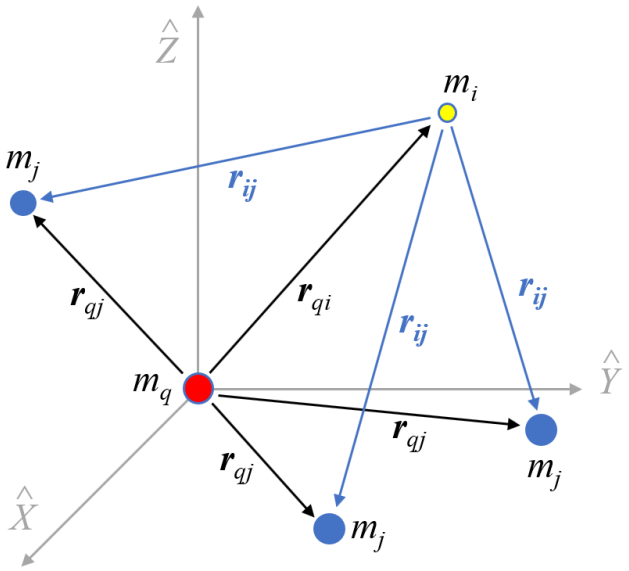

Figure 2.4: Geometry of the N-Body Problem relative to a central mass

where the gravitational force due to the central body has been "pulled" out of the summation. Analogously, the same equation for the central body is given by

$$m_q \mathbf{r}_q'' = -G\frac{m_q m_i}{r_{iq}^3}\mathbf{r}_{iq} - G\sum_{\substack{j=1 \\ j\neq i,q}}^{N} \frac{m_q m_j}{r_{jq}^3}\mathbf{r}_{jq} \tag{2.35}$$

Simplifying the masses and, then, subtracting equation (2.35) from (2.34), it follows

$$\mathbf{r}_{qi}'' = -G\left(m_i + m_q\right)\frac{\mathbf{r}_{qi}}{r_{qi}^3} + G\sum_{\substack{j=1 \\ j\neq i,q}}^{N} m_j\left(\frac{\mathbf{r}_{ij}}{r_{ij}^3} - \frac{\mathbf{r}_{qj}}{r_{qj}^3}\right) \tag{2.36}$$

where the relationship $\mathbf{r}_{rs} = -\mathbf{r}_{sr}$ (being r and s arbitrary indexes) has been used. The position vector $\mathbf{r}_{qj}$ can be easily found by consulting the planetary ephemerides and, then, $\mathbf{r}_{ij} = \mathbf{r}_{qj} - \mathbf{r}_{qi}$.

Within the context of this thesis, the equation of motion for a spacecraft in the Sun-Earth-Moon system (relatively to the Earth) has been extensively exploited

$$\mathbf{r}'' = -G\left(m_{sc} + m_{\oplus}\right)\frac{\mathbf{r}}{r^3} + Gm_{\odot}\left(\frac{\mathbf{r}_{sc\to\odot}}{r_{sc\to\odot}^3} - \frac{\mathbf{r}_{\oplus\odot}}{r_{\oplus\odot}^3}\right) + Gm_{\leftmoon}\left(\frac{\mathbf{r}_{sc\to\leftmoon}}{r_{sc\to\leftmoon}^3} - \frac{\mathbf{r}_{\oplus\leftmoon}}{r_{\oplus\leftmoon}^3}\right) \tag{2.37}$$

Parameter	Value	Units
$m_\oplus$	$5.9722 \cdot 10^{24}$	kg
$m_\leftmoon$	$7.3477 \cdot 10^{22}$	kg
$m_\odot$	$1.9885 \cdot 10^{30}$	kg
M	$6.0457 \cdot 10^{24}$	kg
$\pi_\oplus$	0.9878464009	nondimensional
$\pi_\leftmoon$	0.0121535990	nondimensional
$\pi_\odot$	328920.99404	nondimensional

Table 2.3: Mass parameters for the Sun-Earth-Moon System

For practical reasons, equation (2.37) can be nondimensionalized by using the same characteristic quantities already introduced for the Earth-Moon system in the CRTBP (see Table 2.1), leading to

$$\ddot{\boldsymbol{\rho}} = -\pi_\oplus \frac{\boldsymbol{\rho}}{\rho^3} + \pi_\odot \left(\frac{\boldsymbol{\rho}_{sc\to\odot}}{\rho^3_{sc\to\odot}} - \frac{\boldsymbol{\rho}_{\oplus\odot}}{\rho^3_{\oplus\odot}} \right) + \pi_\leftmoon \left(\frac{\boldsymbol{\rho}_{sc\to\leftmoon}}{\rho^3_{sc\to\leftmoon}} - \frac{\boldsymbol{\rho}_{\oplus\leftmoon}}{\rho^3_{\oplus\leftmoon}} \right) \tag{2.38}$$

Note that the second order derivative of $\boldsymbol{\rho}$ is, now, with respect to the nondimensional time. Nondimensional position vectors are found dividing the dimensional counterparts by the characteristic length L, while the division by the characteristic mass $M = m_\oplus + m_\leftmoon$ yields to the definition of $\pi_\oplus$, $\pi_\odot$ and $\pi_\leftmoon$

$$\pi_\oplus = \frac{m_{sc} + m_\oplus}{M} \approx \frac{m_\oplus}{M} \tag{2.39}$$

$$\pi_\odot = \frac{m_\odot}{M} \tag{2.40}$$

$$\pi_\leftmoon = \frac{m_\leftmoon}{M} \tag{2.41}$$

Mass parameters for the Sun-Earth-Moon system are listed in Table 2.3.

2.2.2 Equations of Motion in the Synodic Frame

Within the context of the N-Body problem, it can be interesting to select two gravitating bodies and write the equations of motion for a spacecraft with respect to their synodic frame (relative to the barycentre of the selected two-body system). For example, an option can be offered by expressing the dynamics of the spacecraft relatively to the barycentre of the Earth-Moon system and projecting the equations onto the axes of its synodic frame. What changes from the CRTBP is that, now, the actual motion of the N-bodies is considered. This is true also for the selected primaries, m_1 and m_2, that are no longer revolving according to a perfect, uniform, circular motion. As a

convention, it will be still valid that $m_1 > m_2$. The geometry of the problem is illustrated in Figure 2.5.

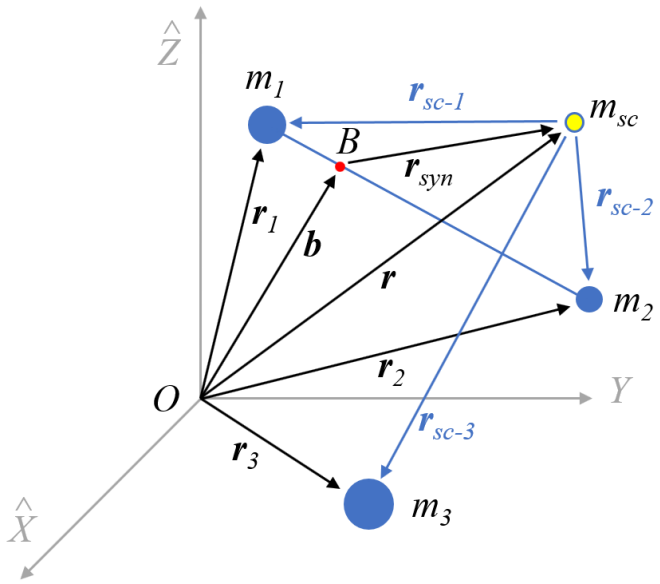

Figure 2.5: Geometry of the N-Body Problem relative to the barycentre of two primaries (m_1 and m_2)

In order to derive the equations of motion in the synodic frame of the masses m_1 and m_2, with reference to Figure 2.5 it follows that

$$\mathbf{r}'' = G \sum_{j=1}^{N} \frac{m_j}{r_{sc\to j}^3} \mathbf{r}_{sc\to j} \tag{2.42}$$

where $\mathbf{r}_{sc\to j} = \mathbf{r}_j - \mathbf{r}$. As already noted, equation (2.42) expresses the acceleration of a particle i in an inertial frame of reference. For the sake of convenience, this frame can be thought to coincide with the J2000 coordinate system, with origin at the barycentre of the Solar System. The J2000 coordinate system is such that the $\hat{X}$-axis is aligned with the mean equinox, the $\hat{Z}$-axis is aligned with the Earth's spin axis (or celestial North Pole) and the $\hat{Y}$-axis completes the right-handed triad. Differently, the mentioned synodic frame of the system $m_1 - m_2$ is centred on its barycentre B and the coordinate system is such that the $\hat{x}$-axis is aligned with the instantaneous relative distance between the two primaries (direction towards the less massive primary m_2), the $\hat{z}$-axis is perpendicular to the osculating plane containing their motion and directed as the relative angular momentum and the $\hat{y}$-axis completes the right-handed triad. Similarly to what has been

done for the derivation of the equations of motion for the CRTBP, by using kinematic relationships it is possible to write the inertial acceleration $\mathbf{r}''$ following another way. Indeed, it is valid that

$$\mathbf{r} = \mathbf{b} + \mathbf{r}_{syn} \tag{2.43}$$

where $\mathbf{b}$ is the position vector of the center of mass of the system $m_1 - m_2$ and $\mathbf{r}_{syn}$ defines the location of the spacecraft relative to B. It is convenient to express $\mathbf{r}_{syn} = k\mathbf{R}\boldsymbol{\rho}$, so equation (2.43) is rewritten as

$$\mathbf{r} = \mathbf{b} + k\mathbf{R}\boldsymbol{\rho} \tag{2.44}$$

where $\boldsymbol{\rho}$ is the nondimensional position vector of the spacecraft whose components are expressed in the synodic frame and relative its origin. The dimensional part is embedded in the time dependent factor k. Since equation (2.44) has to be read and projected onto the $\hat{X}\hat{Y}\hat{Z}$, coherency is granted thanks to the rotation matrix $\mathbf{R}$. Indeed, it is applied to the vector $\boldsymbol{\rho}$, allowing the transformation from the synodic to the inertial frame. Taking the time derivative of equation (2.44), it follows

$$\mathbf{r}' = \mathbf{b}' + k'\mathbf{R}\boldsymbol{\rho} + k\mathbf{R}'\boldsymbol{\rho} + k\mathbf{R}\boldsymbol{\rho}' \tag{2.45}$$

Iterating the procedure to find the second derivative, it is possible to write

$$\mathbf{r}'' = \mathbf{b}'' + k''\mathbf{R}\boldsymbol{\rho} + 2k'\mathbf{R}'\boldsymbol{\rho} + k\mathbf{R}''\boldsymbol{\rho} + 2k'\mathbf{R}\boldsymbol{\rho}' + 2k\mathbf{R}'\boldsymbol{\rho}' + k\mathbf{R}\boldsymbol{\rho}'' \tag{2.46}$$

The comparison between equations (2.42) and (2.46) yields the following relationship

$$\mathbf{b}'' + \left(k''\mathbf{R} + 2k'\mathbf{R}' + k\mathbf{R}''\right)\boldsymbol{\rho} + 2\left(k'\mathbf{R} + k\mathbf{R}'\right)\boldsymbol{\rho}' + k\mathbf{R}\boldsymbol{\rho}'' = G\sum_{j=1}^{N} m_j \frac{\mathbf{r}_{sc\to j}}{r_{sc\to j}^3} \tag{2.47}$$

Note that it is true that

$$\mathbf{r}_{sc\to j} = \mathbf{r}_{B\to j} - \mathbf{r}_{syn} = \mathbf{r}_{B\to j} - k\mathbf{R}\boldsymbol{\rho} \tag{2.48}$$

where $\mathbf{r}_{B\to j}$ is the position vector of the mass m_j measured from the origin B of the synodic frame. Expressing equation (2.47) in terms of $\boldsymbol{\rho}''$, it follows

$$\begin{aligned}\boldsymbol{\rho}'' = &-\left(\frac{k''}{k}\mathbf{I} + 2\frac{k'}{k}\mathbf{R}^T\mathbf{R}' + \mathbf{R}^T\mathbf{R}''\right)\boldsymbol{\rho} - 2\left(\frac{k'}{k}\mathbf{I} + \mathbf{R}^T\mathbf{R}'\right)\boldsymbol{\rho}' \\ &-\frac{1}{k}\mathbf{R}^T\left(\mathbf{b}'' - G\sum_{j=1}^{N} m_j\frac{\mathbf{r}_{sc\to j}}{r_{sc\to j}^3}\right)\end{aligned} \tag{2.49}$$

where $\mathbf{I}$ is the identity matrix. The inversion of the matrix $\mathbf{R}$ is legit: indeed, the transformation matrix $\mathbf{R}$ is orthonormal and its inverse coincides with the transpose matrix $\left(\mathbf{R}^{-1} = \mathbf{R}^T\right)$. Equation (2.49) is a second-order differential equation with respect to the dimensional time. In order to write the dimensionless form, it has to be remembered that the nondimensional time τ is defined (see equation (2.14)) as

$$\tau = \frac{t}{T}$$

being T the characteristic time of the selected primaries. So, in an N-body environment the dimensionless form of the second-order differential equation that describes the dynamics of a particle with respect to the synodic frame of the system $m_1 - m_2$ is the following:

$$\begin{aligned}\ddot{\boldsymbol{\rho}} = -\frac{1}{n^2}\left(\frac{k''}{k}\mathbf{I} + 2\frac{k'}{k}\mathbf{R}^T\mathbf{R}' + \mathbf{R}^T\mathbf{R}''\right)\boldsymbol{\rho} - \frac{2}{n}\left(\frac{k'}{k}\mathbf{I} + \mathbf{R}^T\mathbf{R}'\right)\boldsymbol{\rho}' \\ -\frac{1}{n^2 k}\mathbf{R}^T\left(\mathbf{b}'' - G\sum_{j=1}^{N} m_j \frac{\mathbf{r}_{sc\to j}}{r^3_{sc\to j}}\right)\end{aligned} \tag{2.50}$$

where $n = \frac{1}{T}$ is the mean motion of the selected primaries.

For the sake of completeness, it is important to express some terms that appear in equation (2.50) (in particular, k and $\mathbf{R}$), along with their time derivatives. First, vectorial quantities of the less massive body (m_2) with respect to the main primary (m_1) are denoted by "$\sim$" symbol. So it possible to write

$$\begin{cases}\tilde{\mathbf{r}} = \mathbf{r}_2 - \mathbf{r}_1 \\ \tilde{\mathbf{v}} = \mathbf{v}_2 - \mathbf{v}_1 \\ \tilde{\mathbf{a}} = \mathbf{a}_2 - \mathbf{a}_1 \\ \tilde{\mathbf{j}} = \mathbf{j}_2 - \mathbf{j}_1\end{cases} \tag{2.51}$$

Position and velocity vectors, $\mathbf{r}_i$ and $\mathbf{v}_i$, are known from the ephemeris model. Regarding the acceleration $\mathbf{a}_i$ of the primaries, it is known that

$$\mathbf{a}_i = -G\sum_{\substack{j=1\\ j\neq i}}^{N}\frac{m_j}{r^3_{ji}}\mathbf{r}_{ji} = -G\sum_{j=1}^{N} m_j \frac{\mathbf{r}_i - \mathbf{r}_j}{||\mathbf{r}_i - \mathbf{r}_j||^3} \tag{2.52}$$

The jerk is the rate of change of the acceleration. For each primary, the jerk $\mathbf{j}_i$ can be found by taking the time derivative of equation (2.52)

$$\mathbf{j}_i = G\sum_{\substack{j=1\\ j\neq i}}^{N} m_j \left\{\frac{\mathbf{v}_i - \mathbf{v}_j}{||\mathbf{r}_i - \mathbf{r}_j||^3} - 3\left[(\mathbf{r}_i - \mathbf{r}_j)\cdot(\mathbf{v}_i - \mathbf{v}_j)\right]\frac{\mathbf{r}_i - \mathbf{r}_j}{||\mathbf{r}_i - \mathbf{r}_j||^5}\right\} \tag{2.53}$$

Equations (2.52) and (2.53) must be evaluated separately, once for the main body ($i = 1$) and once for the less massive primary ($i = 2$). The factor k coincides with the value of instantaneous distance between the two primaries. To be clear, it behaves as time dependent factor that is used to nondimensionalize length quantities. The factor k and its time derivatives are written as follows

$$k = ||\tilde{\mathbf{r}}|| \tag{2.54}$$

$$k' = \frac{\tilde{\mathbf{r}} \cdot \tilde{\mathbf{v}}}{k} \tag{2.55}$$

$$k'' = \frac{k\left(\tilde{v}^2 + \tilde{\mathbf{r}} \cdot \tilde{\mathbf{a}}\right) - k'\left(\tilde{\mathbf{r}} \cdot \tilde{\mathbf{v}}\right)}{k^2} \tag{2.56}$$

The columns of the transformation matrix $\mathbf{R}$ coincide with the unit vectors $\mathbf{e}_i$ of the synodic frame of the system $m_1 - m_2$. Recalling that at any time in the synodic frame the $\hat{x}$-axis is parallel to the line connecting the primaries, the $\hat{z}$-axis is directed as their relative angular momentum and the $\hat{y}$-axis completes the right-handed triad, it is possible to write

$$\mathbf{R} = \begin{bmatrix} \mathbf{e}_1 & \mathbf{e}_2 & \mathbf{e}_3 \end{bmatrix} \qquad \text{where} \qquad \begin{cases} \mathbf{e}_1 &= \dfrac{\tilde{\mathbf{r}}}{k} \\ \mathbf{e}_2 &= \mathbf{e}_3 \wedge \mathbf{e}_1 \\ \mathbf{e}_3 &= \dfrac{\tilde{\mathbf{r}} \wedge \tilde{\mathbf{v}}}{h} \end{cases} \tag{2.57}$$

The first time derivative of $\mathbf{R}$ is $\mathbf{R}' = \begin{bmatrix} \mathbf{e}_1' & \mathbf{e}_2' & \mathbf{e}_3' \end{bmatrix}$ where

$$\begin{cases} \mathbf{e}_1' &= \dfrac{k\tilde{\mathbf{v}} - k'\tilde{\mathbf{r}}}{k^2} \\ \mathbf{e}_2' &= \mathbf{e}_3' \wedge \mathbf{e}_1 + \mathbf{e}_3 \wedge \mathbf{e}_1' \\ \mathbf{e}_3' &= \dfrac{h\left(\tilde{\mathbf{r}} \wedge \tilde{\mathbf{a}}\right) - h'\left(\tilde{\mathbf{r}} \wedge \tilde{\mathbf{v}}\right)}{h^2} \end{cases} \tag{2.58}$$

The second derivative of $\mathbf{R}$ is $\mathbf{R}'' = \begin{bmatrix} \mathbf{e}_1'' & \mathbf{e}_2'' & \mathbf{e}_3'' \end{bmatrix}$ where

$$\begin{cases} \mathbf{e}_1'' &= \dfrac{\left[2(k')^2 - kk''\right]\tilde{\mathbf{r}} - 2kk'\tilde{\mathbf{v}} + k^2\tilde{\mathbf{a}}}{k^3} \\ \mathbf{e}_2'' &= \mathbf{e}_3'' \wedge \mathbf{e}_1 + 2\mathbf{e}_3' \wedge \mathbf{e}_1' + \mathbf{e}_3 \wedge \mathbf{e}_1'' \\ \mathbf{e}_3'' &= \dfrac{h^2\left(\tilde{\mathbf{v}} \wedge \tilde{\mathbf{a}} + \tilde{\mathbf{r}} \wedge \tilde{\mathbf{j}}\right) - 2hh'\left(\tilde{\mathbf{r}} \wedge \tilde{\mathbf{a}}\right) + \left[2(h')^2 - hh''\right]\left(\tilde{\mathbf{r}} \wedge \tilde{\mathbf{v}}\right)}{h^3} \end{cases} \tag{2.59}$$

In equations (2.57)-(2.59) the magnitude of the relative angular momentum of the primaries (h) and its time derivatives (h' and h'') appear several time.

Their values are expressed here below:

$$\begin{cases} h &= ||\tilde{\mathbf{r}} \wedge \tilde{\mathbf{v}}|| \\ h' &= \dfrac{(\tilde{\mathbf{r}} \wedge \tilde{\mathbf{v}}) \cdot (\tilde{\mathbf{r}} \wedge \tilde{\mathbf{a}})}{h} \\ h'' &= \dfrac{\tilde{\mathbf{r}} \wedge \tilde{\mathbf{v}}}{h} \end{cases} \tag{2.60}$$

2.2.3 Coordinate Transformations

Often it is very useful to perform coordinate system transformations in order to express state vectors in suitable frames of reference and to design space trajectories under different viewpoints. In particular, it would be desirable to dispose of a transformation that allows to transit between the two systems of reference where the N-body problem equations have been written, that is to say

- Equations of motions relative to a main body with reference to an inertial frame of reference (as the J2000 frame can be);
- Equations of motion relative to the barycentre of the $m_1 - m_2$ system with reference to their synodic frame.

For the sake of convenience, let us assume that the main body ($m_1 = m_E$) is the Earth and that the second primary ($m_2 = m_M$) is the Moon. With reference to Figure 2.6, it is possible write the following relationship:

$$\mathbf{r} = -\mathbf{r}_E + \mathbf{r}_{syn} \tag{2.61}$$

where $\mathbf{r}_E$ is the position vector of the Earth relative to the barycentre B of the Earth-Moon system. Remembering that $\mathbf{r}_{syn} = k\mathbf{R}\boldsymbol{\rho}$, it follows

$$\mathbf{r} = -\mathbf{r}_E + k\mathbf{R}\boldsymbol{\rho} \tag{2.62}$$

Recalling that for the nondimensional time it is true that

$$\tau = \frac{t}{T} \qquad \Rightarrow \qquad dt = Td\tau \tag{2.63}$$

and taking the time derivative of equation (2.62), it is possible to write

$$\mathbf{r}' = -\mathbf{r}'_E + k'\mathbf{R}\boldsymbol{\rho} + k\mathbf{R}'\boldsymbol{\rho} + \frac{k}{T}\mathbf{R}\dot{\boldsymbol{\rho}} \tag{2.64}$$

Joining equations (2.62) and (2.64), it follows

$$\begin{bmatrix} \mathbf{r} \\ \mathbf{r}' \end{bmatrix} = - \begin{bmatrix} \mathbf{r}_E \\ \mathbf{r}'_E \end{bmatrix} + \begin{bmatrix} k\mathbf{R} & \mathbf{0}_{3\times 3} \\ k'\mathbf{R} + k\mathbf{R}' & \frac{k}{T}\mathbf{R} \end{bmatrix} \begin{bmatrix} \boldsymbol{\rho} \\ \dot{\boldsymbol{\rho}} \end{bmatrix} \tag{2.65}$$

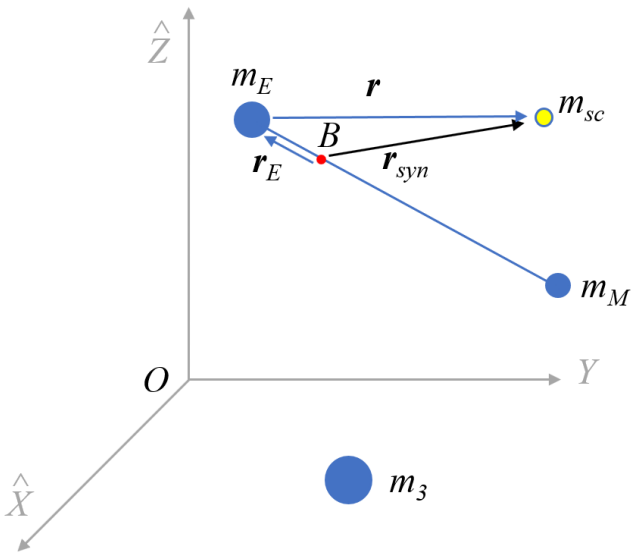

Figure 2.6: Geometry of the N-Body Problem for the coordinate system transformation

where the position and velocity vectors of the Earth relative to the barycentre B ($\mathbf{r}_E$ and $\mathbf{r}'_E$) are known from the planetary ephemerides. Setting

$$\mathbf{M} = \begin{bmatrix} k\mathbf{R} & \mathbf{0}_{3\times 3} \\ k'\mathbf{R} + k\mathbf{R}' & \frac{k}{T}\mathbf{R} \end{bmatrix} \tag{2.66}$$

equation (2.65) can be written more compactly as

$$\begin{bmatrix} \mathbf{r} \\ \mathbf{r}' \end{bmatrix} = -\begin{bmatrix} \mathbf{r}_E \\ \mathbf{r}'_E \end{bmatrix} + \mathbf{M}\begin{bmatrix} \boldsymbol{\rho} \\ \dot{\boldsymbol{\rho}} \end{bmatrix} \tag{2.67}$$

Equation (2.67) allows the transformation of a nondimensional state $(\boldsymbol{\rho}, \dot{\boldsymbol{\rho}})$ expressed in the synodic frame to a dimensional state $(\mathbf{r}, \mathbf{r}')$ relative to the Earth and with respect to inertial axes. In the case that the latter has to be nondimensionalized as well, usual characteristic quantities L and T are used. Reversing equation (2.67), it follows

$$\begin{bmatrix} \boldsymbol{\rho} \\ \dot{\boldsymbol{\rho}} \end{bmatrix} = \mathbf{M}^{-1}\begin{bmatrix} \mathbf{r} + \mathbf{r}_E \\ \mathbf{r}' + \mathbf{r}'_E \end{bmatrix} \tag{2.68}$$

allowing for the inverse transformation: given the dimensional state $(\mathbf{r}, \mathbf{r}')$, it is possible to get the corresponding nondimensional $(\boldsymbol{\rho}, \dot{\boldsymbol{\rho}})$. Similarly to the previous case, if the Earth-relative state (projected along inertial axes) is known in a dimensionless form, dimensionalisation has to be considered before applying equation (2.68).

Chapter 3

Attitude Model

In addition to the motion of the center of mass, another important element is represented by the motion of the spacecraft *about its center of mass*, also denoted as *attitude*. Orbital mechanics and attitude can be considered coupled: the coupling, here considered, is *one-way*, in the sense that the trajectory of the spacecraft influences the attitude motion, but the orientation of the spacecraft does not affect the orbital dynamics. The first part of the previous sentence is adequate: as a matter of fact, orbital mechanics considerations define perturbations that enter in the attitude dynamics. The second part of the previous sentence is less tolerable, and it is accepted with reservations: indeed, solar radiation pressure results in different orbital perturbations depending on the attitude of the spacecraft. Within the context of this study, the effects of solar radiation pressure are neglected and the *one-way* coupling can be justified.

3.1 Dynamics

The rotational dynamics of a spacecraft can be studied considering the motion of a co-moving frame, rigidly attached to the spacecraft itself. This frame is called *body frame* and it is defined by its axes $x_b - y_b - z_b$, defined as the principal axes of inertia of the spacecraft. This means that the inertia matrix of the spacecraft cab be written as a diagonal matrix ($\mathbf{J} = \text{diag}(J_x, J_y, J_z)$) with respect to these axis. Time variations of the spacecraft inertia are not considered.

By considering Newton's second law, the attitude dynamics can be written as

$$\dot{\mathbf{H}} = \mathbf{M}_{net} \tag{3.1}$$

where $\mathbf{H}$ is the angular momentum of the spacecraft and $\mathbf{M}_{net}$ represents

the net sum of the external acting torques. Writing equation (3.1) in the body frame, the so-called *Euler equations* are derived:

$$\dot{\mathbf{H}}_{rel} + \boldsymbol{\omega} \times \mathbf{H} = \mathbf{M}_{net} \tag{3.2}$$

where $\dot{\mathbf{H}}_{rel}$ represents the time derivative of the angular momentum relative to the rotating body frame and $\boldsymbol{\omega} = [\omega_x \ \omega_y \ \omega_z]^T$ is the angular velocity of the body frame (so, of the spacecraft) expressed in the body frame. Expanding equation (3.2), it follows

$$\begin{cases} \dot{\omega}_x &= \dfrac{J_y - J_z}{J_x}\omega_y\omega_z + \dfrac{M_x}{J_x} \\ \dot{\omega}_y &= \dfrac{J_z - J_x}{J_y}\omega_x\omega_z + \dfrac{M_y}{J_y} \\ \dot{\omega}_z &= \dfrac{J_x - J_y}{J_z}\omega_x\omega_y + \dfrac{M_z}{J_z} \end{cases} \tag{3.3}$$

Euler equations allow to determine the angular velocity of the spacecraft at each instant. If the initial attitude of the spacecraft is known, it is possible to rebuild its angular position profiles. The term $\mathbf{M}_{net}$ is used to model external torques that act such to change spacecraft angular momentum and they are represented, in general, by external perturbations (angular momentum variations due to active control is not considered here). The main perturbation, under examination within this study, is the *gravity gradient* torque. Its values strongly depends on the orbital dynamics and it is in this circumstances that *attitude-orbital mechanics* coupling arises.

For numerical purposes, also Euler equations are integrated in their dimensionless form: only a scaling, through the dimensionless time, is required.

3.1.1 Gravity Gradient

Gravity gradient torques are caused when a spacecraft center of gravity is not aligned with its center of mass with respect to the local vertical. The center of gravity is not, in general, the same as the center of mass. This kind of disturbance tends to align the minimum principal axis with the local vertical.

Gravity gradient torque provoked by a central body (denoted as "i") can be expressed as

$$\mathbf{M}_{gg,i} = \frac{3GM_i}{R^5}\begin{bmatrix} (J_z - J_y)\, R_y R_z \\ (J_x - J_z)\, R_x R_z \\ (J_y - J_x)\, R_x R_y \end{bmatrix} \tag{3.4}$$

where G is the universal gravitational constant, M_i the mass of the attracting body and R the norm of $\mathbf{R} = [R_x \ R_y \ R_z]^T$. In order to be coherent with the

formulation, it is very important that $\mathbf{R}$ (spacecraft position vector relative to the central body) is expressed in the body frame. If more attracting bodies are present, the overall perturbing external torque is written as the sum of the single gravity gradient torques, that is

$$\mathbf{M}_{net} = \sum_{i=1}^{N} \mathbf{M}_{gg,i} \tag{3.5}$$

3.2 Kinematics

In order to complete the formulation about attitude, it is important to build the angular configuration of the spacecraft, or its *kinematics*. There are different way to describe spacecraft kinematics. One of the most efficient (but, maybe, less intuitive) ways to solve spacecraft kinematics is represented by *quaternions*. The angular velocities $\boldsymbol{w}$ represent the information needed to solve quaternion dynamics, that can be expressed as follows:

$$\dot{\mathbf{q}} = \frac{1}{2}\boldsymbol{\Xi}\mathbf{q} = \frac{1}{2}\begin{bmatrix} 0 & \omega_z & -\omega_y & \omega_x \\ -\omega_z & 0 & \omega_x & \omega_y \\ \omega_y & -\omega_x & 0 & \omega_z \\ -\omega_x & -\omega_y & -\omega_z & 0 \end{bmatrix} \mathbf{q} \tag{3.6}$$

Once the quaternions are known in time, it is possible to convert their information in order to compute the *direct cosine matrix* $\mathbf{A}_{B/N}$ that, in an equivalent way, describes the attitude configuration of the spacecraft. The generic direct cosine matrix $\mathbf{A}_{x/X}$ is very important, since it represents the transformation matrix that allow to express a vectorial quantity from the "X" to the "x" coordinate system. So, the matrix $\mathbf{A}_{B/N}$ is also used to transform inertial quantities to the body frame coordinate system.

Observation If a direct cosine matrix profile $\mathbf{A}_{x/X}$ is known, it is possible to recover its angular velocity profile $\boldsymbol{\omega}_{x/X}$ (that is, the angular velocities expressed in the "x" frame relative to "X") by exploiting

$$\dot{\mathbf{A}}_{x/X} = -\left[\boldsymbol{\omega}_{x/X}\right]^{\wedge} \mathbf{A}_{x/X} \tag{3.7}$$

where $\left[\boldsymbol{\omega}_{x/X}\right]^{\wedge}$ defines the skew-symmetric matrix obtained starting from $\boldsymbol{\omega}_{x/X}$.

3.3 Coupled Model

In order to solve the attitude-orbital coupled dynamics, it is sufficient to write a system of differential equations of the type

$$\dot{\mathbf{x}} = \mathbf{f}\left(\mathbf{x}, \tau, \varepsilon, \mathbf{J}\right) \tag{3.8}$$

The overall dynamics takes into consideration an augmented state $\mathbf{x}$ defined as follows:

$$\mathbf{x} = \begin{bmatrix} \boldsymbol{\rho} \\ \dot{\boldsymbol{\rho}} \\ \boldsymbol{\omega} \\ \mathbf{q} \end{bmatrix} \tag{3.9}$$

Therefore, the whole dynamics is solved by integrating equations (2.38), (3.3) and (3.6), simultaneously.

Chapter 4

Validation

The aim of this chapter is to verify that the models presented in Chapters 2 and 3 are in agreement with some known results up to a certain degree of precision and that they represent, in a correct way, the phenomena to be studied. So, a reference solution will be compared with the one obtained from numerical integration of the equations of motion, and the relative error will be studied.

A fundamental element that is necessary in order to move on is the numerical integrator. Within the context of this study, a *Runge-Kutta* scheme is used for all the integrations.

4.1 Numerical Propagator

Since all the models presented so far are not characterized by a closed-form, analytical solution, the only way to proceed in order to compute their solution is to numerically integrated the equations of motion. For this reason, different numerical integrators (or propagators) are known and can be exploited. Within this context an explicit Runge-Kutta method is exploited: it integrates a system of ordinary differential equations using 8-7-th order Dormand and Prince formulas [42]. This is a 8th-order accurate integrator and, therefore, the local error normally expected is $O(h^9)$. The propagator requires 13 function evaluations per integration step. The used numerical integration scheme is an already verified version, thanks to the work of Govorukhin V.N. [56].

4.2 SPICE

The *SPICE* tool-kit has been developed at the Jet Propulsion Laboratory (JPL) by the Navigation and Ancillary Information Facility (NAIF), acting under the directions of NASA's Planetary Science Division. This powerful tool-kit allows to assist scientists and engineers in modelling, planning and executing activities needed to conduct planetary exploration missions [1].

The primary SPICE data sets are often called *kernels* and they are composed of navigation and other ancillary information that has been structured and formatted for easy access. The SPICE tool-kit is available for different environments, including MATLAB®. Among the numerous functionalities of SPICE, the retrieval of accurate state vectors of celestial bodies directly enters the equations of motion for the N-body model. Within the context of this study, Jet Propulsion Laboratory DE431 ephemerides kernel is used.

4.3 Validation of N-body Model

Once that the numerical propagator and the ephemerides database have been introduced, it is possible to integrate the N-body models presented in Chapter 2. The validation of the models is carried out comparing the integrated trajectories with the ones coming from the ephemerides database for different Near-Earth asteroids. The celestial bodies used for this purpose are listed in Table 4.1. The integrated trajectories are compared with the

Name	SPK ID	Semi-Major Axis [AU]	Orbit Period [years]	Eccentricity	Inclination [deg]
2008 EV5	2341843	0.958	0.94	0.084	7.436
Bennu	2101955	1.126	1.20	0.203	6.035
1999 JU3	2162173	1.189	1.30	0.190	5.884
2007 UY1	3389197	0.951	0.93	0.175	1.019

Table 4.1: Considered Asteroids for Validation

ones coming from ephemerides evaluation over a period of 10 years (spanning from ε_0 = 1-Jan-2020 to ε_{fin} = 1-Jan-2030). For each one of the bodies in Table 4.1, the verification process evolves in three different main steps:

- The celestial body initial state vector is retrieved from ephemerides database at epoch ε_0 = 1-Jan-2020.

- The initial state vector is used as initial conditions for the numerical integration for the trajectory of the considered body, over a 10 years period. The propagation will give a series of state vectors, each related at a different instant.

- The body ephemerides are evaluated at the same instants of the propagation, in order to obtain the reference trajectory. The difference (at each instant) between the propagated and the reference trajectory allows to define a profile of the relative error (in position or velocity), defined as

$$\varepsilon_{rr}(\tau) = \frac{||\boldsymbol{x}(\tau) - \boldsymbol{x}_{ref}(\tau)||}{||\boldsymbol{x}(\tau)||} \tag{4.1}$$

  where $\boldsymbol{x}(\tau)$ and $\boldsymbol{x}_{ref}(\tau)$ represent the generic state of the propagated and reference trajectory, respectively.

In Figure 4.1 a graphical comparison between the studied trajectory is reported. The continuous blue line represents the integrated trajectories,

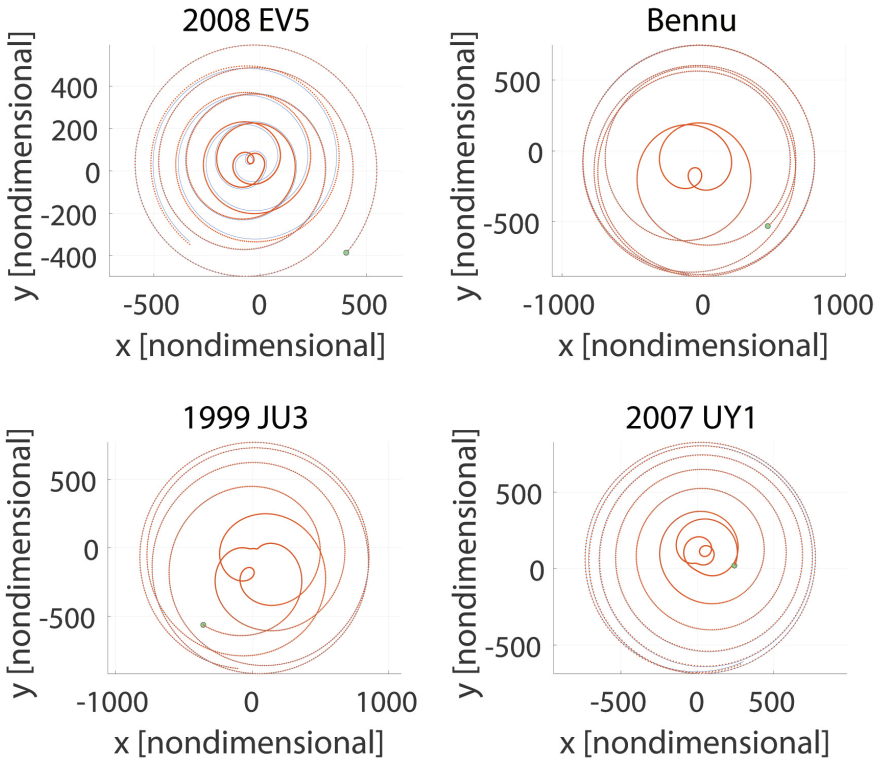

Figure 4.1: Integrated and Reference Trajectories

while orange dots follows the reference ones. The marked point represents

the initial state of the propagation (at ε_0 = 1-Jan-2020). Figure 4.2 reports the profiles of the relative errors (in position) of the two trajectories, for each considered body. Apart from some cases (due to close approaches to central

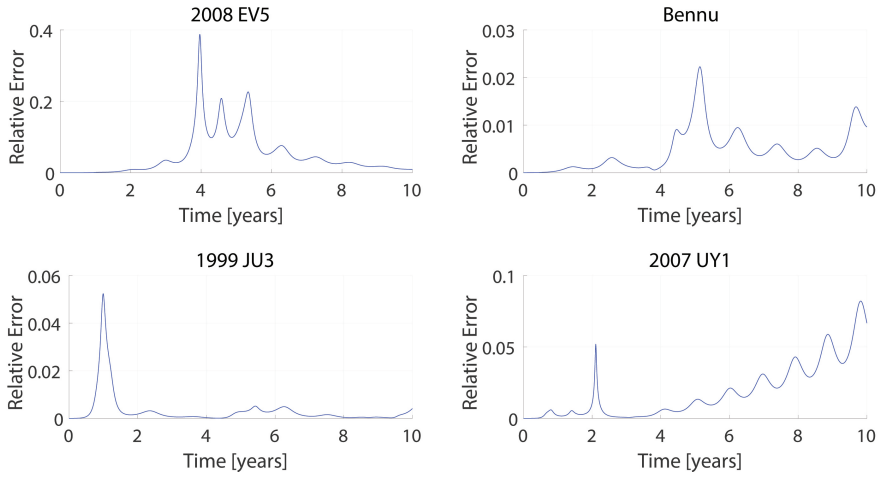

Figure 4.2: Integrated and Reference Trajectories - Relative (Position) Error

bodies) in which a sudden increase in the relative error is observed, the order of magnitude of the error is, usually (10^{-3} or below).

4.4 Validation of the Attitude Model

In order to infer the correctness of the attitude model, some unitary tests have been performed. These tests are related to well known properties and characteristic of spacecraft attitude dynamics, in particular:

- Constancy of angular momentum in the inertial space (if no external torques are acting);
- Stability about major axis of inertia;
- Instability about intermediate axis of inertia;
- Stability regions for gravity gradient torque.

All the above mentioned tests have been performed successfully.

Chapter 5

Numerical Analysis

In order to compute the solution of the CRTBP or N-body problem, the equations of motion must be integrated numerically. Indeed, a closed-form solution doesn't exist. Furthermore, in many circumstances the considered dynamical systems exhibit a chaotic behaviour: slight changes in initial conditions can correspond to large variations in the final conditions. It would be fundamental to have some tools that allow the research of trajectories with given and desired characteristics. Numerical methods, that are presented in this chapter, are essential within the context of trajectory design.

5.1 Information on Derivatives

5.1.1 State Transition Matrix

Dynamical models introduced in the previous chapter can be expressed in a generic way as

$$\dot{\boldsymbol{x}} = \boldsymbol{f}(\boldsymbol{x}, \tau, \varepsilon) \tag{5.1}$$

where the state vector $\boldsymbol{x}$ contains the position and velocity components

$$\boldsymbol{x} = \begin{bmatrix} x \\ y \\ z \\ \dot{x} \\ \dot{y} \\ \dot{z} \end{bmatrix} = \begin{bmatrix} \boldsymbol{\rho} \\ \dot{\boldsymbol{\rho}} \end{bmatrix} \tag{5.2}$$

and τ and ε represent the elapsed time and the reference epoch, respectively. For the sake of convenience, it is possible to think that all the input quantities are in a dimensionless form.

Once some initial conditions $\boldsymbol{x}_0 = [x_0\ y_0\ z_0\ \dot{x}\ \dot{y}\ \dot{z}]$ and an initial epoch ε_0 are specified, the equations in the form (5.1) can be integrated numerically over a time span $\tau_{span} = [\tau_0\ \tau_f]$. Note that the propagation period is $\tau = \tau_f - \tau_0$, where, in general, it will be $\tau_0 = 0$, so that the propagation period coincides with the elapsed time. The resulting trajectory will be denoted as $\boldsymbol{x}(\boldsymbol{x}_0, \tau, \varepsilon_0)$. In order to achieve some desired properties, it is important to understand how the trajectory varies if initial conditions are slightly changed. If a small variation, $\delta\boldsymbol{x}_0$ (in position and velocity), is considered, the resulting trajectory will be slightly different as well. This solution can be denoted as $\boldsymbol{x}(\boldsymbol{x}_0 + \delta\boldsymbol{x}_0, \tau, \varepsilon_0)$ The initial variation $\delta\boldsymbol{x}_0$ repre-

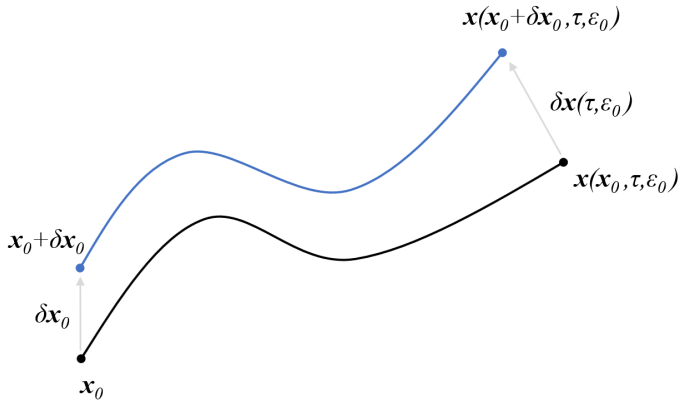

Figure 5.1: Original and perturbed trajectories

sents the difference between the two trajectories when $\tau = \tau_0$. This variation evolves during the propagation and, at the generic time τ, it is true that

$$\boldsymbol{x}(\boldsymbol{x}_0 + \delta\boldsymbol{x}_0, \tau, \varepsilon_0) = \boldsymbol{x}(\boldsymbol{x}_0, \tau, \varepsilon_0) + \delta\boldsymbol{x}(\tau, \varepsilon_0) \tag{5.3}$$

Since the initial variation is small, it is possible to consider the Taylor series of $\boldsymbol{x}(\boldsymbol{x}_0 + \delta\boldsymbol{x}_0, \tau, \varepsilon_0)$, yielding

$$\begin{aligned} \boldsymbol{x}(\boldsymbol{x}_0, \tau, \varepsilon_0) + \frac{\partial \boldsymbol{x}}{\partial \boldsymbol{x}_0}\delta\boldsymbol{x}_0 + \cdots = \boldsymbol{x}(\boldsymbol{x}_0, \tau, \varepsilon_0) + \delta\boldsymbol{x}(\tau, \varepsilon_0) \\ \frac{\partial \boldsymbol{x}}{\partial \boldsymbol{x}_0}\delta\boldsymbol{x}_0 \approx \delta\boldsymbol{x}(\tau, \varepsilon_0) \end{aligned} \tag{5.4}$$

The derivative of $\boldsymbol{x}(\boldsymbol{x}_0, \tau, \varepsilon_0)$ with respect to the initial state $\boldsymbol{x}_0$ gives rise to the *state transition matrix* $\boldsymbol{\Phi}(\tau, \tau_0)$

$$\boldsymbol{\Phi}(\tau, \tau_0) = \frac{\partial \boldsymbol{x}}{\partial \boldsymbol{x}_0} \tag{5.5}$$

Also called *sensitivity matrix*, the state transition matrix expresses how variations in the initial state are related to variations in the final state of the trajectory. Since the state vector $\boldsymbol{x}$ has 6 components, $\boldsymbol{\Phi}(\tau, \tau_0)$ is a 6×6 matrix and it can be written in expanded form as

$$\boldsymbol{\Phi}(\tau, \tau_0) = \begin{bmatrix} \frac{\partial x}{\partial x_0} & \frac{\partial x}{\partial y_0} & \frac{\partial x}{\partial z_0} & \frac{\partial x}{\partial \dot{x}_0} & \frac{\partial x}{\partial \dot{y}_0} & \frac{\partial x}{\partial \dot{z}_0} \\ \frac{\partial y}{\partial x_0} & \frac{\partial y}{\partial y_0} & \frac{\partial y}{\partial z_0} & \frac{\partial y}{\partial \dot{x}_0} & \frac{\partial y}{\partial \dot{y}_0} & \frac{\partial y}{\partial \dot{z}_0} \\ \frac{\partial z}{\partial x_0} & \frac{\partial z}{\partial y_0} & \frac{\partial z}{\partial z_0} & \frac{\partial z}{\partial \dot{x}_0} & \frac{\partial z}{\partial \dot{y}_0} & \frac{\partial z}{\partial \dot{z}_0} \\ \frac{\partial \dot{x}}{\partial x_0} & \frac{\partial \dot{x}}{\partial y_0} & \frac{\partial \dot{x}}{\partial z_0} & \frac{\partial \dot{x}}{\partial \dot{x}_0} & \frac{\partial \dot{x}}{\partial \dot{y}_0} & \frac{\partial \dot{x}}{\partial \dot{z}_0} \\ \frac{\partial \dot{y}}{\partial x_0} & \frac{\partial \dot{y}}{\partial y_0} & \frac{\partial \dot{y}}{\partial z_0} & \frac{\partial \dot{y}}{\partial \dot{x}_0} & \frac{\partial \dot{y}}{\partial \dot{y}_0} & \frac{\partial \dot{y}}{\partial \dot{z}_0} \\ \frac{\partial \dot{z}}{\partial x_0} & \frac{\partial \dot{z}}{\partial y_0} & \frac{\partial \dot{z}}{\partial z_0} & \frac{\partial \dot{z}}{\partial \dot{x}_0} & \frac{\partial \dot{z}}{\partial \dot{y}_0} & \frac{\partial \dot{z}}{\partial \dot{z}_0} \end{bmatrix} \tag{5.6}$$

In order to obtain the elements that build up the state transition matrix, its time derivative is considered, yielding

$$\frac{d}{d\tau}\frac{\partial \boldsymbol{x}}{\partial \boldsymbol{x}_0} = \frac{\partial}{\partial \boldsymbol{x}_0}\frac{d\boldsymbol{x}}{d\tau} = \frac{\partial \dot{\boldsymbol{x}}}{\partial \boldsymbol{x}_0} = \frac{\partial \boldsymbol{f}(\boldsymbol{x}, \tau, \varepsilon)}{\partial \boldsymbol{x}_0} = \frac{\partial \boldsymbol{f}}{\partial \boldsymbol{x}}\frac{\partial \boldsymbol{x}}{\partial \boldsymbol{x}_0} \tag{5.7}$$

Denoting the derivative of the equations of motion with respect to the state vector as the $\mathbf{A}$ matrix, equation (5.7) can be written as

$$\dot{\boldsymbol{\Phi}}(\tau, \tau_0) = \mathbf{A}\boldsymbol{\Phi}(\tau, \tau_0) \tag{5.8}$$

Equation (5.8) is called *variational equation* and it expresses how the components of the state transition matrix varies during time. Its integration leads to the knowledge of the state transition matrix, whereas the initial conditions are defined by the identity matrix

$$\boldsymbol{\Phi}(\tau_0, \tau_0) = \frac{\partial \boldsymbol{x}_0}{\partial \boldsymbol{x}_0} = \mathbf{I}_{6\times 6} \tag{5.9}$$

For the evaluation of the $\mathbf{A}$ matrix, numerical integration of the state transition matrix (36 differential equations) must be carried out along with the integration of the equations of motion (5.1) (6 differential equations).

The $\mathbf{A}$ matrix depends on the considered dynamical models. If equations of motion in an inertial aligned, Earth relative frame are considered (that is, equation (2.38)), the $\mathbf{A}$ matrix can be written as

$$\mathbf{A} = \left[\begin{array}{ccc|c} & \mathbf{0}_{3\times 3} & & \mathbf{I}_{3\times 3} \\ \hline \frac{\partial \ddot{x}}{\partial x} & \frac{\partial \ddot{x}}{\partial y} & \frac{\partial \ddot{x}}{\partial z} & \\ \frac{\partial \ddot{y}}{\partial x} & \frac{\partial \ddot{y}}{\partial y} & \frac{\partial \ddot{y}}{\partial z} & \mathbf{0}_{3\times 3} \\ \frac{\partial \ddot{z}}{\partial x} & \frac{\partial \ddot{z}}{\partial y} & \frac{\partial \ddot{z}}{\partial z} & \end{array}\right] \tag{5.10}$$

where

$$
\begin{aligned}
\frac{\partial \ddot{x}}{\partial x} &= \pi_{\oplus}\left(-\frac{1}{\rho^3}+\frac{3x^2}{\rho^5}\right)+\pi_{\odot}\left(-\frac{1}{\rho_{sc\to\odot}^3}+\frac{3(x_{\odot}-x)^2}{\rho_{sc\to\odot}^5}\right)+\pi_{\mathbb{C}}\left(-\frac{1}{\rho_{sc\to\mathbb{C}}^3}+\frac{3(x_{\mathbb{C}}-x)^2}{\rho_{sc\to\mathbb{C}}^5}\right)\\
\frac{\partial \ddot{x}}{\partial y} &= \pi_{\oplus}\left(\frac{3xy}{\rho^5}\right)+\pi_{\odot}\left(\frac{3(x_{\odot}-x)(y_{\odot}-y)}{\rho_{sc\to\odot}^5}\right)+\pi_{\mathbb{C}}\left(\frac{3(x_{\mathbb{C}}-x)(y_{\mathbb{C}}-y)}{\rho_{sc\to\mathbb{C}}^5}\right)\\
\frac{\partial \ddot{x}}{\partial z} &= \pi_{\oplus}\left(\frac{3xz}{\rho^5}\right)+\pi_{\odot}\left(\frac{3(x_{\odot}-x)(z_{\odot}-z)}{\rho_{sc\to\odot}^5}\right)+\pi_{\mathbb{C}}\left(\frac{3(x_{\mathbb{C}}-x)(z_{\mathbb{C}}-z)}{\rho_{sc\to\mathbb{C}}^5}\right)\\
\frac{\partial \ddot{y}}{\partial x} &= \pi_{\oplus}\left(\frac{3yx}{\rho^5}\right)+\pi_{\odot}\left(\frac{3(y_{\odot}-y)(x_{\odot}-x)}{\rho_{sc\to\odot}^5}\right)+\pi_{\mathbb{C}}\left(\frac{3(y_{\mathbb{C}}-y)(x_{\mathbb{C}}-x)}{\rho_{sc\to\mathbb{C}}^5}\right)\\
\frac{\partial \ddot{y}}{\partial y} &= \pi_{\oplus}\left(-\frac{1}{\rho^3}+\frac{3y^2}{\rho^5}\right)+\pi_{\odot}\left(-\frac{1}{\rho_{sc\to\odot}^3}+\frac{3(y_{\odot}-y)^2}{\rho_{sc\to\odot}^5}\right)+\pi_{\mathbb{C}}\left(-\frac{1}{\rho_{sc\to\mathbb{C}}^3}+\frac{3(y_{\mathbb{C}}-y)^2}{\rho_{sc\to\mathbb{C}}^5}\right)\\
\frac{\partial \ddot{y}}{\partial z} &= \pi_{\oplus}\left(\frac{3yz}{\rho^5}\right)+\pi_{\odot}\left(\frac{3(y_{\odot}-y)(z_{\odot}-z)}{\rho_{sc\to\odot}^5}\right)+\pi_{\mathbb{C}}\left(\frac{3(y_{\mathbb{C}}-y)(z_{\mathbb{C}}-z)}{\rho_{sc\to\mathbb{C}}^5}\right)\\
\frac{\partial \ddot{z}}{\partial x} &= \pi_{\oplus}\left(\frac{3zx}{\rho^5}\right)+\pi_{\odot}\left(\frac{3(z_{\odot}-z)(x_{\odot}-x)}{\rho_{sc\to\odot}^5}\right)+\pi_{\mathbb{C}}\left(\frac{3(z_{\mathbb{C}}-z)(x_{\mathbb{C}}-x)}{\rho_{sc\to\mathbb{C}}^5}\right)\\
\frac{\partial \ddot{z}}{\partial y} &= \pi_{\oplus}\left(\frac{3zy}{\rho^5}\right)+\pi_{\odot}\left(\frac{3(z_{\odot}-z)(y_{\odot}-y)}{\rho_{sc\to\odot}^5}\right)+\pi_{\mathbb{C}}\left(\frac{3(z_{\mathbb{C}}-z)(y_{\mathbb{C}}-y)}{\rho_{sc\to\mathbb{C}}^5}\right)\\
\frac{\partial \ddot{z}}{\partial z} &= \pi_{\oplus}\left(-\frac{1}{\rho^3}+\frac{3z^2}{\rho^5}\right)+\pi_{\odot}\left(-\frac{1}{\rho_{sc\to\odot}^3}+\frac{3(z_{\odot}-z)^2}{\rho_{sc\to\odot}^5}\right)+\pi_{\mathbb{C}}\left(-\frac{1}{\rho_{sc\to\mathbb{C}}^3}+\frac{3(z_{\mathbb{C}}-z)^2}{\rho_{sc\to\mathbb{C}}^5}\right)
\end{aligned}
\tag{5.11}
$$

In the case that equations of motion in a non-inertial, Earth-Moon synodic frame are considered (that is, equation (2.50)), the $\mathbf{A}$ matrix will have the following form:

$$
\mathbf{A} = \left[\begin{array}{c|c}
\mathbf{0}_{3\times 3} & \mathbf{I}_{3\times 3} \\
\hline
-\frac{1}{n^2}\left(\frac{k''}{k}\mathbf{I}+2\frac{k'}{k}\mathbf{R}^T\mathbf{R}'+\mathbf{R}^T\mathbf{R}''\right)+\frac{\partial}{\partial\boldsymbol{\rho}}\left(\boldsymbol{a}_{grav}\right) & -\frac{2}{n}\left(\frac{k'}{k}\mathbf{I}+\mathbf{R}^T\mathbf{R}'\right)
\end{array}\right]
\tag{5.12}
$$

where $\frac{\partial}{\partial\boldsymbol{\rho}}\left(\boldsymbol{a}_{grav}\right)$ represents the derivative of the gravitational acceleration (due to all the considered bodies) with respect the position vector $\boldsymbol{\rho}$, that is

$$
\begin{aligned}
\frac{\partial}{\partial\boldsymbol{\rho}}\left(\boldsymbol{a}_{grav}\right) &= \frac{\partial}{\partial\boldsymbol{\rho}}\left(\frac{1}{n^2k}\mathbf{R}^T G\sum_{j=1}^{N} m_j\frac{\mathbf{r}_j-k\mathbf{R}\boldsymbol{\rho}}{||\mathbf{r}_j-k\mathbf{R}\boldsymbol{\rho}||}\right)\\
&= \frac{1}{n^2k}\mathbf{R}^T G\sum_{j=1}^{N} m_j\frac{\partial}{\partial\boldsymbol{\rho}}\left(\frac{\mathbf{r}_j-k\mathbf{R}\boldsymbol{\rho}}{||\mathbf{r}_j-k\mathbf{R}\boldsymbol{\rho}||}\right)
\end{aligned}
\tag{5.13}
$$

5.1.2 Derivative with respect to Time

When a trajectory is propagated (given some initial conditions $\boldsymbol{x}_0$ and a reference epoch ε_0) for a propagation time T = τ, it is straightforward to obtain information on the time derivative of the final state $\boldsymbol{x}$. Indeed, by

definition it follows

$$\frac{d\boldsymbol{x}}{d\tau} = \dot{\boldsymbol{x}} = \boldsymbol{f}\left(\boldsymbol{x}, \tau, \varepsilon_0\right). \tag{5.14}$$

where $\boldsymbol{f}$ represents the equations of the related dynamical system.

5.1.3 Derivative with respect to Epoch

In contrast to the CRTBP, in an ephemeris N-body model there is a strong dependence on the reference epoch ε with respect to which the trajectory is numerically integrated. This implies that in general the same initial conditions $\boldsymbol{x}_0$ will evolve differently if the starting epoch is changed.

To study the variation of the final state $\boldsymbol{x}$ when the reference epoch is changed, the derivative $\frac{d\boldsymbol{x}}{d\varepsilon}$ is considered. As seen for the state transition matrix, the idea is to obtain a first-order differential equation describing the variation of $\frac{d\boldsymbol{x}}{d\varepsilon}$ as time moves along: its integration will lead to the knowledge of $\frac{d\boldsymbol{x}}{d\varepsilon}$. Taking its time derivative, it follows

$$\frac{d}{d\tau}\left(\frac{d\boldsymbol{x}}{d\varepsilon}\right) = \frac{d}{d\varepsilon}\left(\frac{d\boldsymbol{x}}{d\tau}\right) = \frac{d\boldsymbol{f}\left(\boldsymbol{x}, \tau, \varepsilon\right)}{d\varepsilon} = \frac{\partial \boldsymbol{f}}{\partial \boldsymbol{x}}\frac{d\boldsymbol{x}}{d\varepsilon} + \frac{\partial \boldsymbol{f}}{\partial \varepsilon} = \mathbf{A}\frac{d\boldsymbol{x}}{d\varepsilon} + \frac{\partial \boldsymbol{f}}{\partial \varepsilon} \tag{5.15}$$

If equations of motions in an inertial aligned frame (relative to a central body) are considered, the only epoch-dependent terms in the dynamical system $\boldsymbol{f}$ are the position vectors $\boldsymbol{\rho}_{qj}$ of the massive bodies m_j relative to the central body m_q. So equation (5.15) can be particularized as

$$\frac{d}{d\tau}\left(\frac{d\boldsymbol{x}}{d\varepsilon}\right) = \mathbf{A}\frac{d\boldsymbol{x}}{d\varepsilon} + \sum_{\substack{j=1 \\ j\neq q}}^{N} \frac{\partial \boldsymbol{f}}{\partial \boldsymbol{\rho}_{qj}}\frac{\partial \boldsymbol{\rho}_{qj}}{\partial \varepsilon} = \mathbf{A}\frac{d\boldsymbol{x}}{d\varepsilon} + \sum_{\substack{j=1 \\ j\neq q}}^{N} \frac{\partial \boldsymbol{f}}{\partial \boldsymbol{\rho}_{qj}}\dot{\boldsymbol{\rho}}_{qj} \tag{5.16}$$

being $\dot{\boldsymbol{\rho}}_{qj}$ the velocity of the massive body m_j relative to the central one. In particular, if equation (2.38) is considered, the epoch dependent terms are $\boldsymbol{\rho}_{\oplus\odot}$ and $\boldsymbol{\rho}_{\oplus\mathbb{C}}$ (that appear also in $\boldsymbol{\rho}_{sc\to\odot} = \boldsymbol{\rho}_{\oplus\odot} - \boldsymbol{\rho}$ and $\boldsymbol{\rho}_{sc\to\mathbb{C}} = \boldsymbol{\rho}_{\oplus\mathbb{C}} - \boldsymbol{\rho}$). Equation (5.16) can be rewritten as

$$\frac{d}{d\tau}\left(\frac{d\boldsymbol{x}}{d\varepsilon}\right) = \mathbf{A}\frac{d\boldsymbol{x}}{d\varepsilon} + \frac{\partial \boldsymbol{f}}{\partial \boldsymbol{\rho}_{\oplus\odot}}\dot{\boldsymbol{\rho}}_{\oplus\odot} + \frac{\partial \boldsymbol{f}}{\partial \boldsymbol{\rho}_{\oplus\mathbb{C}}}\dot{\boldsymbol{\rho}}_{\oplus\mathbb{C}} \tag{5.17}$$

The $\mathbf{A}$ matrix has been already derived and it can be found at equations (5.10)-(5.11). $\frac{\partial \boldsymbol{f}}{\partial \boldsymbol{\rho}_{\oplus j}}$ with $j = \odot$ or $\mathbb{C}$ is a 6×3 matrix having the following

structure:

$$\frac{\partial \boldsymbol{f}}{\partial \boldsymbol{\rho}_{\oplus j}} = \left[\begin{array}{ccc} & \mathbf{0}_{3\times 3} & \\ \hline \frac{\partial \ddot{x}}{\partial x_j} & \frac{\partial \ddot{x}}{\partial y_j} & \frac{\partial \ddot{x}}{\partial z_j} \\ \frac{\partial \ddot{y}}{\partial x_j} & \frac{\partial \ddot{y}}{\partial y_j} & \frac{\partial \ddot{y}}{\partial z_j} \\ \frac{\partial \ddot{z}}{\partial x_j} & \frac{\partial \ddot{z}}{\partial y_j} & \frac{\partial \ddot{z}}{\partial z_j} \end{array}\right] \tag{5.18}$$

where (for $j = \odot$ and $\mathbb{C}$)

$$\begin{aligned}
\frac{\partial \ddot{x}}{\partial x_j} &= \pi_j \left(\frac{1}{\rho_{sc\to j}^3} - \frac{3\left(x_j - x\right)^2}{\rho_{sc\to j}^5} - \frac{1}{\rho_{\oplus j}^3} + \frac{3x_j^2}{\rho_{\oplus j}^5} \right) \\
\frac{\partial \ddot{x}}{\partial y_j} &= \pi_j \left(-\frac{3\left(x_j - x\right)\left(y_j - y\right)}{\rho_{sc\to j}^5} + \frac{3x_j y_j}{\rho_{\oplus j}^5} \right) \\
\frac{\partial \ddot{x}}{\partial z_j} &= \pi_j \left(-\frac{3\left(x_j - x\right)\left(z_j - z\right)}{\rho_{sc\to j}^5} + \frac{3x_j z_j}{\rho_{\oplus j}^5} \right) \\
\frac{\partial \ddot{y}}{\partial x_j} &= \pi_j \left(-\frac{3\left(y_j - y\right)\left(x_j - x\right)}{\rho_{sc\to j}^5} + \frac{3y_j x_j}{\rho_{\oplus j}^5} \right) \\
\frac{\partial \ddot{y}}{\partial y_j} &= \pi_j \left(\frac{1}{\rho_{sc\to j}^3} - \frac{3\left(y_j - y\right)^2}{\rho_{sc\to j}^5} - \frac{1}{\rho_{\oplus j}^3} + \frac{3y_j^2}{\rho_{\oplus j}^5} \right) \\
\frac{\partial \ddot{y}}{\partial z_j} &= \pi_j \left(-\frac{3\left(y_j - y\right)\left(z_j - z\right)}{\rho_{sc\to j}^5} + \frac{3y_j z_j}{\rho_{\oplus j}^5} \right) \\
\frac{\partial \ddot{z}}{\partial x_j} &= \pi_j \left(-\frac{3\left(z_j - z\right)\left(x_j - x\right)}{\rho_{sc\to j}^5} + \frac{3z_j x_j}{\rho_{\oplus j}^5} \right) \\
\frac{\partial \ddot{z}}{\partial y_j} &= \pi_j \left(-\frac{3\left(z_j - z\right)\left(y_j - y\right)}{\rho_{sc\to j}^5} + \frac{3z_j y_j}{\rho_{\oplus j}^5} \right) \\
\frac{\partial \ddot{z}}{\partial z_j} &= \pi_j \left(\frac{1}{\rho_{sc\to j}^3} - \frac{3\left(z_j - z\right)^2}{\rho_{sc\to j}^5} - \frac{1}{\rho_{\oplus j}^3} + \frac{3z_j^2}{\rho_{\oplus j}^5} \right)
\end{aligned} \tag{5.19}$$

Integrating numerically to find the evolution of the components of $\frac{d\boldsymbol{x}}{d\varepsilon}$, the initial conditions

$$\frac{d\boldsymbol{x}}{d\varepsilon}\left(\tau_0\right) = \mathbf{0}_{6\times 1} \tag{5.20}$$

shall be considered.

If equations of motion in a non-inertial, Earth-Moon synodic frame are considered (that is, (2.50)), equation (5.15) is still valid, but the term $\frac{\partial \boldsymbol{f}}{\partial \varepsilon}$ becomes very long and complicated to be expressed here (the reader shall

consider that the $\mathbf{R}$ matrix, along with its time derivatives, is epoch dependent). Finite differencing to evaluate $\frac{d\boldsymbol{x}}{d\varepsilon}$ or $\frac{\partial \boldsymbol{f}}{\partial \varepsilon}$ seems the most reasonable solution.

5.2 Towards the Optimization

5.2.1 Newton's Method

The state transition matrix and the derivative of the state with respect to epoch represent the building blocks of gradient-based optimisation methods. Indeed, by exploiting their components, it will be possible to compute the gradient-information. But, before dealing with *nonlinear programming*, it is possible to understand the basic working concepts by considering a preliminary case.

When dealing with trajectory design, it is often be desirable to find the exact values of some variables such that the constraints of the problem are satisfied. This is actually a two-point boundary value problem and it can be solved by using a shooting method based on Newton's algorithm. The variables of the problem can be gathered in the $\boldsymbol{X}$ vector ($n \times 1$ vector)

$$\boldsymbol{X} = \begin{bmatrix} X_1 \\ \vdots \\ X_n \end{bmatrix} \tag{5.21}$$

where the elements of $\boldsymbol{X}$ can be, for example, components of state vectors, times and epochs. The $\boldsymbol{X}$ must satisfy a series of m constraints, that can be grouped in the $\boldsymbol{F}(\boldsymbol{X})$ vector ($m \times 1$ vector)

$$\boldsymbol{F}(\boldsymbol{X}) = \begin{bmatrix} F_1(\boldsymbol{X}) \\ \vdots \\ F_m(\boldsymbol{X}) \end{bmatrix} \tag{5.22}$$

Newton's method allows to find the roots of real-valued functions and it represents a suitable algorithm for the considered problem, allowing to find $\boldsymbol{X}$ such that $\boldsymbol{F}(\boldsymbol{X}) = 0$, given that a solution exists. Imaging that $\boldsymbol{X}^*$ is close to the solution, it is possible to write (by exploiting a Taylor series)

$$\mathbf{0} = \boldsymbol{F}(\boldsymbol{X}) \approx \boldsymbol{F}(\boldsymbol{X}^*) + \frac{\partial \boldsymbol{F}(\boldsymbol{X}^*)}{\partial \boldsymbol{X}} (\boldsymbol{X} - \boldsymbol{X}^*) \tag{5.23}$$

From equation (5.23) it is possible to extract an iterative routine to find the solution of the problem. If $n = m$, the Jacobian of the constraint vector is

squared and invertible and the iterative scheme can be written as

$$\boldsymbol{X}_{j+1} = \boldsymbol{X}_j - \left[\frac{\partial \boldsymbol{F}(\boldsymbol{X}_j)}{\partial \boldsymbol{X}}\right]^{-1} \boldsymbol{F}_j(\boldsymbol{X}) \tag{5.24}$$

If $m < n$, a common choice is to use the following scheme

$$\boldsymbol{X}_{j+1} = \boldsymbol{X}_j - \left(\frac{\partial \boldsymbol{F}(\boldsymbol{X}_j)}{\partial \boldsymbol{X}}\right)^T \left[\left(\frac{\partial \boldsymbol{F}(\boldsymbol{X}_j)}{\partial \boldsymbol{X}}\right)\left(\frac{\partial \boldsymbol{F}(\boldsymbol{X}_j)}{\partial \boldsymbol{X}}\right)^T\right]^{-1} \boldsymbol{F}_j(\boldsymbol{X}) \tag{5.25}$$

Iterations are performed till the output is a solution $\boldsymbol{X}_k$ such that it satisfies the constraints to some acceptable tolerance

$$||\boldsymbol{F}(\boldsymbol{X}_k)|| < tolerance \tag{5.26}$$

Note that, in general, the obtained solution is not necessary optimal.

For the sake of clarity, Newton's method can be summarized with the following steps:

1. Decide the variables $\boldsymbol{X}$ of the problem;
2. Decide the constraints $\boldsymbol{F}(\boldsymbol{X})$ of the problem;
3. Set an initial guess $\boldsymbol{X}_g$;
4. Evaluate the constraints at the current iteration;
5. Evaluate the Jacobian of the constraints at the current iteration;
6. Estimate the new approximation of the solution (by using equation (5.24) or (5.25));
7. Evaluate the constraints and the error by using the new approximation;
8. If the error is less than a decided tolerance, iterations are over; otherwise, return to point 5.

5.2.2 Multiple Shooting

Multiple shooting represents a very effective and useful method for trajectory design. It consists in discretizing the trajectory in n arcs and, then, imposing suitable and desired constraints at the patch points (that is, between the end of an arc and the beginning of the following one). Each arc is characterized by a set of variables, that can be the initial state vector $\boldsymbol{x}_i$, the period of propagation T_i and the reference epoch ε_i. After the propagation of the

initial conditions is performed, for each arc the final state will be denoted as $\boldsymbol{x}_i^t$.

Usually, a requirement for the trajectory is the continuity in position and velocity at the patch points. If only continuity in position is imposed, in general there will be a change (in magnitude and direction) of the velocity vector at the patch points, meaning that a $\Delta \boldsymbol{v}_i$ is introduced. In general, if all the arcs are propagated by using an initial guess of their variables, the result will be a discontinuous trajectory with a mismatch at the patch points, as it can be seen in Figure 5.2. It would be desirable to correct the

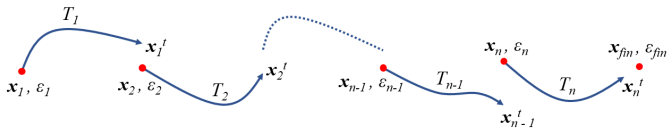

Figure 5.2: Multiple Shooting: discontinuous trajectory

values of the considered variables such that the continuity constraints (in position and velocity) are satisfied within a certain tolerance. The resulting trajectory will be, then, similar to the one depicted in Figure 5.3. This is

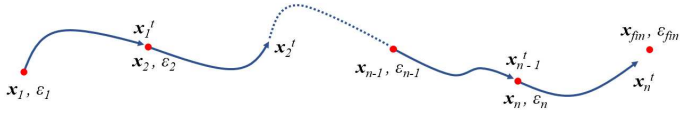

Figure 5.3: Multiple Shooting: continuous trajectory

actually a problem that can be solved by using Newton's method. The free variables of each arc are gathered in a unique $\boldsymbol{X}$ vector and $\boldsymbol{F}(\boldsymbol{X})$ contains

the imposed constraints:

$$\boldsymbol{X} = \begin{bmatrix} \boldsymbol{x}_1 \\ \boldsymbol{x}_2 \\ \vdots \\ \boldsymbol{x}_n \\ \boldsymbol{x}_{fin} \\ \mathrm{T}_1 \\ \mathrm{T}_2 \\ \vdots \\ \mathrm{T}_n \\ \varepsilon_1 \\ \varepsilon_2 \\ \vdots \\ \varepsilon_n \\ \varepsilon_{fin} \end{bmatrix} \qquad \boldsymbol{F}(\boldsymbol{X}) = \begin{bmatrix} \boldsymbol{x}_1^t - \boldsymbol{x}_2 \\ \boldsymbol{x}_2^t - \boldsymbol{x}_3 \\ \vdots \\ \boldsymbol{x}_{n-2}^t - \boldsymbol{x}_{n-1} \\ \boldsymbol{x}_{n-1}^t - \boldsymbol{x}_n \\ \boldsymbol{x}_n^t - \boldsymbol{x}_{fin} \\ \varepsilon_2 - \varepsilon_1 - \mathrm{T}_1 \\ \varepsilon_3 - \varepsilon_2 - \mathrm{T}_2 \\ \vdots \\ \varepsilon_n - \varepsilon_{n-1} - \mathrm{T}_{n-1} \\ \varepsilon_{fin} - \varepsilon_n - \mathrm{T}_n \end{bmatrix} = \mathbf{0} \tag{5.27}$$

where $\boldsymbol{x}_{fin}$ and ε_{fin} represent, respectively, the state vector and the epoch related to the final point of the trajectory ($\boldsymbol{x}_{fin}$ and ε_{fin} can be known quantities, in that case they must be removed from the variable vector $\boldsymbol{X}$). Note that the constraint vector also contains the conditions

$$\varepsilon_{i+1} - \varepsilon_i = \mathrm{T}_i \tag{5.28}$$

stating that the temporal gap between two consecutive patch points is exactly the propagation period of the arc connecting them.

In order to exploit Newton's algorithm, information on the Jacobian of the constraint vector must be known. Derivatives of the final state vector $\boldsymbol{x}_i^t$ with respect to the initial state $\boldsymbol{x}_i$, time period T_i and reference epoch ε_i can be easily found by using considerations expressed in Section 5.1. Note that, of course, the derivative of a variable with respect to itself is equal to the identity; on the contrary, the derivative with respect to another variable is null. Thus, the Jacobian will result in a sparse, block matrix.

5.2.3 Inequality Constraints

Sometimes it is possible to come across some inequality constraints. The generic inequality constraint $F_i(\boldsymbol{X})$ can be expressed as

$$F_{i,LB} \leqslant F_i(\boldsymbol{X}) \leqslant F_{i,UB} \tag{5.29}$$

where $F_{i,LB}$ and $F_{i,UB}$ are the lower and upper bounds for the constraint, respectively. In order to successfully include it within the context of Newton's

method, the inequality must be reformulated as an equality. An inequality constraint with upper boundary

$$F_i(\boldsymbol{X}) \leqslant F_{i,UB} \tag{5.30}$$

can be rewritten as

$$F_i(\boldsymbol{X}) - F_{i,UB} \leqslant 0 \tag{5.31}$$

By introducing a slack variable $\beta_{i,UB}$, it is possible to reformulate equation (5.31) as an equality:

$$F_i(\boldsymbol{X}) - F_{i,UB} + \beta_{i,UB}^2 = 0 \tag{5.32}$$

Similarly, an inequality constraint with lower boundary

$$F_{i,LB} \leqslant F_i(\boldsymbol{X}) \tag{5.33}$$

can be expressed as an equality by exploiting another slack variable $\beta_{i,LB}$:

$$F_i(\boldsymbol{X}) - F_{i,LB} - \beta_{i,LB}^2 = 0 \tag{5.34}$$

When using Newton's method, slack variables β_i must be included in the vector of free variables $\boldsymbol{X}$. Furthermore, when computing the Jacobian of the constraint vector, the derivative of equation (5.32) (or (5.34)) with respect to the slack variable β_i will give rise to a term $2\beta_i$ (or $-2\beta_i$).

5.3 Computing Periodic Solutions

Within the context of the CRTBP and the N-body problem, it is possible to find some particular kinds of periodic solutions. Their computation can be performed considering a peculiar case of the multiple-shooting method, where only one arc is taken in consideration (so, a single-shooting method is obtained). Both for the CRTBP (by definition) and the N-body problem, the description of these orbits has to be performed in the synodic frame. Sometimes the N-body environment can reveal challenging convergence issues. This is why periodic orbit computation is, at first, performed in the CRTBP framework: the obtained solution will be refined in a real ephemeris model.

5.3.1 Symmetric Periodic Solutions in CRTBP

For many (not all) periodic trajectories in the CRTBP it is possible to exploit their inherent symmetry across the xz-plane. This means that the

computation can be limited to find half of the periodic trajectory, where departure and arrival points are constrained to lay on the xz-plane, with velocities perpendicular to it. In view of the above, the generic symmetric periodic solution in the CRTBP is characterized by an initial state vector of the following form:

$$\boldsymbol{x}_0 = \begin{bmatrix} x_0 \\ 0 \\ z_0 \\ 0 \\ \dot{y}_0 \\ 0 \end{bmatrix} \tag{5.35}$$

Setting up a single-shooting problem, the free variables will consist in the non-null components of $\boldsymbol{x}_0$ and the half orbit period T, so

$$\boldsymbol{X} = \begin{bmatrix} x_0 \\ z_0 \\ \dot{y}_0 \\ \mathrm{T} \end{bmatrix} \tag{5.36}$$

In order to guarantee periodicity, symmetry is imposed: a perpendicular arrival at the xz-plane is written as

$$\boldsymbol{F}(\boldsymbol{X}) = \begin{bmatrix} y^t \\ \dot{x}^t \\ \dot{z}^t \end{bmatrix} = 0 \tag{5.37}$$

The derivative of the constraint vector with respect to the free variables leads to the following Jacobian:

$$\frac{\partial \boldsymbol{F}(\boldsymbol{x})}{\partial \boldsymbol{x}} = \begin{bmatrix} \Phi_{21} & \Phi_{23} & \Phi_{25} & \dot{y}^t \\ \Phi_{41} & \Phi_{43} & \Phi_{45} & \ddot{x}^t \\ \Phi_{61} & \Phi_{63} & \Phi_{65} & \ddot{z}^t \end{bmatrix} \tag{5.38}$$

If one component of the initial state vector is prescribed, it is possible to add an appropriate element in the constraint vector. For example, if the x_0 component of starting point is known, an additional term

$$x_0 - x_{0,d} = 0 \tag{5.39}$$

(where $x_{0,d}$ is a constant that specifies the desired initial value for x_0) is included in $\boldsymbol{F}(\boldsymbol{x})$. In order to avoid degenerate orbits, another useful consideration can be setting the half period T larger than a minimum value T_{min}, in that case a term

$$\mathrm{T} - \mathrm{T}_{min} - \beta^2 = 0 \tag{5.40}$$

is added to the constraint vector (and β is included among the free variables). Newton's algorithm is then exploited to find the values of the variables that identify the periodic solution.

Once the first orbit is obtained, the entire family of periodic solutions can be computed by using pseudo-arclength continuation method (see Subsection 5.3.3). In this way, Halo orbits families (Northern and Southern) in the vicinity of collinear points can be found (see Figure 5.4). Continuing to

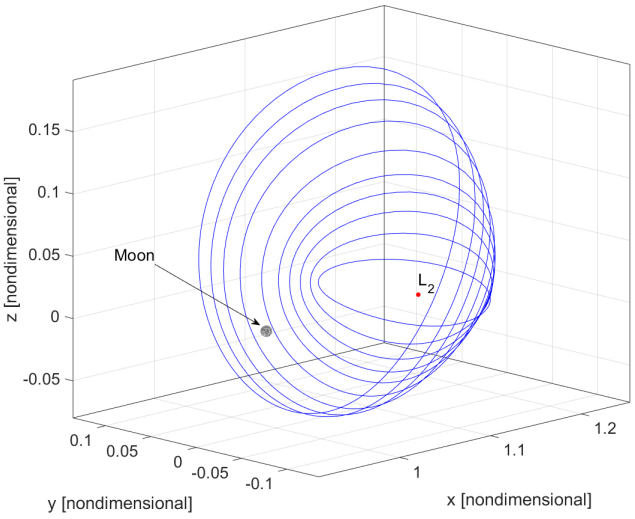

Figure 5.4: L_2 Halo Family (Northern)

propagate the L_1 and L_2 Halo families towards the bifurcation point (that is, towards the Moon), computed periodic solutions will be referred as Near Rectilinear Halo Orbits (NROs). In Figure 5.5 NRO families near L_2 are depicted. In the case that symmetric periodic solutions are required to lay on the xy-plane, initial component z_0 can be removed from the variable vector $\boldsymbol{X}$ (the column related to its derivative is removed from the Jacobian as a consequence). Orbits of such a kind generates planar families. Lyapunov orbits around the collinear points can be obtained. Another family of planar periodic trajectories is represented by Distant Retrograde Orbits (DROs), depicted in Figure 5.6. Distant Retrograde Orbits exist thanks to the intrinsic rotation of the synodic frame and they are characterized by a remarkable stability.

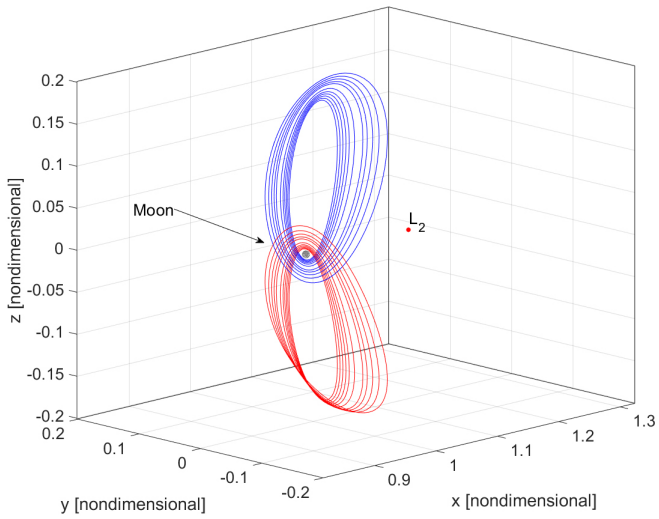

Figure 5.5: L_2 Near Rectilinear Halo Orbits Families (Northern and Southern)

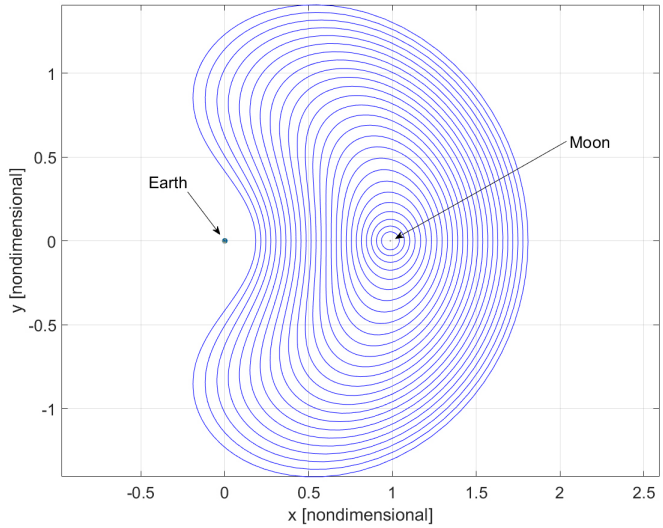

Figure 5.6: Distant Retrograde Orbits

5.3.2 Periodic Solution in the N-body framework

Unlike the CRTBP, the N-body problem is not characterized by intrinsic symmetry. Besides, the problem is epoch dependent, meaning that the same initial conditions usually result in different trajectories if propagated at distinct epochs. This implies that particular initial conditions for a periodic solutions in the N-body framework will be valid for a specific epoch: their

propagation at a different epoch will be very likely to produce an open trajectory.

Periodic solutions computed in the CRTBP can be used as a first guess for the computation of those in the N-body problem. The generic periodic solution can be found setting up a single (or a multiple) shooting problem where the free variables consist in the components of the initial state vector $\boldsymbol{x}$ and the (entire) orbit period T at a specific reference epoch ε_0

$$\boldsymbol{X} = \begin{bmatrix} \boldsymbol{x} \\ \mathrm{T} \end{bmatrix} \tag{5.41}$$

The constraint vector has to impose the periodicity condition, that is the final state of the trajectory must coincide with the initial one:

$$\boldsymbol{F}(\boldsymbol{x}) = \left[\boldsymbol{x}^t - \boldsymbol{x} \right] = 0 \tag{5.42}$$

In the considered case the Jacobian of the constraint vector is a 6×7 matrix with the following form:

$$\frac{\partial \boldsymbol{F}(\boldsymbol{X})}{\partial \boldsymbol{x}} = \begin{bmatrix} & & \\ & [\boldsymbol{\Phi} - \boldsymbol{I}_{6\times 6}] & \dot{\boldsymbol{x}} \\ & & \end{bmatrix} \tag{5.43}$$

As already noted, if one component of the initial state vector is known, it is possible to add an appropriate element in the constraint vector. For example, if the starting point is constrained to lay on the xz-plane, an additional term $y - y_d = 0$ (where y_d is a constant that specifies the desired initial value for y, so in this case $y_d = 0$) is included in $\boldsymbol{F}(\boldsymbol{x})$. Similarly, slack variables and connected constraints can be added, if necessary.

The outlined procedure has been used to compute periodic orbits in a real ephemeris environment. Figure 5.7 represents a Near Rectilinear Halo Orbit characterized by an aposelene $r_a = 78000\ km$ (reference epoch set on 13 February 2026). Figure 5.8 depicts a Distant Retrograde Orbit in a real ephemeris model (reference epoch set on 15 October 2026). The orbit is, then, propagated over one year period: even under the effects of several gravitational fields, the Distant Retrograde Orbit results effectively stable.

5.3.3 Pseudo-Arclength Continuation

Once a converged solution is available, it is possible to find the entire family of orbits by exploiting a continuation method. In contrast to other simpler continuation methods (for example, the single-parameter continuation

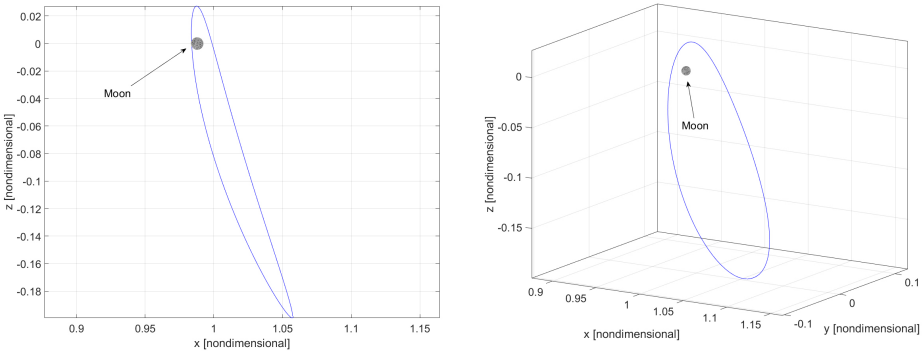

(a) NRO - Projection on xz-plane *(b) NRO*

Figure 5.7: NRO in N-body framework (Epoch = 13 Feb 2026)

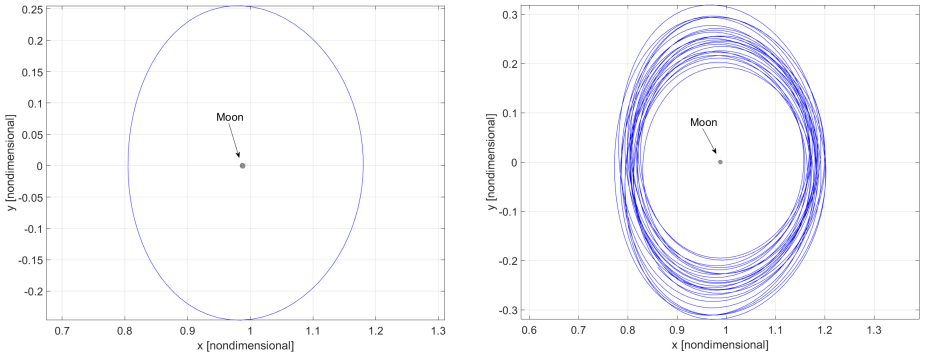

(a) DRO *(b) DRO (propagated for 1 year)*

Figure 5.8: DRO in N-body framework (Epoch = 15 Oct 2026)

method) that search for the next member of the family moving along a prescribed direction (so, evolution of the family has to be known *a priori* for a successful application of the method), pseudo-arclength continuation schemes modify initial conditions taking a step Δs in the direction tangent to the family. Free variables of last converged solution are denoted as $\boldsymbol{X}_i^*$ and they satisfy the constraint vector $\boldsymbol{F}\left(\boldsymbol{X}_i^*\right) = 0$. The tangential direction $\Delta \boldsymbol{X}_i^*$ is computed as the null space of the Jacobian of the constraint vector (evaluated at $\boldsymbol{X}_i^*$)

$$\Delta \boldsymbol{X}_i^* = \text{Null}\left(\frac{\partial \boldsymbol{F}\left(\boldsymbol{X}_i^*\right)}{\partial \boldsymbol{X}}\right) \tag{5.44}$$

In order to move towards the next orbit of the family (identified by free variables $\boldsymbol{X}_{i+1}$), a step along the tangential direction must be included in the constraint vector. The augmented constraint vector, now denoted as

$\boldsymbol{G}(\boldsymbol{X})$, can be written as

$$\boldsymbol{G}(\boldsymbol{X}_{i+1}) = \begin{bmatrix} \boldsymbol{F}(\boldsymbol{X}_{i+1}) \\ (\boldsymbol{X}_{i+1} - \boldsymbol{X}_i^*)^T \Delta \boldsymbol{X}_i^* - \Delta s \end{bmatrix} = 0 \tag{5.45}$$

The Jacobian of the augmented constraint vector yields

$$\frac{\partial \boldsymbol{G}(\boldsymbol{X}_{i+1})}{\partial \boldsymbol{X}} = \begin{bmatrix} \frac{\partial \boldsymbol{F}(\boldsymbol{X}_{i+1})}{\partial \boldsymbol{X}} \\ \Delta \boldsymbol{X}_i^{*T} \end{bmatrix} = 0 \tag{5.46}$$

By exploiting Newton's method, it is possible to iterate and converge towards the solution $\boldsymbol{X}_{i+1}^*$ (that identifies the $(i+1)^{th}$ orbit of the family). The generic iteration for Newton's method can be written as

$$\boldsymbol{X}_{k+1} = \boldsymbol{X}_k - \left(\frac{\partial \boldsymbol{G}(\boldsymbol{X}_k)}{\partial \boldsymbol{X}} \right)^{-1} \boldsymbol{G}(\boldsymbol{X}_k) \tag{5.47}$$

The great advantage of pseudo-arclength continuation method is that the information to compute next member of the family is intrinsically obtained, without the need of its *a priori* knowledge.

5.3.4 Stability of CRTBP Periodic Solutions

In CRTBP, that is an autonomous problem, it is possible to exploit time-invariant system theory to study the stability of periodic orbits. Once the initial condition $\mathbf{x}_0^*$ of a periodic solution is obtained through a correction scheme, it is possible to obtain the *monodromy matrix* $\mathbf{M}$ by integrating the variational equation (5.8) over one period of the orbit. Indeed, by definition, the monodromy matrix is the state transition matrix after one period T

$$\mathbf{M} = \boldsymbol{\Phi}(\tau_0 + \mathrm{T}, \tau_0) \tag{5.48}$$

By studying the eigenvalues λ_i of the monodromy matrix, it is possible to obtain information on the stability of the considered periodic solution. For periodic orbits in CRTBP, eigenvalues of the monodromy matrix occur in reciprocal pair. Depending to the magnitude of the eigenvalues, it is possible to note that:

- If $|\lambda_i| < 1$, an asymptotically stable eigenstructure is associated to the orbit;
- If $|\lambda_i| \leqslant 1$, a marginally stable eigenstructure is associated to the orbit;
- If $|\lambda_i| > 1$, an unstable eigenstructure is associated to the orbit.

For orbits around collinear points, one asymptotically stable eigenstructure and one unstable eigenstructure are always observed, producing a non-stable (saddle) behaviour for the orbits. These one-dimensional stable and unstable eigenstructures are also called *manifolds* and they can be obtained propagating the corrected initial condition $\mathbf{x}_0^*$ of the orbit perturbed in the direction of the eigenvector $\boldsymbol{Y}^s(\mathbf{x}_0^*)$ (or $\boldsymbol{Y}^u(\mathbf{x}_0^*)$) associated to the stable (or unstable) eigenvalue λ_i

$$\boldsymbol{X}^s(\mathbf{x}_0^*) = \mathbf{x}_0^* \pm \varepsilon \boldsymbol{Y}^s(\mathbf{x}_0^*) \tag{5.49}$$

$$\boldsymbol{X}^u(\mathbf{x}_0^*) = \mathbf{x}_0^* \pm \varepsilon \boldsymbol{Y}^u(\mathbf{x}_0^*) \tag{5.50}$$

where $\boldsymbol{X}^s(\mathbf{x}_0^*)$ represents the initial condition of the stable manifold arriving to the orbit (and it has to be propagated backward), while $\boldsymbol{X}^u(\mathbf{x}_0^*)$ represents the initial condition of the unstable manifold departing from the orbit (and it has to be propagated forward). In equations (5.49) and (5.50), ε is the magnitude of the perturbation.

It is also possible to find the initial conditions for stable and unstable manifolds related to any point $\mathbf{x}(t)$ of the periodic solution, different from the corrected state $\mathbf{x}_0^*$ at which the monodromy matrix has been computed. In order to do this operation, it is sufficient to transport the eigenvectors by multiplying them by the state transition matrix from τ_0 to τ, that is $\boldsymbol{\Phi}(\tau, \tau_0, \mathbf{x}_0^*)$. So, the initial conditions for the stable and unstable manifolds related to the generic state $\mathbf{x}(t)$ of the orbit are given by

$$\boldsymbol{X}^s(\mathbf{x}(t)) = \mathbf{x}(t) \pm \varepsilon \frac{\boldsymbol{\Phi}(\tau, \tau_0, \mathbf{x}_0^*)\, \boldsymbol{Y}^s(\mathbf{x}_0^*)}{||\boldsymbol{\Phi}(\tau, \tau_0, \mathbf{x}_0^*)\, \boldsymbol{Y}^s(\mathbf{x}_0^*)\,||} \tag{5.51}$$

$$\boldsymbol{X}^u(\mathbf{x}(t)) = \mathbf{x}(t) \pm \varepsilon \frac{\boldsymbol{\Phi}(\tau, \tau_0, \mathbf{x}_0^*)\, \boldsymbol{Y}^u(\mathbf{x}_0^*)}{||\boldsymbol{\Phi}(\tau, \tau_0, \mathbf{x}_0^*)\, \boldsymbol{Y}^u(\mathbf{x}_0^*)\,||} \tag{5.52}$$

Manifolds are really effective in trajectory design, since they allows to obtain low-cost transfers to leave or to reach the orbit.

5.3.5 Lagrangian Coherent Structures

The theory of time-invariant systems is non applicable to the N-body problem (that is non-autonomous) and the illustrated procedure for the computation of invariant manifolds does not hold anymore. Lagrangian Coherent Structures (LCS) can be seen as the extension of invariant manifolds for the N-body problem. It is possible to distinguish attracting (*attractors*) and repulsing (*repulsors*) LCS, being the structures that attract or repulse the neighbouring portions of the flow the most. Heuristically, it is possible to identify the LCS as the *ridges* of the flow, being the structure through which

the flow flux is null. One common way to identify LCS is to exploit the *Finite-time Lyapunov exponent* (FTLE).

Finite-Time Lyapunov Exponent

FTLE can be used as a measure to identify LCS ([48]) and, in particular, local high values of FTLE indicate LCS. Starting from a particular initial condition, FTLE measures how much the neighbouring trajectories are attracted or repulsed over a fixed propagation time. Denoting as $\mathbf{\Phi}(\tau, \tau_0, \mathbf{x}_0)$ the state transition matrix computed evolving the initial condition $\mathbf{x}_0$ from time τ_0 to τ, FTLE is computed as the largest normalized eigenvalue of $\sqrt{\mathbf{\Phi}^T(\tau, \tau_0, \mathbf{x}_0)\,\mathbf{\Phi}(\tau, \tau_0, \mathbf{x}_0)}$, so, more formally, it follows

$$FLTE = \frac{1}{\tau - \tau_0}\tilde{\lambda}_{max}\left(\sqrt{\mathbf{\Phi}^T(\tau, \tau_0, \mathbf{x}_0)\,\mathbf{\Phi}(\tau, \tau_0, \mathbf{x}_0)}\right) \tag{5.53}$$

where the operator $\tilde{\lambda}_{max}()$ is used to extract the largest eigenvalue of the argument. This eigenvalue is then normalized by using the propagation period $\tau - \tau_0$. Given a prescribed initial conditions $\mathbf{x}_0$ (with n_s components), it is possible to map (in terms of FLTE) the neighbouring states of the design space by considering a n_s-dimensional mesh centred in $\mathbf{x}_0$. For attracting LCS, propagations must be carried out backward.

Chapter 6

Trajectory Optimization

In this chapter the bases of trajectory optimization are presented. The final goal is to apply them to a *low-thrust* trajectory design and optimization. Low-thrust propulsion systems are very efficient but produce a small amount of thrust. As a consequence, electric propulsion systems have to operate for an extended period of time, implying a more complex strategy for trajectory optimization. One way to optimize low-thrust trajectories consists in using *indirect* methods, based on calculus of variations. The main complication of these methods is that they are very sensible to initial conditions and a good guess is required solved. The presence of gravity-assists enhances the sensitivity and the difficulty. Differently, strategies that are used within the context of this work are *direct* methods and they are solved using Nonlinear Programming (NLP). Once the NLP framework is presented, a low-medium fidelity Sims-Flanagan based method is explained. Then, a direct transcription, shooting method (based on Chebyshev polynomials) is presented.

6.1 Nonlinear Programming (NLP)

6.1.1 Introduction

Multiple-shooting techniques exploit Newton's method in order to correct a set of free variables such that some imposed constraints are verified. When dealing with trajectory design, it is usually desirable to achieve this convergence while optimizing a scalar objective function. In practice, the problem can be related to the minimisation of the Δv or the time-of-flight. The well-known Newton's algorithm will help in understanding the new numerical challenge and it will be, once again, at the base for its solution.

A Nonlinear Programming problem consists in finding the n-dimensional vector $\mathbf{x}$ such that it minimizes the scalar function

$$F(\mathbf{x}) \tag{6.1}$$

and subject to the m constraints

$$\mathbf{c}_L \leqslant \mathbf{c}(\mathbf{x}) \leqslant \mathbf{c}_U \tag{6.2}$$

and bounds

$$\mathbf{x}_L \leqslant \mathbf{x} \leqslant \mathbf{x}_U \tag{6.3}$$

Equality constraints can be imposed by setting $c_{i,L} = c_{i,U}$.

6.1.2 Equality-Constrained Optimization

The first case consists in finding the value of $\mathbf{x}$ while optimizing of the objective function $F(\mathbf{x})$ and satisfying a set of equality constraints $\mathbf{c}(\mathbf{x}) = 0$. The variable vector $\mathbf{x}$ contains n elements, whereas the constraint vector $\mathbf{c}(\mathbf{x})$ has m components (with $m \leqslant n$). In order to move towards the solution, the approach envisages the definition of the *Lagrangian* $L(\mathbf{x}, \boldsymbol{\lambda})$

$$L(\mathbf{x}, \boldsymbol{\lambda}) = F(\mathbf{x}) - \boldsymbol{\lambda}^T \mathbf{c}(\mathbf{x}) = F(\mathbf{x}) - \sum_{i=1}^{m} \lambda_i c_i(\mathbf{x}) \tag{6.4}$$

where $\boldsymbol{\lambda}$ is the $(m \times 1)$ vector of *Lagrangian multipliers*. The necessary condition for $(\mathbf{x}^*, \boldsymbol{\lambda}^*)$ to be an optimum point is that the gradient of the Lagrangian (both with respect to $\mathbf{x}$ and to $\boldsymbol{\lambda}$) is null:

$$\nabla L(\mathbf{x}^*, \boldsymbol{\lambda}^*) = \begin{bmatrix} \nabla_x L(\mathbf{x}^*, \boldsymbol{\lambda}^*) \\ \nabla_\lambda L(\mathbf{x}^*, \boldsymbol{\lambda}^*) \end{bmatrix} = \mathbf{0} \tag{6.5}$$

The gradient of the Lagrangian with respect to $\mathbf{x}$ yields

$$\nabla_x L(\mathbf{x}, \boldsymbol{\lambda}) = \mathbf{g} - \mathbf{G}^T \boldsymbol{\lambda} \tag{6.6}$$

where $\mathbf{g}(\mathbf{x}) = \nabla_x F(\mathbf{x})$ is the gradient of the objective function and $\mathbf{G}(\mathbf{x}) = \nabla_x \mathbf{c}(\mathbf{x})$ is the Jacobian of the constraint vector. The gradient of the Lagrangian with respect to $\boldsymbol{\lambda}$ leads to

$$\nabla_\lambda L(\mathbf{x}, \boldsymbol{\lambda}) = -\mathbf{c} \tag{6.7}$$

Assuming that $(\mathbf{x}_0, \boldsymbol{\lambda}_0)$ is a guess close to the solution, it is possible to consider a Taylor series expansion of equations 6.6 and 6.7, yielding

$$\mathbf{g} - \mathbf{G}^T \boldsymbol{\lambda} + \mathbf{H}_L (\mathbf{x} - \mathbf{x}_0) - \mathbf{G}^T (\boldsymbol{\lambda} - \boldsymbol{\lambda}_0) = \mathbf{0} \tag{6.8}$$

$$-\mathbf{c} - \mathbf{G}(\mathbf{x} - \mathbf{x}_0) = \mathbf{0} \tag{6.9}$$

where $\mathbf{H}_L$ is the Hessian of the Lagrangian

$$\mathbf{H}_L = \nabla^2_{xx} L(\mathbf{x}, \boldsymbol{\lambda}) = \nabla^2_{xx} F - \sum_{i+1}^{m} \lambda_i \nabla^2_{xx} c_i \tag{6.10}$$

Rewriting the linear system made up by equations 6.8 and 6.9 as

$$\begin{bmatrix} \mathbf{H}_L & \mathbf{G}^T \\ \mathbf{G} & \mathbf{0} \end{bmatrix} \begin{bmatrix} \mathbf{p} \\ -\boldsymbol{\lambda} \end{bmatrix} = \begin{bmatrix} -\mathbf{g} \\ -\mathbf{c} \end{bmatrix} \tag{6.11}$$

where $\mathbf{p} = \mathbf{x} - \mathbf{x}_0$, it is possible to apply Newton's method to find its solution, that is the value of the $(n+m)$-dimensional vector $(\mathbf{x}^*, \boldsymbol{\lambda}^*)$. The system 6.11 is called *Karush-Kuhn-Tucker* (KKT) system and it expresses *necessary conditions* for $(\mathbf{x}^*, \boldsymbol{\lambda}^*)$ to be an optimum point of the nonlinear programming problem.

6.1.3 Inequality Constraints

The general case envisages that inequality constraints are imposed as well. So the problem consists now in finding the n-dimensional vector $\mathbf{x}$ such that it minimizes the scalar function $F(\mathbf{x})$ and satisfies the m inequalities constraints

$$\mathbf{c}(\mathbf{x}) \geqslant \mathbf{0} \tag{6.12}$$

In this case, it can be that $m \geqslant n$. Imagining that the solution $\mathbf{x}^*$ is available, the constraints can be divided in two classes:

1. Constraints that are strictly verified, that is

   $$c_i(\mathbf{x}^*) > 0 \tag{6.13}$$

   are called *inactive*;

2. Constraints that are verified as equalities, that is

   $$c_i(\mathbf{x}^*) = 0 \tag{6.14}$$

   are called *active*.

If the set of *active* constraints (also called *active set*) is known, it is possible to ignore the remaining constraints and to solve the problem by using the strategy for equality-constrained optimization. Complex algorithms are used to determine the active set. A common implementation is the *sequential quadratic programming* (SQP) approach, that can be found in many packages, including MATLAB® and SNOPT. The basic idea behind these schemes is to solve a sequence of optimization sub-problems. Indeed, at each iterate $\mathbf{x}$, a quadratic programming sub-problem is solved in order to find the search direction $\mathbf{p}$, allowing to define the next iterate $\mathbf{x}_{k+1}$.

6.2 Sims-Flanagan Transcription Method

Sims-Flanagan algorithm represents a direct method that can be used for a preliminary design of low-thrust trajectories ([55], [49], [15], [50] and [60]), also in presence of gravity-assists. It is possible to refer to it as a *transcription* method, since it envisages a discretization of the optimal control problem.

6.2.1 Trajectory Structure

Figure 6.1 represents a diagram explaining how a space *mission* can be structured, from the trajectory hierarchy point of view. First of all, a mission can

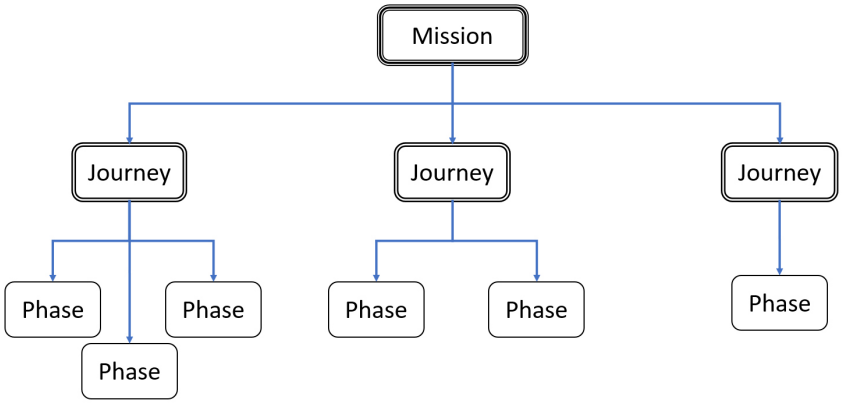

Figure 6.1: Trajectory Structure Diagram

be seen a set of journeys, each identifying an extended trajectory related to the main events (namely, *arrival* and/or *departure*) at the target bodies. For example, an asteroid sample return mission would be composed of two journeys: the first leaving the Earth and *arriving* to the asteroid, the second *departing* from the asteroid and coming back to the Earth. Usually, two consecutive journeys are separated by a certain period of time, during which some mission operations are carried out. Each journey can be represented by a complex trajectory and this is the reason why journeys are studied independently. In turn, a journey is identified by *control nodes*, usually associated with planets or small bodies. So, for each journey, it is possible to identify the following control nodes:

- *Departure* control node, where the journey starts;
- *Arrival* control node, where the journey ends;

- *Intermediate* control nodes, associated with bodies where temporary and relevant events occur (usually, gravity-assists and rendezvous, if present).

Two consecutive control nodes specify a trajectory *phase*, which can be split into two legs: a *forward* leg and a *backward* one. Indeed, in a *phase*, the trajectory is propagated *forward* from the earlier control node and *backward* from the later control node. Two different propagations are preferred in order to reduce the sensitivity to initial conditions. As a matter of fact, a single forward branch could be characterized by propagation errors that grow during time, yielding a more difficult convergence. Final points (denoted as *match points*) of forward and backward legs will have to converge to the same value, in order to guarantee continuity in position, within a certain tolerance. Looking more into the detail, Figure 6.2 depicts how a trajectory phase is structured. A trajectory phase is made up of n segments: the

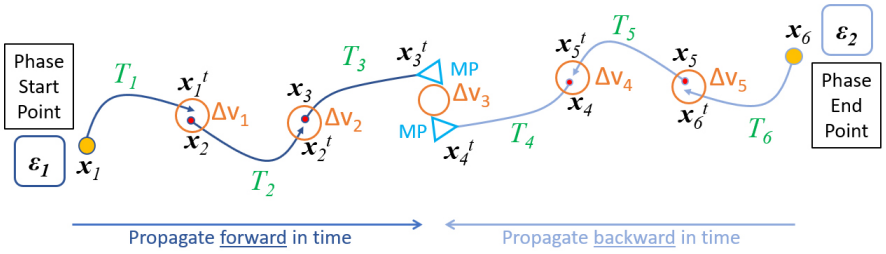

Figure 6.2: Phase Between Two Control Node (n = 6)

first $n/2$ segments have to be propagated forward in time (building up the forward leg), while the remaining $n/2$ segments are propagated backward in time (building up the backward leg). Each segment is specified by initial conditions $\boldsymbol{x}_i$ and is propagated over a period T_i, being the periods positive in the forward leg and negative in the backward one. The final state of the segment is denoted as $\boldsymbol{x}_i^t$. The reference epoch at the start control node is denoted as ε_k, while the one at the end control node will be ε_{k+1}. It is important to ensure the continuity in position between the segments, but in general there will be a velocity discontinuity (in magnitude and direction). As a matter of fact, low-thrust is modelled as a series of impulses, whose magnitude is limited by the amount Δv_i that can be accumulated during the propagation period. Figure 6.3 illustrates a journey made up of two trajectories phases (with a gravity-assist between them).

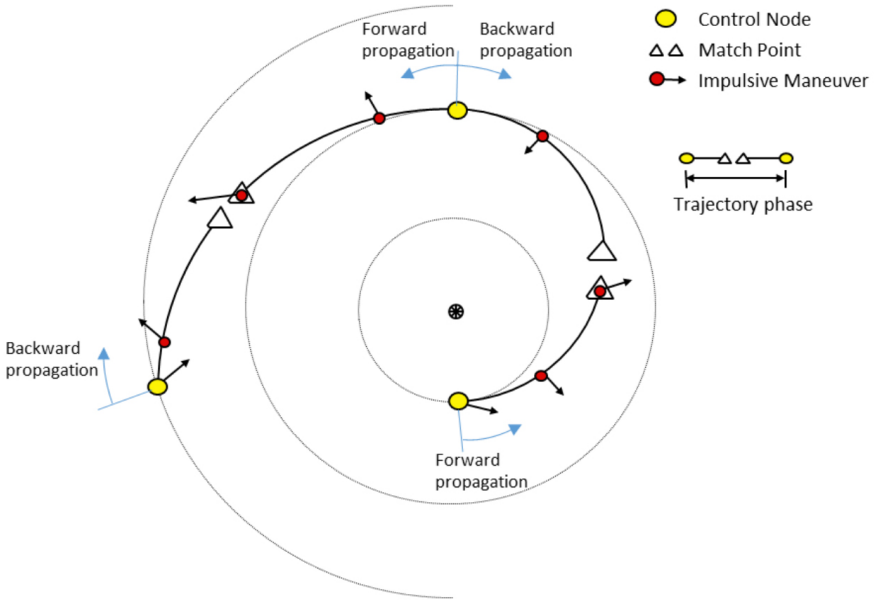

Figure 6.3: Sims-Flanagan Transcription Method: Journey

6.2.2 Variables

Variables are defined for each journey, containing one or multiple phases depending whether some gravity-assists are included. Juxtaposing the segments of all the phases in the journey, the first set of variables is given by the initial conditions $\boldsymbol{x}_i$ of each segment, starting from the departure control node to the arrival one. So, the generic vector $\boldsymbol{x}_i$ contains the position and velocity components of the i-th segment initial state vector. In presence of an intermediate control node (joining two phases), two vectors of initial conditions are specified: the first one will originate the backward leg of the previous phases, while the second one is related to the forward leg of the following leg. The second set of variables is given by the propagation periods T_i of each segment. Finally, a variable for the reference epochs ε_k is associated to each control node. In general, in presence of multiple trajectory phases, there is no guarantee that all the phases contain an equal number of segments (this is a decision for the programmer). Assuming that a considered journey consists of M trajectory phases (so, it is possible to identify $M+1$ control nodes) with a total number N of segments, the variable vector for

the NLP problem is written as

$$\mathbf{x} = \begin{bmatrix} \boldsymbol{x}_1 \\ \boldsymbol{x}_2 \\ \vdots \\ \boldsymbol{x}_{N-1} \\ \boldsymbol{x}_N \\ \mathrm{T}_1 \\ \mathrm{T}_2 \\ \vdots \\ \mathrm{T}_{N-1} \\ \mathrm{T}_N \\ \varepsilon_1 \\ \varepsilon_2 \\ \vdots \\ \varepsilon_M \\ \varepsilon_{M+1} \end{bmatrix} \tag{6.15}$$

In general, then it is possible to include all the *slack* variables β_i arising from the presence of inequality constraints (see Subsection 5.2.3). Although SQP algorithms can deal with inequality constraints and the conversion from inequality to equality constraints is not necessarily needed, the inclusion of slack variables has been used successfully.

6.2.3 Objective Function

An *objective function* (also called *cost function* and denoted as J) must be provided to the NLP solver. Within the context of the Sims-Flanagan transcription method, the objective function J that has to be minimized is the sum of all the Δv_i along the trajectory. Indeed, it is important to recall that the effect of the low thrust is, here, modelled as a series of small impulses, each occurring at the intersection between two consecutive segments. So, for each journey of the trajectory, it is possible to define the cost function as follows

$$J = \sum_{i=1}^{N} \Delta v_i \qquad \text{for } i = 1, \ldots, N \tag{6.16}$$

Note that the generic Δv_i can be expressed as

$$\Delta v_i = \begin{cases} ||\boldsymbol{x}^t_{\boldsymbol{v},i} - \boldsymbol{x}_{\boldsymbol{v},i+1}|| & \text{for Forward Segments} \\ ||\boldsymbol{x}^t_{\boldsymbol{v},i} - \boldsymbol{x}^t_{\boldsymbol{v},i+1}|| & \text{for Match Points} \\ ||\boldsymbol{x}_{\boldsymbol{v},i} - \boldsymbol{x}^t_{\boldsymbol{v},i+1}|| & \text{for Backward Segments} \end{cases} \tag{6.17}$$

In general, the last element of the sum in equation (6.16) (for $i = N$) is present if a last impulse is required to match a target velocity (for example, to match an asteroid velocity). If the final state of the journey is constrained to be equal to a prescribed state vector (as it can be the case in which the final state of the journey must be exactly equal to a NRO or DRO state), the term Δv_i, for $i = N$, can be omitted (if present, it will turn out to be null).

6.2.4 Constraints and Derivatives

In the spirit of multiple-shooting algorithms, it is important to understand the most common constraints that will build up the constraint vector $\mathbf{c}$ for the NLP problem. Also their derivatives with respect to the problem variables are fundamental, since they build up the Jacobian that will be supplied to the optimization solver. Since, depending on the case, it is necessary to constrain the initial (and final) state vectors of the segments with respect to position or velocity, it is useful to consider the following partition:

$$\boldsymbol{x}_i = \left[\begin{array}{c} x_i \\ y_i \\ z_i \\ \hline \dot{x}_i \\ \dot{y}_i \\ \dot{z}_i \end{array}\right] = \left[\begin{array}{c} \boldsymbol{x}_{\boldsymbol{r},i} \\ \hline \boldsymbol{x}_{\boldsymbol{v},i} \end{array}\right] \tag{6.18}$$

If the final state of the segments is considered, a "t" superscript is added.

Constraints on Position

One fundamental requirement for the trajectory journey is represented by the continuity in position. At a phase level, this condition is written by imposing the continuity in position between all the segments. The continuity between segments "i" and "$i + 1$" is written as

$$\mathbf{c}_i(\mathbf{x}) = \begin{cases} \boldsymbol{x}^t_{\boldsymbol{r},i} - \boldsymbol{x}_{\boldsymbol{r},i+1} = \mathbf{0} & \text{for Forward Segments} \\ \boldsymbol{x}^t_{\boldsymbol{r},i} - \boldsymbol{x}^t_{\boldsymbol{r},i+1} = \mathbf{0} & \text{for Match Points} \\ \boldsymbol{x}_{\boldsymbol{r},i} - \boldsymbol{x}^t_{\boldsymbol{r},i+1} = \mathbf{0} & \text{for Backward Segments} \end{cases} \tag{6.19}$$

In general, it is important to set some conditions on the departure and arrival control point of the journey

$$\mathbf{c}_i(\mathbf{x}) = \begin{cases} \boldsymbol{x}_{\boldsymbol{r},1} - \boldsymbol{x}_{\boldsymbol{r},in} = \mathbf{0} & \text{for Departure Control Node} \\ \boldsymbol{x}_{\boldsymbol{r},N} - \boldsymbol{x}_{\boldsymbol{r},fin} = \mathbf{0} & \text{for Arrival Control Node} \end{cases} \tag{6.20}$$

For instance, position vectors $\boldsymbol{x}_{\boldsymbol{r},in}$ and $\boldsymbol{x}_{\boldsymbol{r},fin}$ can be represented by a target body location or the initial conditions for a Halo orbit. In that case, their dependence on the reference epoch ε_k must be taken in consideration. Finally, if some gravity-assists are included, the continuity in position is applied also at the intermediate control nodes (each connecting consecutive phases) and it is written as

$$\mathbf{c}_i(\mathbf{x}) = \boldsymbol{x}_{\boldsymbol{r},i} - \boldsymbol{x}_{\boldsymbol{r},i+1} = \mathbf{0} \qquad \text{for Intermediate Control Node} \tag{6.21}$$

So, constraints with the form expressed in equations 6.19, 6.20 and 6.21 can be included in the overall constraint vector $\mathbf{c}(\mathbf{x})$. Considering their derivatives with respect to the free variables, the differentiation is quite straightforward. Indeed, it is important to remember that

$$\frac{\partial \boldsymbol{x}^t_{\boldsymbol{r},i}}{\partial \boldsymbol{x}_i} = \left[\begin{array}{c} \\ \boldsymbol{\Phi}_i\left[\alpha,\beta\right] \\ \\ \end{array}\right] = \begin{bmatrix} \Phi_{11} & \Phi_{12} & \Phi_{13} & \Phi_{14} & \Phi_{15} & \Phi_{16} \\ \Phi_{21} & \Phi_{22} & \Phi_{23} & \Phi_{24} & \Phi_{25} & \Phi_{26} \\ \Phi_{31} & \Phi_{32} & \Phi_{33} & \Phi_{34} & \Phi_{35} & \Phi_{36} \end{bmatrix} \tag{6.22}$$

where $\alpha = \{1,2,3\}$ and $\beta = \{1,2,3,4,5,6\}$. So, $\boldsymbol{\Phi}_i\left[\alpha,\beta\right]$ represents a submatrix formed from the first three rows and all the columns of $\boldsymbol{\Phi}_i$. Besides,

$$\frac{\partial \boldsymbol{x}^t_{\boldsymbol{r},i}}{\partial \mathrm{T}_i} = \boldsymbol{x}^t_{\boldsymbol{v},i} \qquad \text{and} \qquad \frac{\partial \boldsymbol{x}^t_{\boldsymbol{r},i}}{\partial \varepsilon_k} = \begin{bmatrix} \frac{\partial x^t_i}{\partial \varepsilon_k} \\ \frac{\partial y^t_i}{\partial \varepsilon_k} \\ \frac{\partial z^t_i}{\partial \varepsilon_k} \end{bmatrix} \tag{6.23}$$

where ε_k is the reference epoch of the phase leg to which $\boldsymbol{x}^t_{r,i}$ belongs. If $\boldsymbol{x}^t_{r,i}$ is not related to the first segment of a phase leg, in general it is characterized by non-null derivatives with respect to the propagation periods of the antecedent segments. For example, with reference to Figure 6.2, $\boldsymbol{x}^t_{r,3}$ has a dependence on T_1 and T_2, while $\boldsymbol{x}^t_{r,4}$ on T_5 and T_6. Variations of these periods behave like variations of the related reference epochs (ε_1 and ε_2, respectively). So, if a phase has n segments, it is possible to write

$$\frac{\partial \boldsymbol{x}^t_{\boldsymbol{r},i}}{\partial \mathrm{T}_j} = \begin{cases} \dfrac{\partial \boldsymbol{x}^t_{\boldsymbol{r},i}}{\partial \varepsilon_k} & \text{for } j = 1,\ldots,i-1 \quad \text{for Forward Segment} \\ \dfrac{\partial \boldsymbol{x}^t_{\boldsymbol{r},i}}{\partial \varepsilon_{k+1}} & \text{for } j = i+1,\ldots,n \quad \text{for Backward Segment} \end{cases} \tag{6.24}$$

Considering the initial position vector of the i-th segment, the only non-null derivative is the one with respect to the state vector itself, yielding

$$\frac{\partial \boldsymbol{x}_{\boldsymbol{r},i}}{\partial \boldsymbol{x}_i} = \left[\begin{array}{c|c} \mathbf{I}_{3\times 3} & \mathbf{0}_{3\times 3} \end{array}\right] \tag{6.25}$$

Constraints on Altitude

It is very useful to constraint the magnitude of the position vector relative to a celestial body within a lower and an upper bound

$$d_{i,min} < d_i < d_{i,max} \tag{6.26}$$

where $d_i = ||\boldsymbol{x_r}_{,i} - \boldsymbol{x_r}_{,body}|| = \sqrt{(x_i - x_{body})^2 + (y_i - y_{body})^2 + (z_i - z_{body})^2}$. This condition can be included by adding two components to the constraint vector:

$$\mathbf{c}_i(\mathbf{x}) = \begin{bmatrix} d_i - d_{i,max} \\ -d_i + d_{i,min} \end{bmatrix} < \mathbf{0} \tag{6.27}$$

By introducing slack variables into the $\mathbf{x}$ vector, equation 6.27 can be written as

$$\mathbf{c}_i(\mathbf{x}) = \begin{bmatrix} d_i - d_{i,max} + \beta_j^2 \\ d_i - d_{i,min} - \beta_{j+1}^2 \end{bmatrix} = \mathbf{0} \tag{6.28}$$

The magnitude d_i has non-null derivative with respect to $\boldsymbol{x}_i$, yielding

$$\frac{\partial d_i}{\partial \boldsymbol{x}_i} = \frac{1}{d_i}\begin{bmatrix} x & y & z & 0 & 0 & 0 \end{bmatrix} \tag{6.29}$$

It is important to consider the dependence of $\boldsymbol{x_r}_{,body}$ on its reference epoch ε_k, so

$$\frac{\partial d_i}{\partial \varepsilon_k} = \frac{1}{d_i}(\boldsymbol{x_r}_{,i} - \boldsymbol{x_r}_{,body}) \cdot (-\boldsymbol{x_v}_{,body}) \tag{6.30}$$

Finally, note that the differentiation with respect to the slack variables yield the terms $\pm 2\beta$.

Constraints on Velocity

In this case, the magnitude of the velocity vector relative to a celestial body is constrained to remain between a lower and an upper limit

$$v_{i,min} < v_i < v_{i,max} \tag{6.31}$$

where $v_i = ||\boldsymbol{x_v}_{,i} - \boldsymbol{x_v}_{,body}|| = \sqrt{(\dot{x} - \dot{x}_{body})^2 + (\dot{y} - \dot{y}_{body})^2 + (\dot{z} - \dot{z}_{body})^2}$. Two components are added to the constraint vector:

$$\mathbf{c}_i(\mathbf{x}) = \begin{bmatrix} v_i - v_{i,max} \\ -v_i + v_{i,min} \end{bmatrix} < \mathbf{0} \tag{6.32}$$

Equation 6.32 is equivalent to (by exploiting slack variables)

$$\mathbf{c}_i(\mathbf{x}) = \begin{bmatrix} v_i - v_{i,max} + \beta_j^2 \\ v_i - v_{i,min} - \beta_{j+1}^2 \end{bmatrix} = \mathbf{0} \tag{6.33}$$

This kind of constraint can be applied to constraint the magnitude of the relative velocity during a gravity-assist. In this case, a good estimation for $v_{i,min}$ is represented by the two-body escape velocity

$$v_{esc,i} = \sqrt{\frac{2\mu}{d_i}} \tag{6.34}$$

where μ is the (nondimensionalized) gravitational parameter related to the body around which the gravity-assist takes place and $d_i = ||\boldsymbol{x_r}_{,i} - \boldsymbol{x_r}_{,body}||$. The derivatives of v_i with respect to initial conditions $\boldsymbol{x}_i$ and the reference epoch ε_k are written as

$$\begin{cases} \dfrac{\partial v_i}{\partial \boldsymbol{x}_i} &= \dfrac{1}{v_i}\begin{bmatrix} 0 & 0 & 0 & \dot{x} & \dot{y} & \dot{z} \end{bmatrix} \\ \dfrac{\partial v_i}{\partial \varepsilon_i} &= \dfrac{1}{v_i}\left(\boldsymbol{x_v}_{,i} - \boldsymbol{x_v}_{,body}\right) \cdot \left(-\boldsymbol{x_a}_{,body}\right) \end{cases} \tag{6.35}$$

where $\boldsymbol{x_a}_{,body}$ is the acceleration of the celestial body. In the case that $v_{esc,i}$ is included in the formulation, it is possible to write its derivatives as well:

$$\begin{cases} \dfrac{\partial v_{esc,i}}{\partial \boldsymbol{x}_i} &= -\dfrac{\sqrt{2\mu}}{2}\dfrac{1}{d_i^{5/2}}\begin{bmatrix} (x_i - x_{body}) & (y_i - y_{body}) & (z_i - z_{body}) & 0 & 0 & 0 \end{bmatrix} \\ \dfrac{\partial v_{esc,i}}{\partial \varepsilon_i} &= -\dfrac{\sqrt{2\mu}}{2}\dfrac{1}{d_i^{5/2}}\left(\boldsymbol{x_r}_{,i} - \boldsymbol{x_r}_{,body}\right) \cdot \left(-\boldsymbol{x_v}_{,body}\right) \end{cases} \tag{6.36}$$

Constraints on Δv

In order to simulate the low-thrust trajectory as best as possible, it is very important limit the magnitudes of the inserted impulses. Indeed, each Δv is limited by the amount of thrust that can be accumulated over the duration of a segment. Denoting as Δv_i the impulse that occurs at the end of the i-th segment, the constraint is expressed as

$$c_i\left(\mathbf{x}\right) = \begin{cases} \Delta v_i < \dfrac{D\ n_{thr}\ T_{max}}{m_0}\mathrm{T}_i & \text{for } \mathrm{T}_i > 0 \\ \Delta v_i < -\dfrac{D\ n_{thr}\ T_{max}}{m_0}\mathrm{T}_i & \text{for } \mathrm{T}_i < 0 \end{cases} \tag{6.37}$$

where D is the thruster duty cycle, n_{thr} is the number of thrusters, T_{max} is the maximum value of thrust deliverable by one single thruster and m_0 is a reference mass of the spacecraft. Inequality constraints equation 6.37 can be transformed into equality ones by using slack variables, yielding

$$c_i\left(\mathbf{x}\right) = \begin{cases} \Delta v_i - \dfrac{D\ n_{thr}\ T_{max}}{m_0}\mathrm{T}_i + \beta_j^2 = 0 & \text{for } \mathrm{T}_i > 0 \\ \Delta v_i + \dfrac{D\ n_{thr}\ T_{max}}{m_0}\mathrm{T}_i + \beta_j^2 = 0 & \text{for } \mathrm{T}_i < 0 \end{cases} \tag{6.38}$$

The form of Δv_i changes depending on the point of the trajectory where it takes place:

$$\Delta v_i = \begin{cases} ||\boldsymbol{x}_{\boldsymbol{v},i+1} - \boldsymbol{x}^t_{\boldsymbol{v},i}|| & \text{in Forward Legs} \\ ||\boldsymbol{x}^t_{\boldsymbol{v},i+1} - \boldsymbol{x}^t_{\boldsymbol{v},i}|| & \text{for Match Points} \\ ||\boldsymbol{x}^t_{\boldsymbol{v},i+1} - \boldsymbol{x}_{\boldsymbol{v},i}|| & \text{in Backward Legs} \\ ||\boldsymbol{x}_{\boldsymbol{v},i+1} - \boldsymbol{x}_{\boldsymbol{v},i}|| & \text{for Control Nodes} \end{cases} \tag{6.39}$$

Also the structure of its derivatives changes as a consequence. For illustrative purposes, considering a

$$\Delta v_i = ||\boldsymbol{x}_{\boldsymbol{v},i+1} - \boldsymbol{x}^t_{\boldsymbol{v},i}|| = \sqrt{\left(\dot{x}_{i+1} - \dot{x}^t_i\right)^2 + \left(\dot{y}_{i+1} - \dot{y}^t_i\right) + \left(\dot{z}_{i+1} - \dot{z}^t_i\right)}$$

in a forward leg, it follows

$$\frac{\partial \Delta v_i}{\partial \boldsymbol{x}_i} = -\frac{1}{\Delta v_i} \begin{bmatrix} & \boldsymbol{\Phi}_i \left[\alpha, \beta\right]^T & \end{bmatrix} \begin{bmatrix} \dot{x}_{i+1} - \dot{x}^t_i \\ \dot{y}_{i+1} - \dot{y}^t_i \\ \dot{z}_{i+1} - \dot{z}^t_i \end{bmatrix} \tag{6.40}$$

where $\alpha = \{4, 5, 6\}$ and $\beta = \{1, 2, 3, 4, 5, 6\}$. Then, the derivatives with respect to propagation period T_i and reference epoch ε_k are written as

$$\frac{\partial \Delta v_i}{\partial \mathrm{T}_i} = \frac{1}{\Delta v_i} \left(\boldsymbol{x}_{\boldsymbol{v},i+1} - \boldsymbol{x}^t_{\boldsymbol{v},i}\right) \cdot \left(-\boldsymbol{x}^t_{\boldsymbol{a},i}\right) \tag{6.41}$$

and

$$\frac{\partial \Delta v_i}{\partial \varepsilon_k} = \frac{1}{\Delta v_i} \left(\boldsymbol{x}_{\boldsymbol{v},i+1} - \boldsymbol{x}^t_{\boldsymbol{v},i}\right) \cdot \left(-\frac{\partial \boldsymbol{x}^t_{\boldsymbol{v},i}}{\partial \varepsilon_k}\right) \tag{6.42}$$

respectively. Equation 6.42 is valid also to find derivatives with respect to antecedent propagation periods. When differentiating constraints in equation 6.38 with respect to the propagation period T_i, also the term $\frac{D\ n_{thr}\ T_{max}}{m_0}$ arises.

Constraints on Propagation Periods

Depending if propagation periods are referred to forward or backward segments, constraints of the kind

$$c_i\left(\mathbf{x}\right) = \begin{cases} \mathrm{T}_i > 0 & \text{for Forward Segments} \\ \mathrm{T}_i < 0 & \text{for Backward Segments} \end{cases} \tag{6.43}$$

must be considered. By exploiting slack variables, constraints in equation 6.43 are rewritten as

$$c_i\left(\mathbf{x}\right) = \begin{cases} \mathrm{T}_i - \beta_j^2 = 0 & \text{for Forward Segments} \\ \mathrm{T}_i + \beta_j^2 = 0 & \text{for Backward Segments} \end{cases} \tag{6.44}$$

Derivatives of constraints in equation 6.44 are straightforward.

Constraints on Epochs and Propagation Periods

In order to ensure continuity in time within the segments, the sum of all the propagation periods in a trajectory phase must equal the difference between the reference epochs at the start and end points. So, considering a trajectory phase with n segments, it follows that

$$c_j(\mathbf{x}) = \varepsilon_{k+1} - \varepsilon_k - \sum_{i=1}^{n/2} \mathrm{T}_i + \sum_{i=\frac{n}{2}+1}^{n} \mathrm{T}_i \tag{6.45}$$

where summations are referred to forward and backward legs, respectively. Also in this case, derivatives are straightforward.

Bounds on Epochs

It is very useful to constraint and limit the field of existence of reference epochs. For each epoch, it is possible to specify a lower and an upper bound

$$\varepsilon_{k,min} < \varepsilon_k < \varepsilon_{k,max} \tag{6.46}$$

By introducing slack variables into the $\mathbf{x}$ vector, equation 6.46 can be written as

$$\mathbf{c}_i(\mathbf{x}) = \begin{bmatrix} \varepsilon_k - \varepsilon_{k,max} + \beta_j^2 \\ \varepsilon_k - \varepsilon_{k,min} - \beta_{j+1}^2 \end{bmatrix} = \mathbf{0} \tag{6.47}$$

Also in this case, derivatives are trivial and they exist only with respect to the reference epoch itself and the related slack variable.

6.3 Optimal Control

6.3.1 Introduction

The introduced Sims-Flanagan method represents a low-medium fidelity tool for low-thrust trajectory design and optimization. The main problem related to this method is that the overall dynamics is not perfectly considered. Although each Δv is constrained to be smaller than the accumulated thrust on the considered segment, velocity changes are modelled as impulsive variations. In addition, the acceleration due to thrusters is not included in the dynamical equations and the mass variations in the spacecraft are not studied.

The next step aims to consider the complete dynamics of the N-body problem, including the effects of the thrust as well. Then, the optimization process consists in finding the optimal profiles (magnitude and direction)

of the thrust, such that it minimizes the propellant consumption and the mission constraints are satisfied. This outlines an optimal control problem.

6.3.2 Optimal Control Problem

The inclusion of a manoeuvrable action is reflected by the introduction of a control $\boldsymbol{u}(t)$ in the equations of motions. For many applications, even if the problem can be seen as a series of *phases*, it is possible to focus on a single k-th phase, defined in the region $t_0 \leqslant t \leqslant t_f$. In a general way, the considered optimal control problem is characterized by a governing dynamics of the kind

$$\dot{\boldsymbol{x}} = \boldsymbol{f}(\boldsymbol{x}, \boldsymbol{u}, \boldsymbol{\lambda}, \varepsilon, \tau) \tag{6.48}$$

where $\boldsymbol{x}$ is the state vector (n_x components), $\boldsymbol{u}$ is the control vector (n_u components), $\boldsymbol{\lambda}$ is a vector that contains n_p parameters, ε and τ are, respectively, the reference epoch and time (that has been nondimensionalized). Note that, in general, the parameters in $\boldsymbol{\lambda}$ are time independent (for example, they can be used to describe the propulsive properties of the spacecraft). Between two consecutive phases, it is not excluded to have changes in the governing dynamics and discontinuities in some of the states (for example, a mass discontinuity if a stage is released). Initial and final conditions ($\boldsymbol{\psi}_0$ and $\boldsymbol{\psi}_f$ respectively) for the considered phase are expressed as

$$\boldsymbol{\psi}_{0l} \leqslant \boldsymbol{\psi}\left[\boldsymbol{x}(\tau_0), \boldsymbol{u}(\tau_0), \boldsymbol{\lambda}, \varepsilon, \tau_0\right] \leqslant \boldsymbol{\psi}_{0u} \tag{6.49}$$

$$\boldsymbol{\psi}_{fl} \leqslant \boldsymbol{\psi}\left[\boldsymbol{x}(\tau_f), \boldsymbol{u}(\tau_f), \boldsymbol{\lambda}, \varepsilon, \tau_f\right] \leqslant \boldsymbol{\psi}_{fu} \tag{6.50}$$

Besides, generally the solution of the problem has satisfy algebraic path constraints of the form

$$\boldsymbol{g}_l \leqslant \boldsymbol{g}\left[\boldsymbol{x}(\tau), \boldsymbol{u}(\tau), \boldsymbol{\lambda}, \varepsilon, \tau\right] \leqslant \boldsymbol{g}_u \tag{6.51}$$

where the vector $\boldsymbol{g}$ has n_g components. Finally, the components of the state and control vectors are subject to the following bounds

$$\boldsymbol{x}_l \leqslant \boldsymbol{x}(\tau) \leqslant \boldsymbol{x}_u \tag{6.52}$$

$$\boldsymbol{u}_l \leqslant \boldsymbol{u}(\tau) \leqslant \boldsymbol{u}_u \tag{6.53}$$

Solving the optimal control problem corresponds to determine the n_u dimensional control vector $\boldsymbol{u}(\tau)$ that minimize the performance index J

$$J = \Phi\left[\boldsymbol{x}(\tau_0), \tau_0, \boldsymbol{x}(\tau_f), \tau_f\right] + \int_{t_0}^{t_f} \boldsymbol{q}\left[\boldsymbol{x}(\tau), \boldsymbol{u}(\tau), \boldsymbol{\lambda}, \varepsilon, \tau\right] d\tau \tag{6.54}$$

If the cost function J contains the term Φ (evaluated at the ends of the phase) and the integral of the function $\boldsymbol{q}$, the presented formulation is also referred as a problem of *Bolza*. If only the former term is present, it is called problem of *Mayer* while, if only the latter is included, it is a problem of *Lagrange*.

6.3.3 Low-Thrust Dynamical Model

Considering the actual dynamics of a low-thrust problem implies the addition of a state variable related to the mass m of the spacecraft. So, the augmented state vector can be written as

$$\boldsymbol{x} = \begin{bmatrix} \boldsymbol{\rho} \\ \dot{\boldsymbol{\rho}} \\ m \end{bmatrix} \tag{6.55}$$

The dynamics of the problem is then modified by considering the acceleration due to the thrusters and the mass evolution:

$$\dot{\boldsymbol{x}} = \begin{bmatrix} \dot{\boldsymbol{\rho}} \\ \ddot{\boldsymbol{\rho}} \\ \dot{m} \end{bmatrix} = \begin{bmatrix} \dot{\boldsymbol{\rho}} \\ \boldsymbol{f}\left(\boldsymbol{x}, \varepsilon, \tau\right) + \frac{T_h}{m}\hat{\boldsymbol{u}} \\ -\frac{T_h}{I_{sp} g_0} \end{bmatrix} \tag{6.56}$$

where T_h is the magnitude of the thrust, $\hat{\boldsymbol{u}}$ is the unit vector defining the direction of the thrust, I_{sp} and g_0 are, respectively, the specific impulse of the propulsive system and the standard acceleration due to gravity near the surface of the Earth (9.80665 m/s^2). Note that the term $\boldsymbol{f}\left(\boldsymbol{x}, \varepsilon, \tau\right)$ can be replaced by the the second term of equation (2.37) or (2.50), depending on whether N-body equations are projected onto inertial axes (and relative to a central mass) or onto an appropriate synodic frame. It is equally important to note that the added terms have to be nondimensionalized in order to obtain a coherent expression with the remaining quantities.

The new dynamics expressed in (6.56) has, actually, the form of equation (6.48), where a control vector $\boldsymbol{u}$ is included. As a matter of fact, a desired dynamics (within feasibility limits) can be achieved manoeuvring the value of the thrust vector $\boldsymbol{T_h}$ (magnitude and direction) in time. So, trivially, the selection for the components of the control vector must allow guidance of the magnitude T_h and the direction $\hat{\boldsymbol{u}}$ of the thrust. The choice of the control vector is not unique, a suitable selection is represented by

$$\boldsymbol{u} = \begin{bmatrix} \alpha \\ \beta \\ P \end{bmatrix} \tag{6.57}$$

where α and β represent two angular spherical coordinates and P is the provided power for the thrusters. The angles α and β allow to describe the direction $\boldsymbol{u}$ (see Figure 6.4) as

$$\hat{\boldsymbol{u}} = \begin{bmatrix} \cos\alpha\cos\beta \\ \sin\alpha\cos\beta \\ \sin\beta \end{bmatrix} \tag{6.58}$$

while the provided power P is linked to the thrust magnitude according to

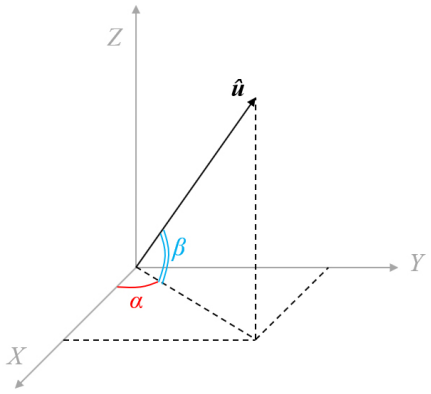

Figure 6.4: Thrust Direction

$$T_h = \frac{2P}{I_{sp}g_0} \tag{6.59}$$

The first angular coordinate α must be bounded within the region $0 \leqslant \alpha \leqslant 2\pi$, while for β it must be $-\pi/2 \leqslant \beta \leqslant \pi/2$. Similarly, the domain for the power is $0 \leqslant P \leqslant P_{max}$ and, as a consequence, the thrust magnitude will be bounded as well. Such a selection of the control vector has the notable advantage to automatically satisfy the condition (for the direction $\hat{\boldsymbol{u}}$)

$$\hat{u}_x^2 + \hat{u}_y^2 + \hat{u}_z^2 = 1 \tag{6.60}$$

Usually, in low-thrust trajectory optimization the optimal control problem aims at the definition of the control vector such that it minimizes a performance index in the Mayer form

$$\text{Min } J = -m(t_f) \tag{6.61}$$

Equation (6.61) corresponds to the maximization of the final mass and, so, at the minimization of the fuel consumption.

Within the context of this study, a *constant specific impulse* (CSI) scenario is considered, in contrast to a *variable specific impulse* (VSI) case.

6.3.4 Direct Methods

In opposition to *indirect* methods, *direct* optimization aims to solve the optimal control problem by discretizing it with a finite set of variables and converting it to a NLP problem. This allows to overcome the main difficulties of indirect methods (in particular, sensitivity to initial conditions) and to obtain robust tool in terms of convergence. The price to pay is that these methods are usually more expensive in terms of computational speed. The process of discretizing an optimal control problem is called *transcription*. Usually, the idea behind discretization schemes is to write quantities that appear in the considered dynamics as polynomial functions. If polynomials of degree N are exploited, each particular quantity is described by its values at $N + 1$ points, placed at suitable locations.

Depending on which quantities are parametrized, direct transcription methods are divided into two main types (see Figure 6.5):

- If only control components are parametrized, *shooting methods* are obtained. In this case, dynamics is satisfied by integrating equations of motions through a ODE solver (Runge-Kutta schemes, for instance). Depending on the number of segments into which the considered phase is subdivided, schemes can be single or multiple shooting methods.

- If state and control components are parametrized simultaneously, *collocation method* are obtained. In this case, dynamics is imposed by constraining the slope at nodes of polynomial functions. Depending on the number of segments into which the considered phase is subdivided, collocation schemes can be local or global.

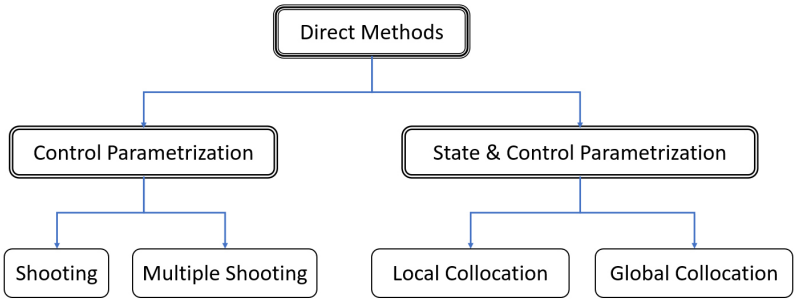

Figure 6.5: Direct Methods for Optimal Control

Within the context of this study, a single shooting scheme is adopted and parametrization is achieved by exploiting Chebyshev polynomials.

Single Shooting

Focusing on a single phase (going from τ_0 to τ_f) of the optimal control problem, the basic idea behind single shooting scheme is to write the control vector $\boldsymbol{u}(\tau)$ (n_u components) as a polynomial function of order N

$$\boldsymbol{u}(\tau) = \sum_{i=0}^{N} \boldsymbol{c}_i \psi_i(\tau) \tag{6.62}$$

where $\boldsymbol{c}_i$ is a column vector containing the coefficients for appropriate base functions ψ_i. In order to do that, its values at $N+1$ nodes, placed at suitable locations, are exploited. First of all, time domain of the phase is normalized in order to be $[-1, 1]$, according to

$$\tilde{\tau} = \frac{2}{\tau_f - \tau_0}(\tau - \tau_0) - 1 \tag{6.63}$$

Then, the new time domain is meshed according to $N+1$ increasing points

$$S = \{\tilde{\tau}_0, \tilde{\tau}_1, \ldots, \tilde{\tau}_i, \ldots, \tilde{\tau}_{N-1}, \tilde{\tau}_N\} \tag{6.64}$$

At each point of the set S, a corresponding value of the control vector is associated

$$Z = \{\boldsymbol{u}(\tilde{\tau}_0), \ldots, \boldsymbol{u}(\tilde{\tau}_i), \ldots, \boldsymbol{u}(\tilde{\tau}_N)\} = \{\boldsymbol{u}_0, \ldots, \boldsymbol{u}_i, \ldots, \boldsymbol{u}_N\} \tag{6.65}$$

Z will represent the set containing the variables of the problem (solved through NLP). More compactly, it is possible to write

$$\mathbf{U} = [\boldsymbol{u}_0, \boldsymbol{u}_1, \ldots, \boldsymbol{u}_i, \ldots, \boldsymbol{u}_{N-1}, \boldsymbol{u}_N] = \mathbf{CA} \tag{6.66}$$

where $\mathbf{C}$ is the $(n_u \times (N+1))$ matrix containing the coefficients $\boldsymbol{c}_i$

$$\mathbf{C} = [\boldsymbol{c}_0, \boldsymbol{c}_1, \ldots, \boldsymbol{c}_i, \ldots, \boldsymbol{c}_{N-1}, \boldsymbol{c}_N] \tag{6.67}$$

and the $((N+1) \times (N+1))$ matrix $\mathbf{A}$ contains the base functions

$$\mathbf{A} = \begin{bmatrix} \psi_0(\tilde{\tau}_0) & \psi_0(\tilde{\tau}_1) & \cdots & \psi_0(\tilde{\tau}_{N-1}) & \psi_0(\tilde{\tau}_N) \\ \psi_1(\tilde{\tau}_0) & \psi_1(\tilde{\tau}_1) & \cdots & \psi_1(\tilde{\tau}_{N-1}) & \psi_1(\tilde{\tau}_N) \\ \vdots & \vdots & \cdots & \vdots & \vdots \\ \psi_{N-1}(\tilde{\tau}_0) & \psi_{N-1}(\tilde{\tau}_1) & \cdots & \psi_{N-1}(\tilde{\tau}_{N-1}) & \psi_{N-1}(\tilde{\tau}_N) \\ \psi_N(\tilde{\tau}_0) & \psi_N(\tilde{\tau}_1) & \cdots & \psi_N(\tilde{\tau}_{N-1}) & \psi_N(\tilde{\tau}_N) \end{bmatrix} \tag{6.68}$$

Once the values $\boldsymbol{u}_i$ are known, it is possible to recover the coefficients $\boldsymbol{c}_i$ thanks to

$$\mathbf{C} = \mathbf{U}\mathbf{A}^{-1} \tag{6.69}$$

Then, it is possible to estimate the value of $\boldsymbol{u}(\tilde{\tau})$ according to

$$\boldsymbol{u}(\tilde{\tau}) = \mathbf{C} \begin{bmatrix} \psi_0(\tilde{\tau}) \\ \vdots \\ \psi_i(\tilde{\tau}) \\ \vdots \\ \psi_N(\tilde{\tau}) \end{bmatrix} \tag{6.70}$$

Thanks to equation 6.70, the control vector $\boldsymbol{u}(\tau)$, can be included into the dynamics (paying attention to the passage from normalized time $\tilde{\tau}$ to the dimensionless one τ).

The values of $\boldsymbol{u}_i$ at nodes are the variables of the NLP problem, aiming to minimize the fuel consumption. The problem is, in general, associated to some equality and inequality constraints. In particular, it is important to constrain the final state of the propagation equal to a desired condition. For the low-thrust problem, values of the provided power P (at each instant, not only at nodes) must be positive. Similarly, it is possible to bound the rate of change of control components, considering that

$$\frac{d}{d\tilde{\tau}}\mathbf{U} = \frac{d}{d\tilde{\tau}}\left(\mathbf{CA}\right) = \mathbf{C}\frac{d}{d\tilde{\tau}}\left(\mathbf{A}\right) = \mathbf{CD} \tag{6.71}$$

where the $((N+1)\times(N+1))$ matrix $\mathbf{D}$ contains the derivatives of the base functions ψ_i.

Within the context of this study, *Chebyshev polynomials* of the first kind are used as base functions and the mesh S for the time domain is set according to *Chebyshev points* (also called *Chebyshev nodes*).

Chebyshev Polynomials

Chebyshev polynomials are largely appreciated in approximation theory and they represent a sequence of orthogonal polynomials. Chebyshev polynomials of the first kind are denoted as T_k and they are defined by the following recurrence relation:

$$\begin{cases} T_0(x) = 1 \\ T_1(x) = x \\ T_{n+1}(x) = 2xT_n(x) - T_{n-1}(x) \end{cases} \tag{6.72}$$

For the sake of convenience, they are defined over the domain $[-1, 1]$, where they satisfy $-1 \leqslant T_k(x) \leqslant 1$. Chebyshev nodes are the extrema of T_n within the range $[-1, 1]$ and they are located according to

$$x_k = \cos\left(\frac{k}{n}\pi\right) \quad , \qquad \text{for } k = 0, 1, \ldots, n \tag{6.73}$$

At the Chebyshev nodes, the polynomial T_k has value 1 or -1. In Figure 6.6, Chebyshev polynomials T_n, up to $n = 5$, are depicted.

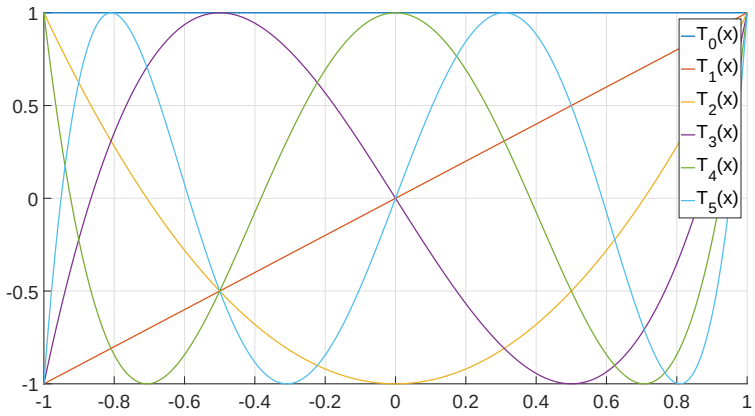

Figure 6.6: Chebyshev Polynomials ($n = 0, 1, \ldots, 5$)

In the theory of approximation, using Chebyshev nodes as points in polynomial interpolation has admirable advantages, since this minimizes the problem of Runge's phenomenon and leads to greater accuracy. Supposing $f(x)$ is a Lipschitz continuous function on $[1, 1]$, a good approximation of $f(x)$ is the polynomial $p_n(x)$ obtained by interpolation at Chebyshev nodes

$$p_n(x) = \sum_{k=0}^{n} c_k T_k(x) \tag{6.74}$$

Since every Lipschitz continuous function $f(x)$ on $[1, 1]$ is characterized by a unique representation as an absolutely and uniformly convergent series

$$f(x) = \sum_{k=0}^{\infty} a_k T_k(x) \tag{6.75}$$

and since Chebyshev coefficients a_k are related to interpolating ones c_k (see [52]), it is possible to understand that large values of n leads to higher precisions.

Derivatives of Chebyshev polynomials of the first kind can be handles easily as well. Indeed, it is true that

$$\frac{dT_n}{dx} = nU_{n-1} \tag{6.76}$$

where the generic U_k represents Chebyshev polynomial of the second kind. The recurrence relation that defines Chebyshev polynomials of the second

kind is

$$\begin{cases} U_0(x) = 1 \\ U_1(x) = 2x \\ U_{n+1}(x) = 2xU_n(x) - U_{n-1}(x) \end{cases} \tag{6.77}$$

Chapter 7

Simulation

In this chapter simulations and results, exploiting numerical methods for trajectory optimization introduced in Chapter 4, are presented. Simulations have been performed taking inspiration from *Asteroid Redirect Robotic Mission* (ARRM), part of the more extended *Asteroid Redirect Mission* (ARM). This mission was proposed by NASA and it was supposed to be achieved in the near future, in order test some deep space exploration capabilities and to be preparatory for other missions. The main objective of the mission is the exploration of a Near-Earth Asteroid and the retrieval of a boulder from its surface. The above mentioned boulder is, then, supposed to be place on a stable DRO around the Moon, exploiting a NRO as a gateway.

7.1 Trajectory Structure

In terms of trajectory design, the presented mission has been divided into three different journeys:

1. **Earth-to-Asteroid Trajectory**. This trajectory is expected to be characterized by a double lunar gravity assist (LGAs or *double lunar swing-by*) to leave the Earth-Moon system. Placing two intermediate control nodes (one for each gravity assist), in turn this trajectory can be subdivided into three phases:
   (a) A *first* phase, from the launch from the Earth to the first LGA;
   (b) A *second* phase, from the first to the second LGA;
   (c) A *third* phase, from the second LGA to the arrival at the asteroid.
2. **Asteroid-to-NRO Trajectory**. This trajectory represents the return into the Earth-Moon region and it exploits an Earth gravity assist

Asteroid	Asteroid Estimated Diameter [m]	Semi-Major Axis [AU]	Orbit Period [years]	Eccentricity	Inclination [deg]
2008 EV5	400	0.958	0.94	0.084	7.436
Bennu	500	1.126	1.20	0.203	6.035
2014 YD	24-107	1.070	1.11	0.087	1.735
2000 SG344	20-89	0.978	0.97	0.067	0.112
2013 BS45	11-51	0.993	0.99	0.084	0.772
2001 QJ142	33-142	1.060	1.09	0.086	3.103
2012 UV136	14-62	1.010	1.01	0.138	2.211
1999 JU3	251-1124	1.189	1.30	0.190	5.884
2001 CQ36	55-246	0.938	0.91	0.178	1.258
2006 FH36	46-205	0.955	0.93	0.198	1.586
2007 UY1	46-205	0.951	0.93	0.175	1.019

Table 7.1: Possible Targets

(EGA) in order to enter a NRO. So, this journey can be divided into two phases:

(a) A *first* phase, from the asteroid departure to the EGA;

(b) A *second* phase, from the EGA to the arrival at NRO.

3. **NRO-to-DRO Trajectory**. Since NRO is a non-stable orbit, this single-phase journey is scheduled in order to move the boulder into a DRO, a stable periodic solution within the Earth-Moon region (where it can be reached more easily to carried out on-site studies).

Several asteroids have been identified as possible targets for the mission. The most important options are listed in Table 7.1. Asteroid 2008 EV5 results to be one of the most interesting because of its scientific attractiveness, composition and size. Within the context of this study, asteroid 2008 EV5 has been selected as the target for the mission analysis. The diagram inherent to the trajectory structure of the mission is reported in Figure 7.1.

7.1.1 Earth-to-Asteroid Trajectory

Sims-Flanagan Transcription Method

The initial step of trajectory design for the considered mission consists on applying the Sims-Flanagan transcription method to the first journey. All the variables related to the journey are defined for the NLP problem. Surely,

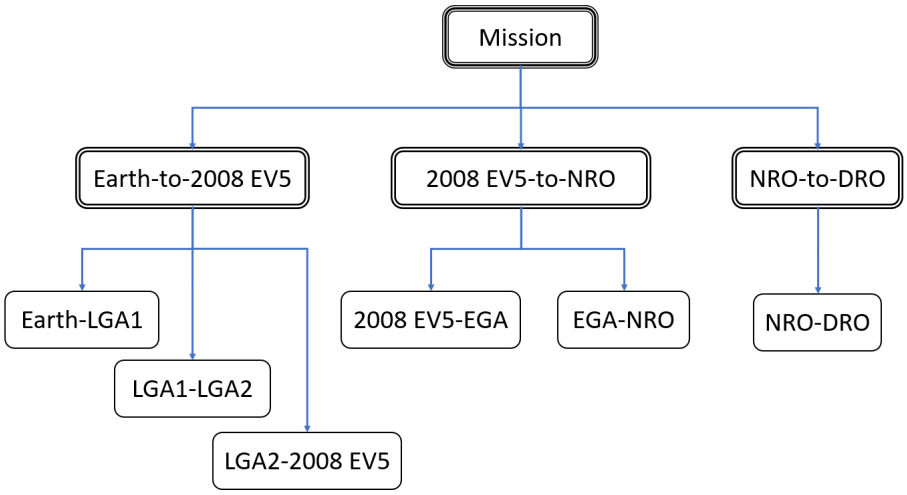

Figure 7.1: Trajectory Structure

the total number of variables takes into consideration $6n$ components of the state vectors $\boldsymbol{x}_i$ (related to the n segments into which the journey is discretized), other n variables concerning the propagation period T_i for each segment and k epoch variables ε_j, where k is equal to the number of control nodes of the journey (in this case, $k = 4$, being ε_j the generic variable related to the epoch of the departure, first LGA, second LGA or arrival to the asteroid). In addition, some slacks variables β are considered:

- For each gravity assist in the journey (p denotes the number of GAs in the journey), slack variables related to altitude and velocity constraints (equations (6.28) and (6.33)) are included, for a total of $(2 + 2)p = 4p$ additional slack variables;
- For each Δv_i (one at the end of each segment), conditions expressed in equation (6.38) must be included, resulting in other n slack variables;
- For each propagation period T_i, conditions of the kind (6.44) must be included, this results in other n slack variables;
- For each epoch variable, bounds are imposed by using equation (6.47), giving other $2k$ additional variables.

As a consequence, the total amount of variables N_v can be expressed as

$$N_v = 6n + n + k + 4p + n + n + 2k = 9n + 3k + 4p \tag{7.1}$$

Within the proposed study, $n = 26$ segments are considered in the first journey. The first phase is modelled by 2 segments, the second one by 16 segments and the third one by 8. In each phase, the first half of the segments is propagated forward (from the phase start control node), while the second half is propagated backward (from the phase end control node). The considered journey results in 254 components for the variable vector $\mathbf{x}$.

Concerning the constraints, it is important to impose the continuity $(3(n-1))$ conditions in terms of position for consecutive segments (equation (6.19)) and 3 conditions to ensure continuity at the journey final point (equation (6.20)); then there are $k-1$ conditions for continuity between propagation periods and epochs (equation (6.45)), $(2+2)p = 4p$ constraints for altitude and velocity at GAs (equations (6.28) and (6.33)), n conditions to bound the magnitude of Δvs (equation (6.38)), other n equations to discriminate forward and backward propagation periods (equation (6.44)) and, finally, $2k$ conditions to set bounds on epochs (equation (6.47)). So, the total number of constraint N_c for the considered journey is

$$N_c = 3n + (k-1) + 4p + n + n + 2k = 5n + 4p + 3k - 1 \tag{7.2}$$

For $n = 26$ segments, it means a total of 149 constraints. Since, in the first phase, also continuity in velocity is considered between the 2 (only) segments (3 additional constraints), one Δv cancels out (one slack variable and one constraint are eliminated). Besides, the journey start point is constrained to have a fixed magnitude $d_0 = 7000$ km (one additional equality constraint). So, at the end, this translates into a problem with $N_v = 253$ variables and $N_c = 152$ constraints. The simulation is performed by using the *SQP fmincon* algorithm in MATLAB®. Propagations are carried out by using a *Runge-Kutta* 78 scheme.

The solution of the first journey by using the proposed Sims-Flanagan transcription method is presented in Figure 7.2. Trajectory is depicted in the inertial frame. Zooming at the center of Figure 7.2, a more detailed image related to the first two phases of the journey is obtained (Figure 7.3). Recalling equation (6.37), some propulsive parameters are required to solve the problem. In particular, the initial mass of the spacecraft has been set to $m_0 = 5000$ kg, the duty cycle has been fixed to $D = 0.9$ and the number of thrusters to $n_{thr} = 3$. The maximum deliverable thrust can be computed exploiting the relation

$$T_{h,max} = \frac{2P_{max}}{I_{sp} g_0} \tag{7.3}$$

Setting the maximum provided power (per thruster) equal to $P = 13$ kW and the specific impulse $I_{sp} = 4000$ s, a value of $T_{h,max} = 0.6625$ N is obtained.

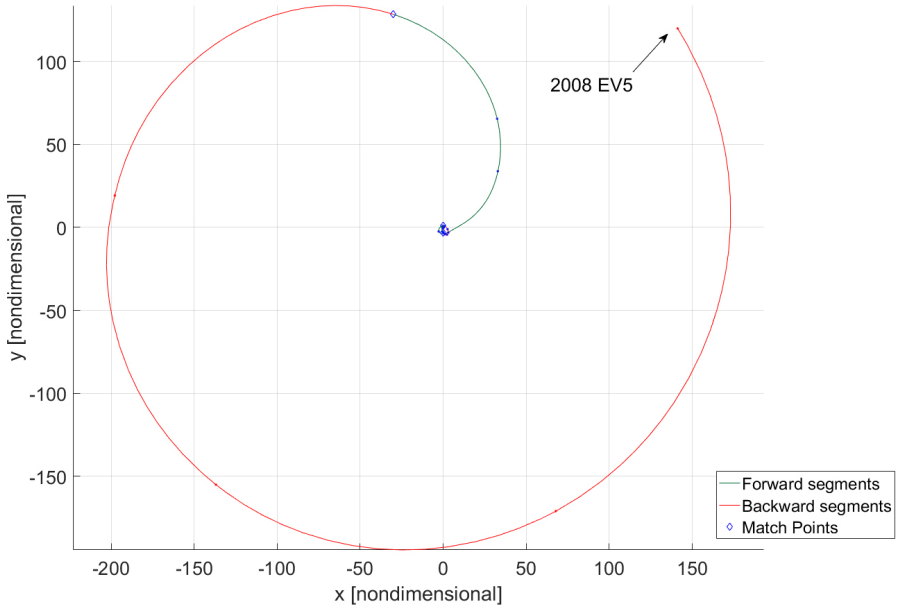

Figure 7.2: Earth-to-2008 EV5 Journey

Event	Date
Earth Departure	18 February 2021
LGA1	23 February 2021
LGA2	7 June 2021
2008 EV8 Arrival	9 February 2023

Table 7.2: Journey 1: Epochs

The first Lunar Gravity Assist (LGA1) is constrained to have an altitude in the range 100km $\leqslant h_{LGA1} \leqslant$ 3000km, while fort the second one (LGA2) the considered relation is 100km $\leqslant h_{LGA1} \leqslant$ 10000km. The presented method is quite robust, but in order to deal with the most sensitive variables (in particular, the epochs ε_k), multiple runs are performed, changing the components of the initial guess randomly, within reasonable bounds. The best obtained solution is characterized by a $\Delta v = 4.511$ km/s. In Table 7.2, the epochs related to the control nodes are reported.

Sims-Flanagan transcription method is a quite effective to find a low-medium fidelity optimized trajectory and the epochs of multiple gravity assists. Nevertheless, discontinuities in velocities are present in the low thrust modelling. The next step is the refinement of the found trajectory considering the complete low thrust dynamics and the referred optimal control

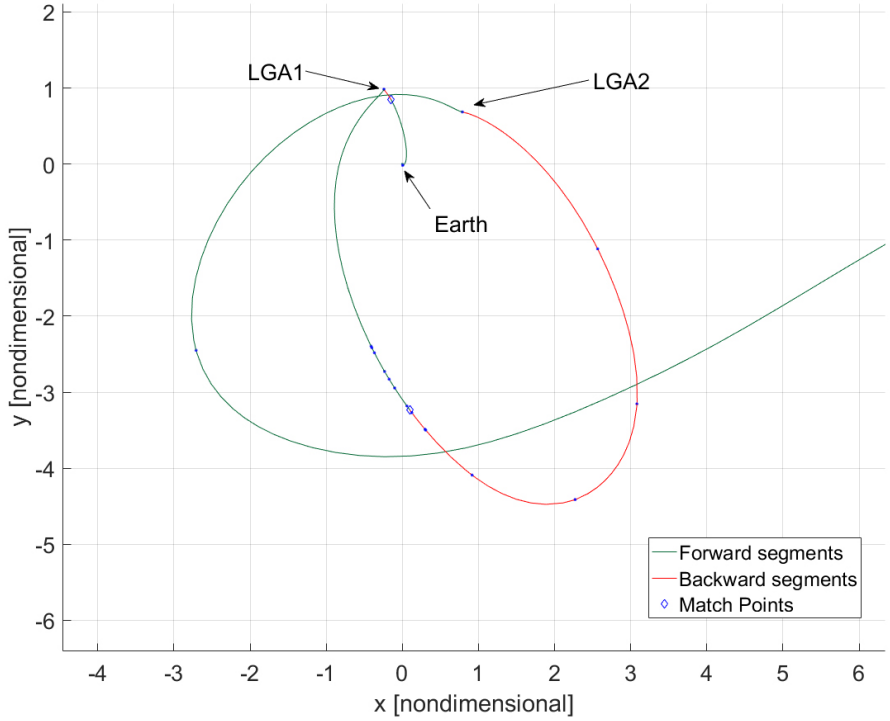

Figure 7.3: Earth-to-2008 EV5 Journey, in detail

problem.

Optimal Control: Shooting

The optimal control problem for the first journey from the Earth to the 2008 EV5 asteroid is subdivided into a series of 3 sub-problems, in which each different phase is analysed and solved through simple shooting. So, for each phase, the control vector is represented by

$$\boldsymbol{u}(\tau) = \begin{bmatrix} \alpha(\tau) \\ \beta(\tau) \\ P(\tau) \end{bmatrix} \tag{7.4}$$

whose components are, then, discretized and transcripted into a polynomial of degree q by using Chebyshev interpolation. So, the variables for the related NLP problem are the values of the controls at $q+1$ points, distributed according to Chebyshev points. In total, the number of variables is $n_u(q+1) = 3(q+1)$. As constraints, first of all the shooting method has to connect the last state vector of the previous phase to the final state vector of the

current phase. These values have been retrieved from the Sims-Flanagan method, as well as the reference epochs. Regarding to inequality constraints, the interpolating polynomials have to respect the bounds of their interval of existence (not only at nodes, but for every τ). If necessary, also conditions on the slopes can be includes (in particular, to limit the rate of variations of the control angles).

Phase 1: Earth-LGA1 This arc has been modelled as a continuous trajectory, in terms of position and velocity, by using Sims-Flanagan method. Once the spacecraft has been inserted in the right orbit, a coasting will lead to the next phase.

Phase 2: LGA1-LGA2 Knowing the epochs of the Lunar Gravity Assists, an optimal problem through single shooting is solved to connect the positions of the spacecraft at the two LGAs. Sims-Flanagan solution is used to obtain the starting state vector. Chebyshev interpolation of degree $q = 13$ is used. Figure 7.4 depicts the obtained solution, while Figure 7.5 illustrates the optimal profile for the control variables.

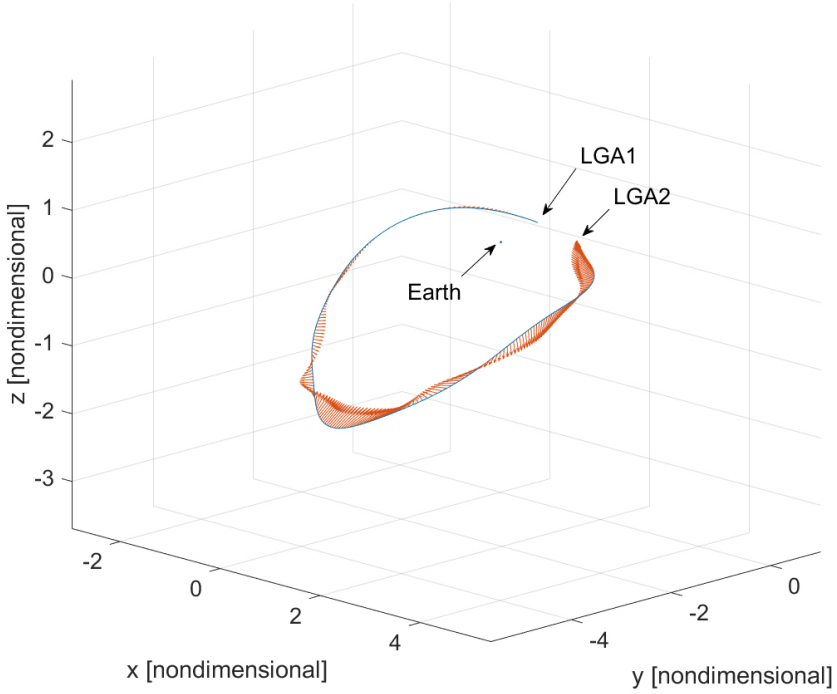

Figure 7.4: LGA1-LGA2 Phase

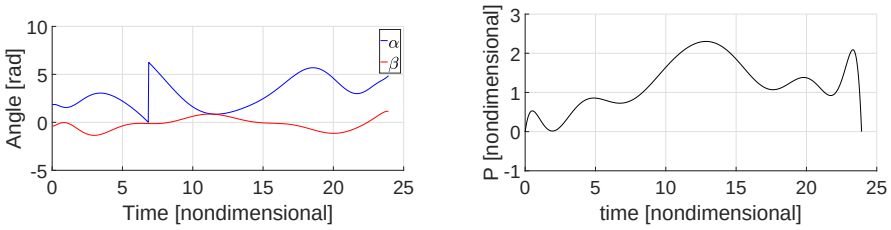

(a) Control Angles $\alpha(\tau)$ and $\beta(\tau)$ *(b) Power $P(\tau)$*

Figure 7.5: Journey 1: LGA1-LGA2 Phase - Control Variables, $q = 13$

Phase 3: LGA2-2008 EV5 The last phase of the first journey connects the second Lunar Gravity Assist to the target, the asteroid 2008 EV5. The optimal control problem is solved in order to have a rendezvous with the asteroid. Also in this case, control variables are modelled as interpolating polynomials of degree $q = 13$. Figure 7.6 illustrates the continuous trajec-

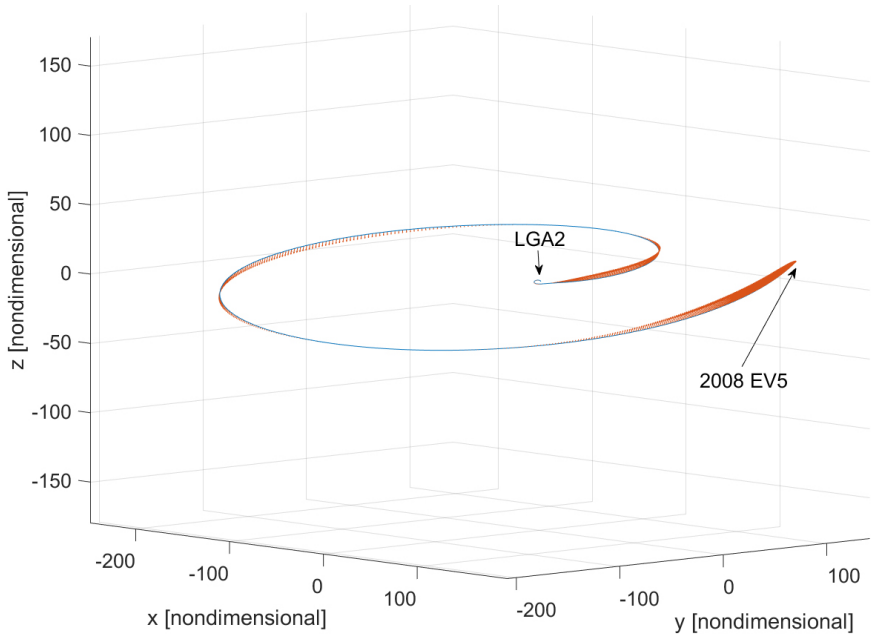

Figure 7.6: LGA2-2008 EV5 Phase

tory, together with the thrust vector. Figure 7.7 completes the obtained results.

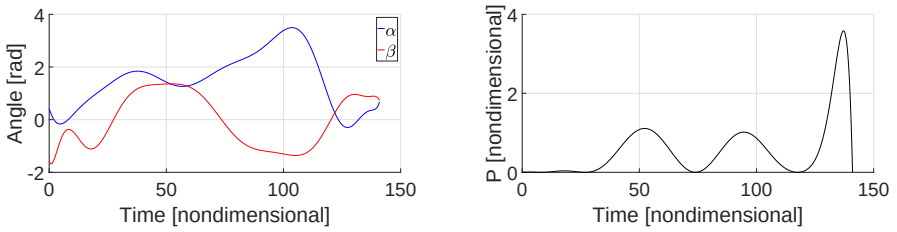

(a) Control Angles $\alpha(\tau)$ and $\beta(\tau)$ *(b) Power $P(\tau)$*

Figure 7.7: Journey 1: LGA2-2008 EV5 Phase - Control Variables, q = 13

7.1.2 Asteroid-to-NRO Trajectory

Sims-Flanagan Transcription Method

After the exploration of the asteroid and the collection of a small boulder from its surface, the spacecraft can proceed to come back into the Earth-Moon region. While the *double lunar swing-by* is a viable and known strategy that can be exploited to reach *Near-Earth Asteroids*, the structure of the way back has not been imposed *a priori*. Indeed, the structure including an Earth Gravity Assist has been after a preliminary run of Sims-Flanagan method (with 8 segments), in which the conditions for a gravity assist have not been imposed (equations (6.28) and (6.33)). After that, the solution has been refined including directly the above mentioned gravity assist.

Particularizing equation (7.1) for $n = 12$ segments, $k = 3$ control nodes and $p = 1$ gravity assist, it follows that the number of variables for the second journey is $N_v = 121$. Since the last point of the trajectory (at NRO insertion) is constrained to be equal to the state vector related to the attractive LCS departing from the aposelene of the NRO, a last Δv is not imposed (it would be null) and a slack variable can be removed. As a consequence, the number of considered variables is $N_v = 120$.

Regarding the constraints, in this case it is important to match a prescribed state vector at the beginning (departure from the asteroid) and at the end (NRO insertion) of the trajectory. So, equation (7.2) can be rewritten as

$$N_c = 6(1+1)+3(n-1)+(k-1)+4p+n+n+2k = 5n+4p+3k+8 \quad (7.5)$$

Particularizing for $n = 12$ (and considering that a last Δv is omitted), it follows $N_c = 80$. It is important to note that, during this and the following journey, the spacecraft mass is increased by the collected boulder: an additional estimated mass of $m_{boulder} = 15$ tons is included in the computation. The solution obtained by applying Sims-Flanagan transcription method is

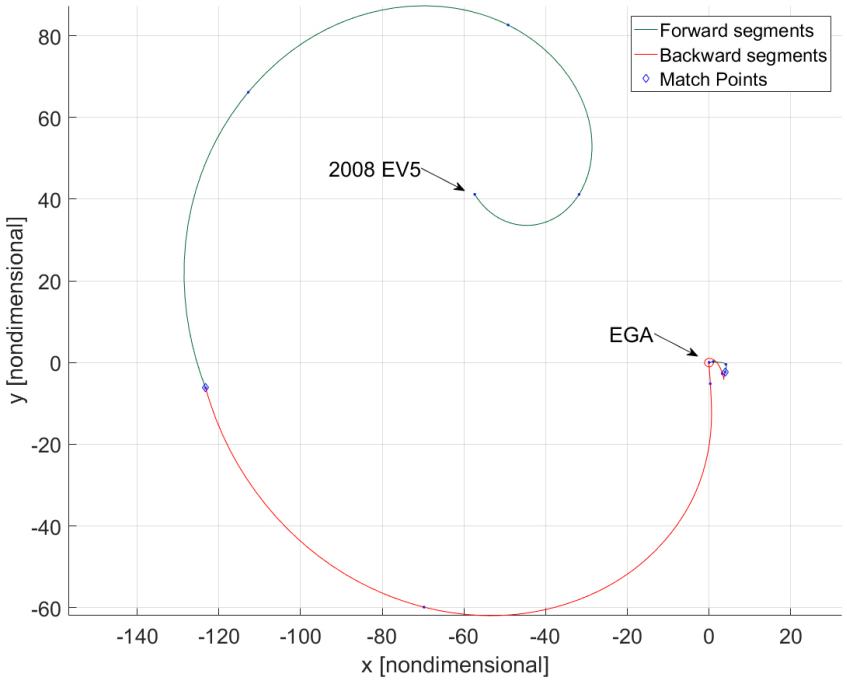

Figure 7.8: 2008 EV5-to-NRO Journey

Event	Date
2008 EV8 Departure	19 June 2024
EGA	23 June 2025
NRO Arrival	28 December 2025

Table 7.3: Journey 2: Epochs

presented in Figure 7.8. The NRO insertion phase (after the EGA) is presented with a higher level of detail in Figure (7.9). The sum of all the impulses within the second journey of the mission leads to a $\Delta v = 2.450$ km/s. Control nodes epochs, that are obtained by the optimization process, are summarized in Table 7.3.

Observation It is fundamental that all the quantities that enter in the NLP problem have derivative information. In general, it is true that, referring to equation (6.20), the quantities $\boldsymbol{x}_{\boldsymbol{r},in}$ and $\boldsymbol{x}_{\boldsymbol{r},fin}$ are dependent on epochs of the first and last control nodes of the journey, so $\boldsymbol{x}_{\boldsymbol{r},in}(\varepsilon_1)$ and $\boldsymbol{x}_{\boldsymbol{r},fin}(\varepsilon_k)$. While asteroid states (along with their derivatives) are known from the ephemeris database, particular attention must be paid for states

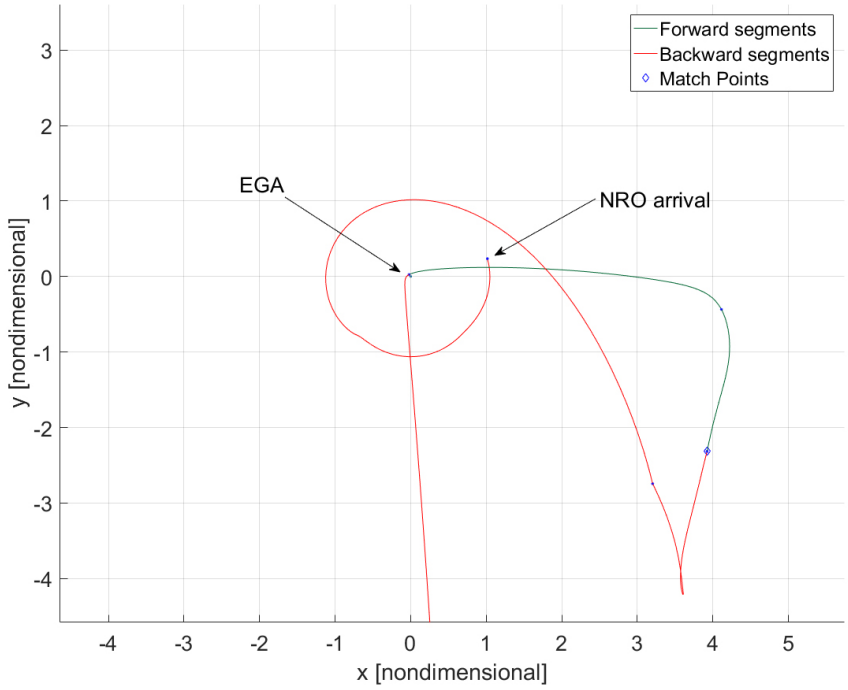

Figure 7.9: 2008 EV5-to-NRO Journey, in detail

related to periodic solutions. Indeed, since periodic solutions are epoch dependent within the N-body framework and $\boldsymbol{x}_{\boldsymbol{r},fin}(\varepsilon_k)$ represents the state (it must be propagated backward) of the attracting LCS that leads to the NRO at epoch $\varepsilon = \varepsilon_k$, a smooth $\boldsymbol{x}_{\boldsymbol{r},fin}(\varepsilon_k)$ profile must be considered. This is why a reference NRO (aposelene $r_a = 78000$ km) has been corrected within the N-body model over a large period (year 2025 and 2026) with a discrete time-step. The corrected initial states, along with the related states characterizing the attracting LCS, have been used to create a smooth database (by performing a piecewise cubic regression). Thanks to this information, the state at the final control node (and its derivative with respect to ε_k) can be known for every instant over the considered period.

Optimal Control

Also in this case, the overall journey is divided into its phases and a series of two sub-problems is solved.

Phase 1: 2008 EV5-EGA Within this phase, the control vector $\boldsymbol{u}(\tau)$, including the provided power and the angular spherical coordinates for the

direction, are written as interpolating polynomials of degree $q = 13$ by exploiting Chebyshev functions. Figure 7.10 depicts the optimal trajectory

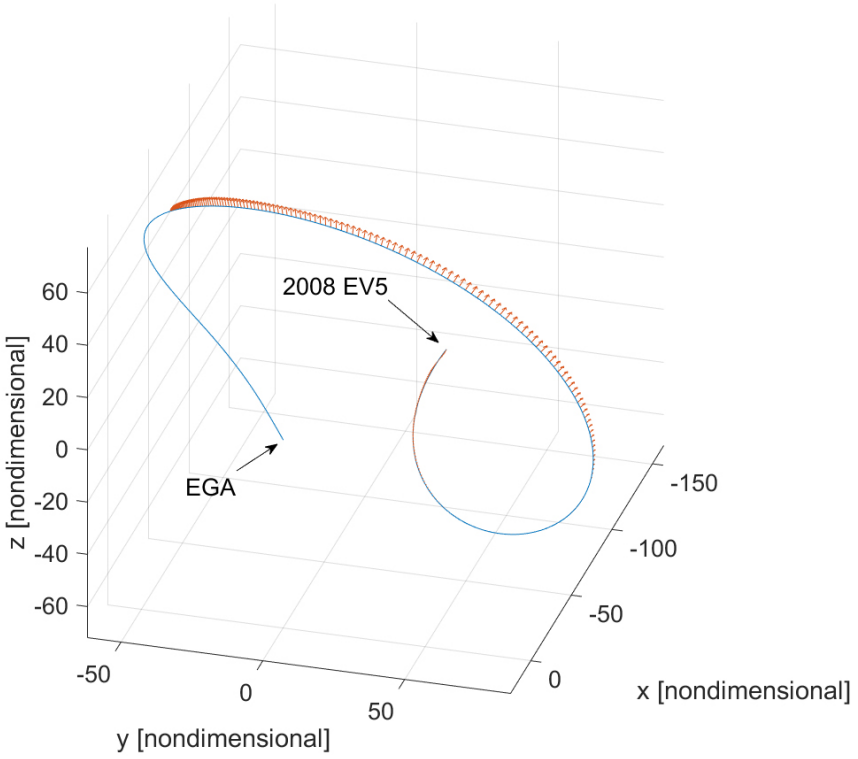

Figure 7.10: 2008 EV5-EGA Phase

departing from the asteroid and aiming to the EGA. Optimal control solution is completed by power and direction angles profiles, reported in Figure 7.11.

Phase 2: EGA-NRO For this phase of the journey, the degree of the interpolating polynomials has been increased to $q = 21$ in order to have more flexibility in the convergence. Besides, the single shooting takes place such that to reach the state at the middle of the last segment[1] (according to the Sims-Flanagan discretization), in order to have a period of coasting that drives the spacecraft into the NRO automatically. The solution is reported in Figure 7.12. The related profiles for $\alpha(\tau)$, $\beta(\tau)$ and $P(\tau)$ are illustrated in Figure (7.13).

[1]Last segment corresponds to the attracting LCS.

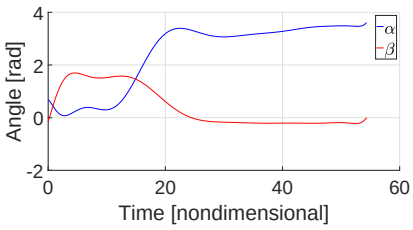

(a) Control Angles $\alpha(\tau)$ and $\beta(\tau)$

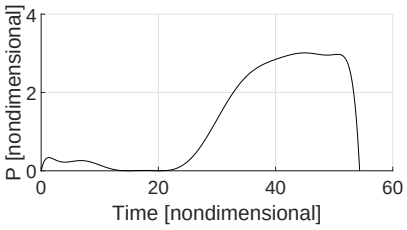

(b) Power $P(\tau)$

Figure 7.11: Journey 2: 2008 EV5-EGA Phase - Control Variables, q = 13

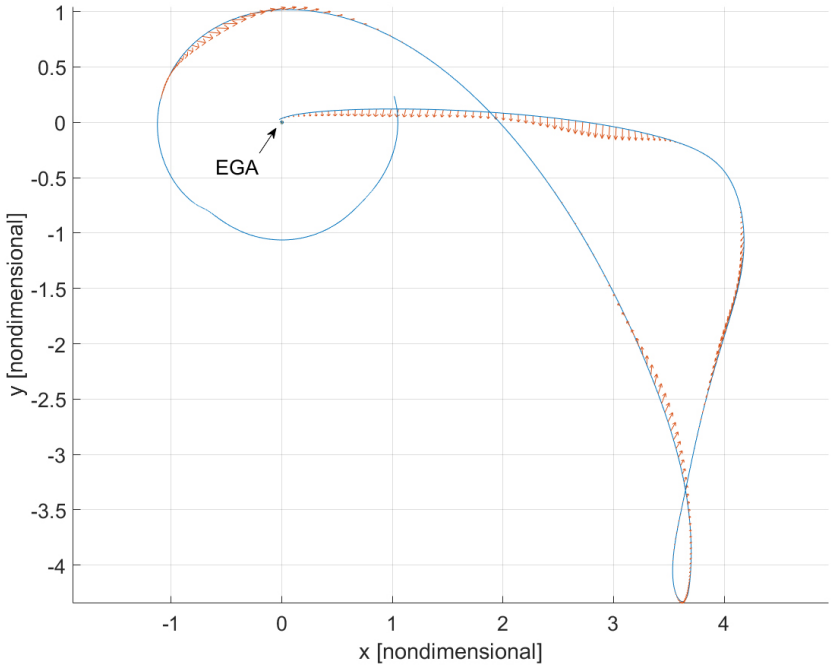

Figure 7.12: EGA-NRO Phase

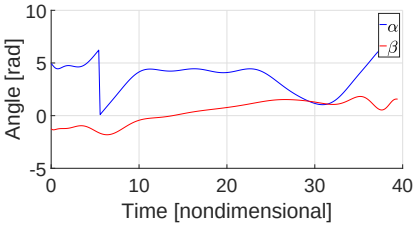

(a) Control Angles $\alpha(\tau)$ and $\beta(\tau)$

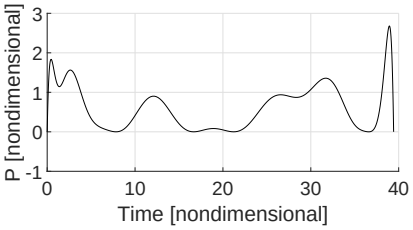

(b) Power $P(\tau)$

Figure 7.13: Journey 2: EGA-NRO Phase - Control Variables, q = 13

7.1.3 NRO-to-DRO Trajectory

Sims-Flanagan Transcription Method

The achieved NRO is unstable and it is used as a temporary location and as a gateway to move the collected boulder to a stable DRO. The journey under consideration is, actually, a single phase journey, since no intermediate gravity assists are necessary (so $p = 0$). Particularizing equation (7.5) for $n = 8$ segments and $k = 2$, it follows that the number of variables under consideration is $N_v = 53$ (a last Δv is omitted). In this case, it is more suitable to study the considered trajectory in the synodic frame by using the related equations of motions. The obtained solution (in the synodic frame) is presented in Figure 7.14. The departure from the NRO and the arrival

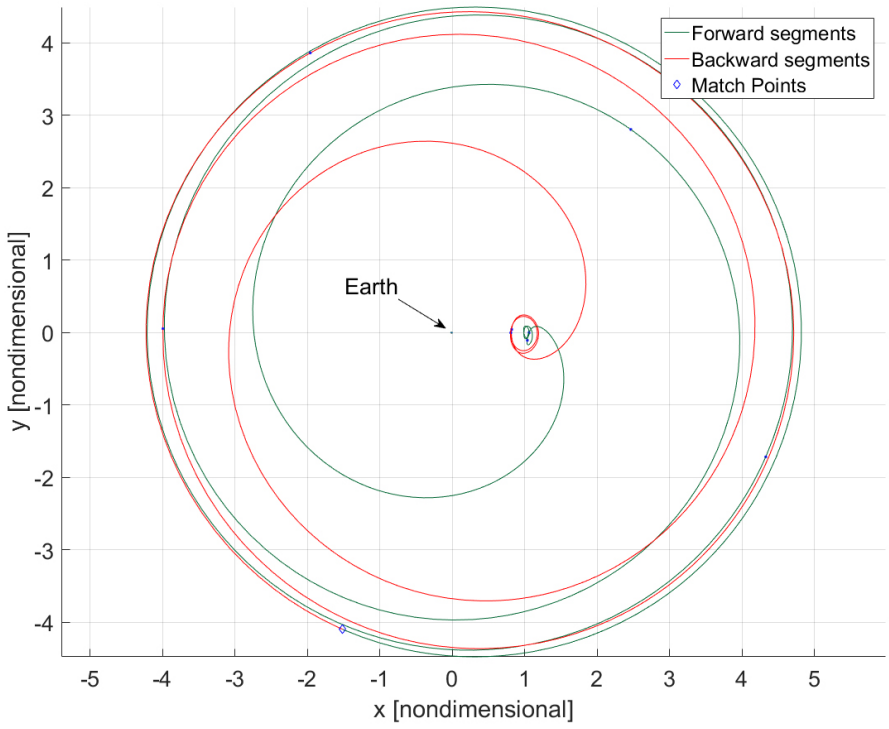

Figure 7.14: NRO-to-DRO Journey (Synodic Frame)

to the DRO can be appreciated in Figure 7.15. The obtained solution is characterized by a total $\Delta v = 0.550$ km/s; the departing and the arrival dates of the journey are presented in Table 7.4.

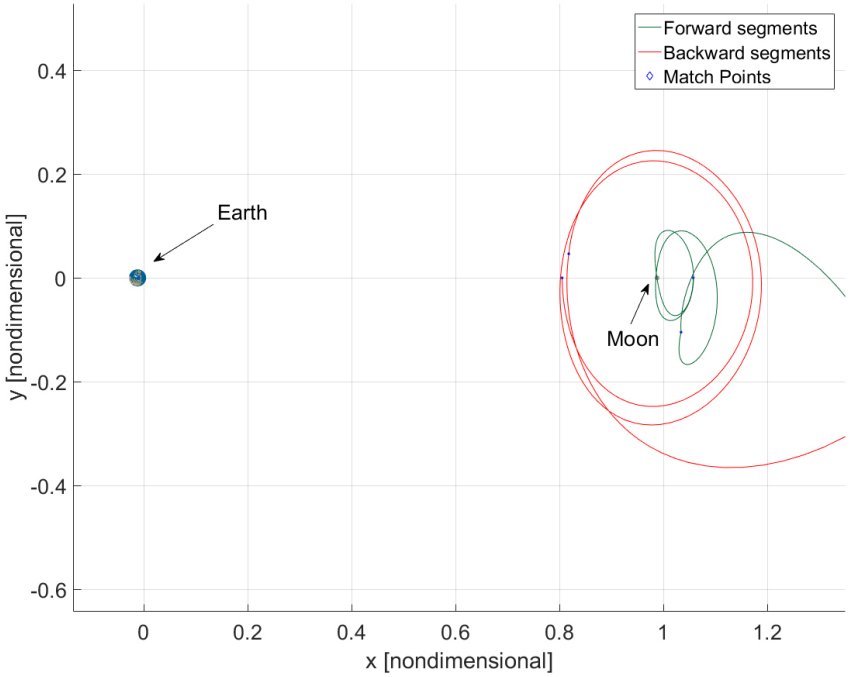

Figure 7.15: NRO-to-DRO Journey, in detail (Synodic Frame)

Event	Date
NRO Departure	13 February 2026
DRO Arrival	15 October 2026

Table 7.4: Journey 3: Epochs

Observation Derivative information with respect to epochs is computed numerically when N-body equations of motions are expressed in the synodic frame. As already seen for the second journey, also in this case it is very important to rely on a smooth database describing the states of the NRO repulsive LCS and of the arriving DRO. For this reason, NRO initial conditions (along with associated repulsive LCS) are corrected over the first half of year 2026. Similarly, initial conditions of a resonant 2:1 DRO are computed over the period from 1-Jul-2026 to 1-Mar-2027.

Optimal Control

In order to solve the optimal control problem, the trajectory has been studied by using equations of motion with respect to an inertial frame an relative to the Earth (as all the other optimal controls problem). So, the shooting for

the optimal control problem has been carried out by converting the initial guess (found by using Sims-Flanagan method) to the inertial frame and by connecting the repulsing LCS (related to the NRO departure) to the final DRO. To have a more precise convergence, the single shooting has been split and an intermediate node (equal to the initial state of the fifth segment, according to Sims-Flanagan transcription) has been considered, defining, hence, a multiple shooting scheme where control variables have been described as polynomials of degree $q = 13$ within each of the two segments. Figure 7.16 depicts the obtained solution (in the inertial frame). For the sake of completeness, profiles of the provided power and of angular

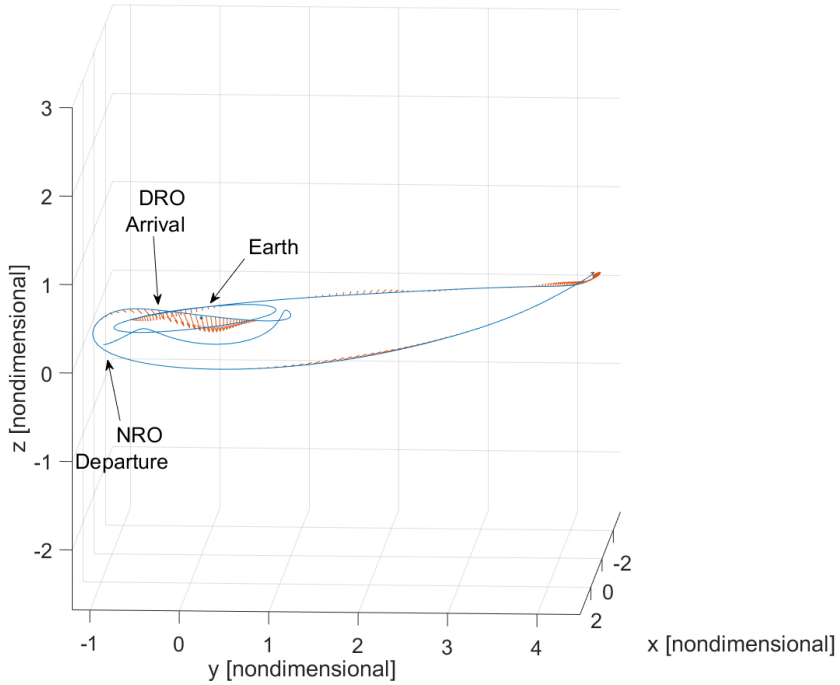

Figure 7.16: NRO-DRO Phase

coordinates of the thrust direction are reported in Figure 7.17

7.2 Conclusions on Results

All the simulations are performed with a view to minimize the cost in terms of propellant, hence to maximize the final mass of the spacecraft. Table 7.5 reports the most important figures obtained from the simulation. As already noted, it is important to stress the fact that an additional boulder

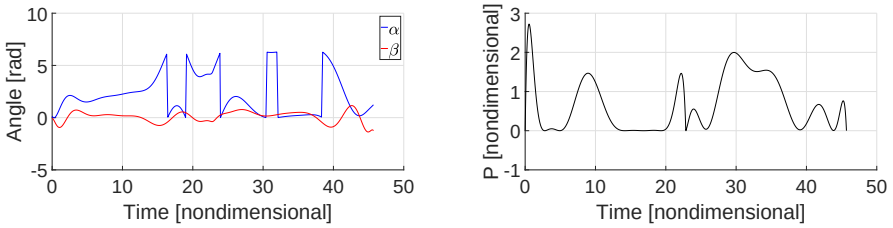

(a) Control Angles $\alpha(\tau)$ and $\beta(\tau)$ *(b) Power $P(\tau)$*

Figure 7.17: Journey 3: NRO-DRO Phase - Control Variables, q = 13

	Sims-Flanagan		**Optimal Control**	
Journey	Δv [km/s]	m_{fin}/m_0	m_{fin}/m_0	Phase
Earth-to-2008 EV5	4.511	0.891	1	Earth-LGA1
			0.960	LGA1-LGA2
			0.852	LGA2-2008 EV5
2008 EV5-to-NRO	2.450	0.656	0.756	2008 EV5-EGA
			0.678	EGA-NRO
NRO-to-DRO	0.550	0.605	0.621	NRO-DRO

Table 7.5: Results

mass ($m_{boulder}$ = 15 tons) is considered in the computation of the trajectories. What it is possible to note is that the mass ratios computed by using a Sims-Flanagan method or an optimal control-based approach are $(m_{fin}/m_0)_{S-F} = 0.605$ and $(m_{fin}/m_0)_{OC} = 0.621$, respectively. The two values are quite in agreement, with the optimal control figure that is slightly less that the Sims-Flanagan counterpart. This is reasonable considering the fact that no mass variation is taken into account within the Sims-Flanagan framework (it could be included in the formulation). The results are quite coherent with the ones reported in a preliminary Mission Design Description of *ARM* mission (obtained by using MALTO, *Mission Analysis Low-Thrust Optimizer*, a NASA software based on Sims-Flanagan approach).

Chapter 8

Attitude Strategies

In this chapter some attitude considerations, coupled with orbital mechanics aspects in multi-body regimes, are discussed. The focus about this topic arises directly from the analysis of the Asteroid Redirect Mission (ARM) scenario, simulated in Chapter 7. Indeed, the NRO and DRO environments are extensively exploited within the context of the mission. It could be interesting to study the behaviour of attitude dynamics in these Non-Keplerian orbits.

The main aim of this analysis is to leverage the free natural attitude dynamics (under the perturbation of Earth and Moon gravity gradient disturbance torques) along these periodic solutions in order to minimize the active control. First, the NRO environment is considered, trying to search for initial configurations that allow to maintain a bounded mismatch with the LVLH frame of the orbit. Then, DRO environment is analysed and some period attitude-orbit solutions in multi-body regimes are presented.

8.1 Attitude in NRO

The first coupled analysis involves the study of the spacecraft attitude in a NRO. Referring to the ARM simulation carried out in Chapter 7, NROs have a significant role, since one orbit of this family is used as an intermediate stage and as a gateway before the final transfer that drives the spacecraft to a DRO. From the simulation, it clearly appears that the waiting time to be spent in the NRO is a little more than one month. The target NRO has been fixed throughout the simulation: it corresponds to a NRO with aposelene $r_a = 78000$ km and it is, actually, a $4:1$ resonant NRO, meaning that the NRO orbital period is 1/4 of the synodic period of the Moon (that is, approximately, 29.53 days). Between the moments of arrival and of departure

within the ARM simulation framework, the spacecraft can orbit the targeted NRO without remarkable station-keeping issues (in practice, some corrective manoeuvres are likely to be performed). Figure 8.1 depicts the targeted NRO.

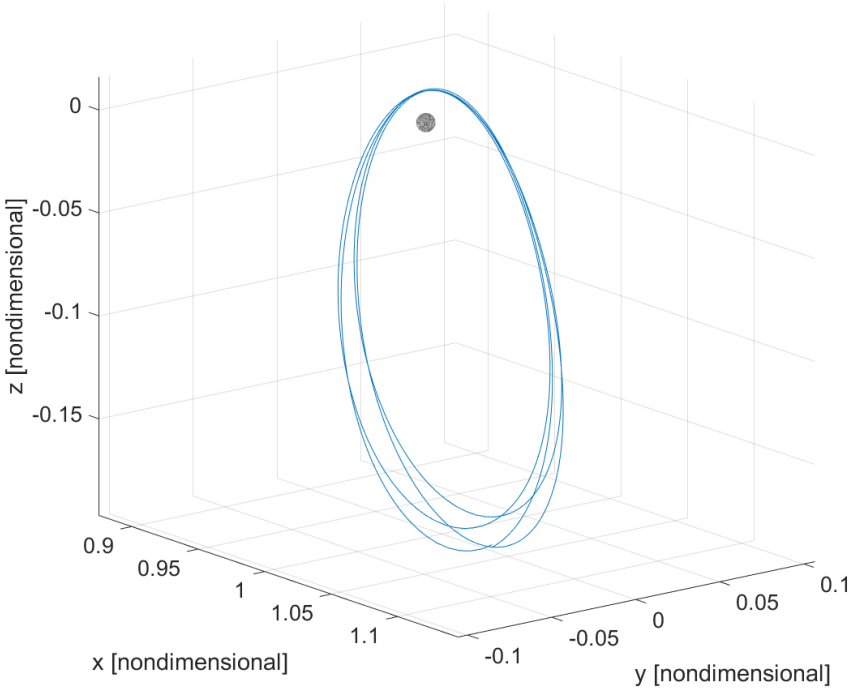

Figure 8.1: 4:1 Resonant NRO

8.1.1 The LVLH Frame

In general, a NRO is characterized by a complicated three-dimensional shape and this increases the complexity in the search for some interesting periodic patterns from the attitude point of view. A configuration that is worth to be studied is the one dictated by the NRO LVLH frame. The Local Vertical-Local Horizon coordinate system (denoted as $\check{x}\check{y}\check{z}$) for a NRO is defined (for every time τ) such that the $\check{x}$-axis is directed as the spacecraft position vector relative to the Moon (therefore, outgoing and radial), the $\check{z}$-axis points towards the instantaneous orbital angular momentum and the $\check{y}$-axis completed the right-handed triad.

It would be interesting to search for configurations that grant the spacecraft attitude to follow the LVLH kinematics or that, at worst, have a bounded mismatch with the LVLH frame. This would translate into a space-

craft that, from the attitude point of view, moves in accordance with the LVLH. Such an attitude would be very interesting in particular if pointing requirements towards the Moon are asked.

By building up the profile in time of the LVLH frame direct cosine matrix (that corresponds to the transformation matrix $\mathbf{A}_{LVLH/Syn}$, allowing the passage from the synodic frame to the LVLH frame), it is possible to recover the angular velocity profile $\boldsymbol{\omega}_{LVLH/Syn}$ that satisfies the LVLH frame kinematics, by exploiting:

$$\dot{\mathbf{A}}_{LVLH/Syn} = -\left[\boldsymbol{\omega}_{LVLH/Syn}\right]^{\wedge} \mathbf{A}_{LVLH/Syn} \tag{8.1}$$

where $\boldsymbol{\omega}_{LVLH/Syn}$ represents the angular velocity (expressed in the LVLH frame) of the LVLH frame with respect the synodic frame. Surely, it would be more interesting to recover the angular velocity of the LVLH frame with respect to the inertial space. In order to do so, also the profile in time of the synodic frame direct cosine matrix is required: the matrix $\mathbf{A}_{Syn/N}$ can be reconstructed from ephemerides evaluation. Thanks to this, the direct cosine matrix of the LVLH frame with respect to the inertial space can be recovered: simply applying transformation matrices properties, it follows

$$\mathbf{A}_{LVLH/N} = \mathbf{A}_{LVLH/Syn}\mathbf{A}_{Syn/N} \tag{8.2}$$

By applying the analogous version of equation (8.1), the profile of the angular velocity (expressed in the LVLH frame) of the LVLH frame with respect the inertial frame (that is, $\boldsymbol{\omega}_{LVLH/N}$) can be recovered. The value of $\boldsymbol{\omega}_{LVLH/N}$ is reported in Figure 8.2 over an entire synodic period of the 4:1 resonant NRO. In order to follow perfectly the LVLH frame kinematics, a spacecraft must have the angular velocity profile shown in Figure 8.2. To see if this is possible in the NRO environment, different initial configurations have been considered.

8.1.2 Parametric Analysis

Different inertia conditions for the spacecraft have been considered in order to analyse the response in attitude. The performed parametric study has been characterized by the following elements:

- Varying inertia properties about each one of the main axes of inertia. For each axis, a range going from $J_{min} = 10^4$ kg m^2 to $J_{max} = 4 \cdot 10^4$ kg m^2 has been considered, allowing to obtain different combinations of the K_x, K_y and K_z values, where

$$K_x = \frac{J_z - J_y}{J_x}, \qquad K_y = \frac{J_z - J_x}{J_y}, \qquad K_z = \frac{J_y - J_x}{J_z}.$$

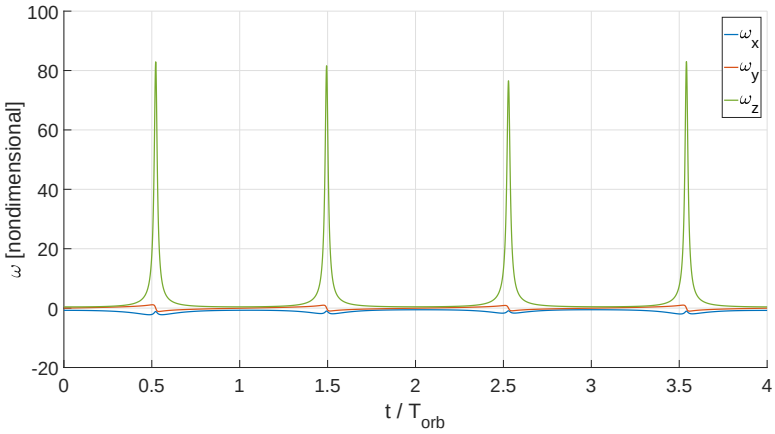

Figure 8.2: NRO LVLH Angular Velocity, with respect inertial space

- Prescribed initial condition for attitude kinematics, dictated by the perfect alignment with the LVLH frame.

- Prescribed initial condition for attitude dynamics, dictated by the initial values of the LVLH frame angular velocity (with respect to the inertial space).

The simulation suggests that there are not configurations of inertia properties that allows to follow the LVLH frame kinematics, given the prescribed initial velocity and orientation. Indeed, by using a classical Pitch-Roll-Yaw [1] Euler sequence, it is possible to note that there are always two angles that are characterized by a drift, making impossible a synchronous rotation of the spacecraft with the LVLH frame. As a representative selection, Figure 8.3 shows the results for the case $K_x = 0.666$, $K_y = 0.8$ and $K_z = 0.285$. The explanation of the phenomenon is quite simple and it is due to the enhanced gravity gradient torque at the periselene of the NRO: indeed, near this point the gravity gradient due to the Moon becomes suddenly three order of magnitude larger and it is able to destabilize irretrievably the spacecraft attitude.

[1] The angular orientation of a xyz frame can be described with reference to a XYZ frame through the pitch(ϕ), roll(θ) and yaw(ψ) angles. The Pitch-Roll-Yaw sequence is characterized by the first rotation is around the Z ($= z_1$) axis through the pitch angle ϕ. This takes X into x_1 and Y into y_1. The second rotation is around the y_2 ($= y_1$) axis through the roll angle θ. This carries x_1 and z_1 into x_2 and z_2, respectively. The third and final rotation is around the x ($= x_2$) axis through the yaw angle ψ, which takes y_2 into y and z_2 into z.

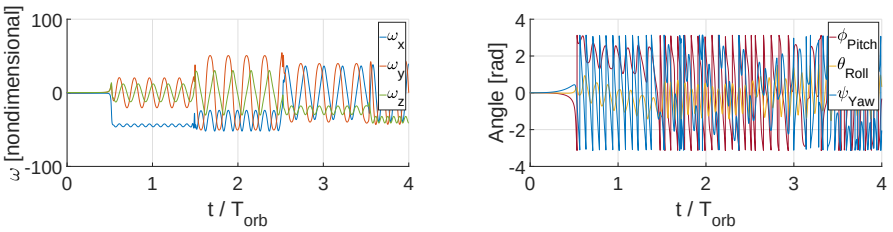

(a) Absolute Angular Velocity $\boldsymbol{\omega}_{b/N}$ *(b) Euler Angles, with respect to LVLH*

Figure 8.3: Attitude in NRO ($K_x = 0.666$, $K_y = 0.8$ and $K_z = 0.285$)

The only case in which one single angle drift is observed is for completely symmetric spacecraft. In this case, the spacecraft is not affected gravity gradient torque (it cancels out) and the angular velocity remains constant. Figure 8.4 depicts this case.

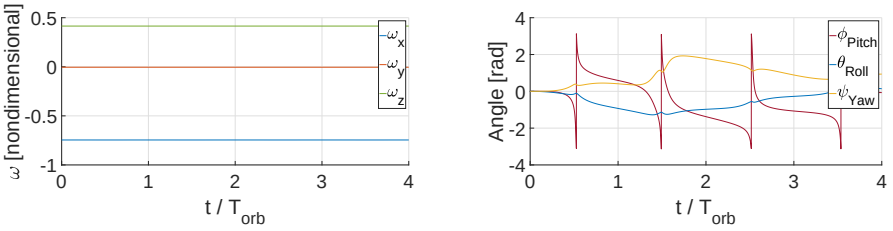

(a) Absolute Angular Velocity $\boldsymbol{\omega}_{b/N}$ *(b) Euler Angles, with respect to LVLH*

Figure 8.4: Attitude in NRO (Symmetric Spacecraft)

Concluding, the simulations suggest that some active control is desirable if the motion of the NRO LVLH frame has to be followed. The magnitude of the control is not very large: the order of magnitude of the angular momentum can be seen in Figure 8.5 (inertial components). In the same Figure, also the components of the perturbing angular accelerations are depicted.

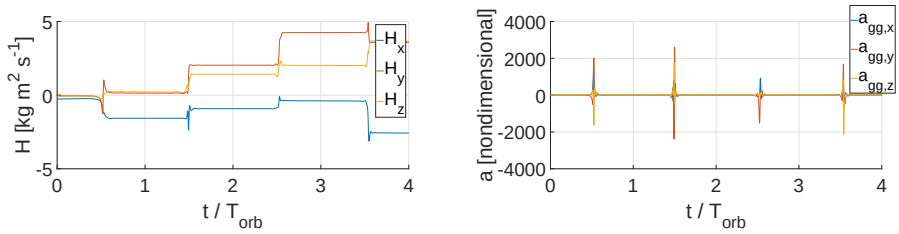

(a) Angular Momentum $\mathbf{H}$ *(b) Disturbance Torque Accelerations*

Figure 8.5: Angolar Momentum and Disturbance Torque Accelerations in NRO ($K_x = 0.666$, $K_y = 0.8$ and $K_z = 0.285$)

8.2 Attitude in DRO

The starting point for the attitude analysis in DRO is offered by the targeted final orbit coming from the ARM simulation. It consists in a 2:1 resonant DRO, meaning that the orbital period is 1/2 of the synodic period of the Moon. In Figure 8.6 the considered orbital path is illustrated. It is important to note how the periodicity is recovered after a synodic period.

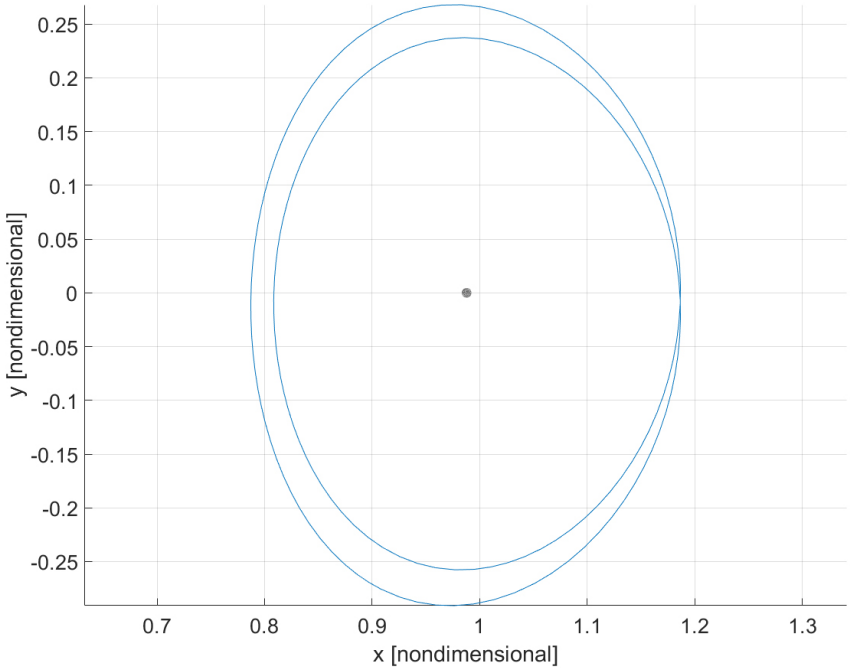

Figure 8.6: 2:1 Resonant DRO

The geometry of the problem is, in this case, less complex than the NRO counterpart. The motion in a DRO can be considered planar (out-of-plane motion is, actually, present when multi-body regime and the actual motion of the Moon are considered) and it suggests to search for attitude-orbital periodic solutions. Assuming a spacecraft oriented as the DRO LVLH frame at the initial instant, it could be interesting to identify for which conditions the spacecraft performs an integer number of rotations (with reference to the synodic frame) about its z-axis per orbital period. Actually, this is the same path that has been developed in [6], with the study of attitude-orbital periodic solutions in the CR3BP environment. It clearly appears that such a problem is governed by the inertia ration $(J_x - J_y)/J_z$ that appears in the z-projection of Euler equations.

8.2.1 Attitude-Orbital Periodic Solutions

In this case, a parametric study has been adopted in order to find, when K_z is varied, different values of the z-component of spacecraft angular velocity (relative to the synodic frame) $\boldsymbol{\omega}_{b/Syn}$ such that it grants an integer number of rotations per orbital period (with respect the synodic frame). The main considered elements for the analysis are:

- Varying inertia properties through a variation of the K_z term. A range going from $K_{z,min} = 0.1$ to $K_{z_max} = 1$ is considered.
- Prescribed initial condition for attitude kinematics, dictated by perfect alignment with the DRO LVLH frame.

The value of the z-component of spacecraft angular velocity (relative to the synodic frame) $\boldsymbol{\omega}_{b/Syn}$ is found via correction scheme, imposing that a number N (where $N = -2, -1, 0, 1$ or 2) of rotations are performed per orbital period.

The analysis has led to the definition of Figure 8.7. It is possible to

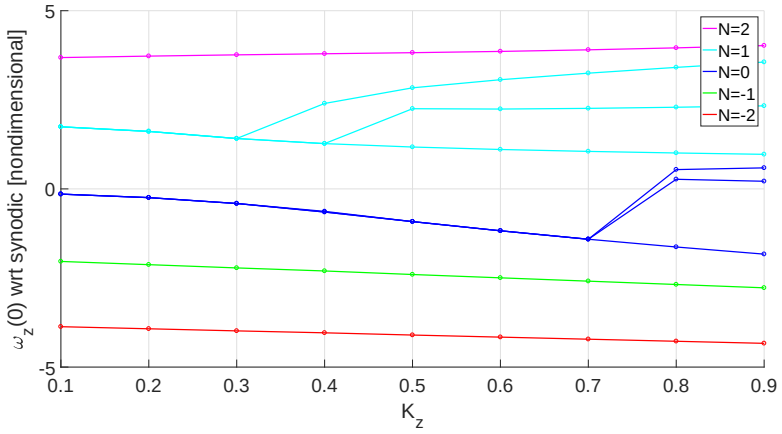

Figure 8.7: Attitude-Orbital Periodic Solutions for 2:1 Resonant DRO

note that, for $0.1 \leqslant K_z \leqslant 0.3$, one single initial angular velocity exists such that it implies a specific number N of spacecraft rotations (with respect the synodic frame) per orbital period. For $K_z > 0.3$, a bifurcation for the branch $N = 1$ appears, meaning that multiple values of the initial angular velocity can grant that number of spacecraft rotations. Similarly, a bifurcation for $N = 0$ is observed for $K_z > 0.7$.

It is interesting to note how solutions characterized by low gyroscopic stiffness are more likely to be destabilized in a long run propagation, due

to the rise of out-of-plane DRO segments and, therefore, of all the three components of the gravity gradient torque. Figures 8.8 and 8.9 are a example of this situation, valid for $K_z = 0.8$ and characterized by an initial angular velocity that should grant $N = 1$.

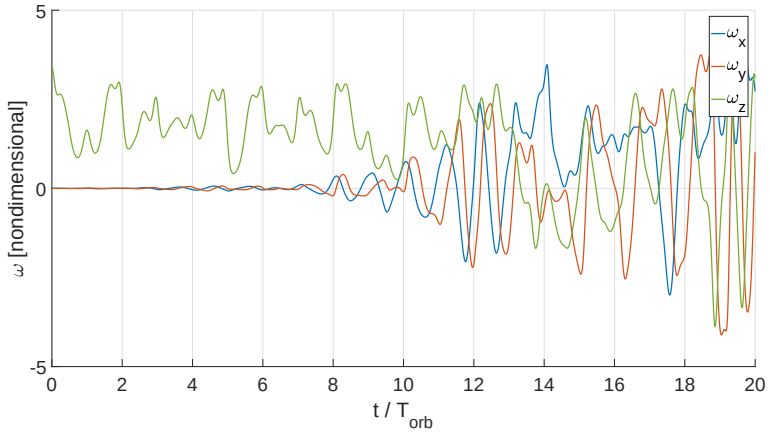

Figure 8.8: Angular Velocity with respect Synodic Frame, $\boldsymbol{\omega}_{b/Syn}$

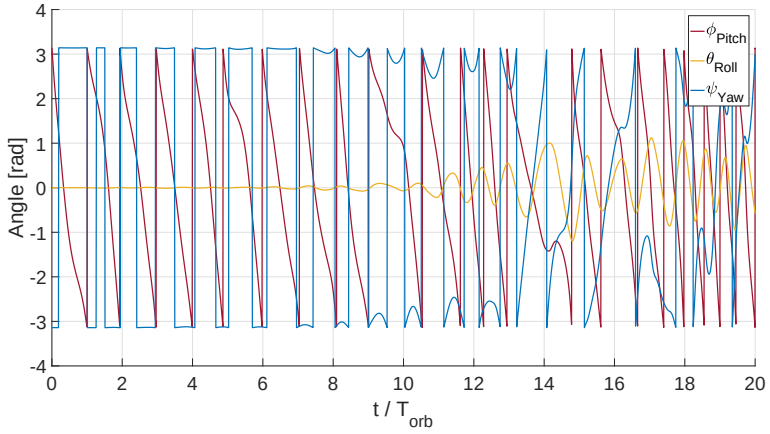

Figure 8.9: Euler Angles with respect to Synodic, $K_z = 0.8$ (propagation over 10 synodic periods)

Chapter 9

Conclusions

The main objective of the present work is the search for a higher level of accuracy in mission analysis design at an academic level. For this reason, an improvement of classical orbital mechanics models - RTBP and CRTBP - is presented: the effects of multiple gravity fields are included in the dynamical formulation to describe the equations of motion of a particle characterized by negligible mass. The N-body model equations of motion are presented with respect two different coordinate systems. Some basic notions about spacecraft attitude dynamics are recalled and the attitude-orbital mechanics coupling is clarified. The main steps of the validation process for the models are presented.

The discussion about numerical methods for dynamical models is presented, leading directly to the presentation of corrections schemes and basic concepts of optimization problems. Trajectory design is discussed in detail, with particular reference to low thrust trajectory model. Low thrust trajectory optimization is handled by presenting two direct optimization schemes: a low-medium fidelity tool, inspired to a classical Sims-Flanagan transcription method, and a high fidelity tool, considering the entire actual dynamics of the problem and based on an optimal control approach exploiting Chebyshev interpolation. The two presented methods are applied to a real mission scenario, offering coherent results.

The increasing interest for the Earth-Moon system and the exploitation of its Non-Keplerian orbits pushes towards the design of viable attitude strategies, capable of minimizing the active control. Attitude-orbital coupling is faced in NRO and DRO environments. While complex challenges seem to suggest that active control is required for the former, interesting attitude-orbital periodic solutions are computed for the latter.

9.1 Future Work

Multi-body regimes fundamentals are presented throughout this work. All the simulations have been carried out considering the gravity fields of the Earth, the Moon and the Sun. Higher level of accuracy can be attained including additional bodies of the Solar System, introducing, yet, new challenges in the numerical methods formulation. In order to count on a more and more precise model, also the effects of the solar radiation pressure could be considered. This aspect involves not only the orbital mechanics section, but also the attitude one.

Regarding the optimization processes, due to convergence challenges (that have been solved increasing gradually the size of the problems), it could be nice to create a global optimization algorithm before the application of Sims-Flanagan transcription method. The main aim of this passage would be a preliminary detection of a good candidate initial guess.

Concerning the attitude-orbital coupled study, even if the behaviour of the N-body models can be hardly predictable, it would be nice to extend the presented analysis to a wider range of periodic solution of the same families, and not only.

Bibliography

[1] Navigation and Ancillary Information Facility (NAIF), SPICE, https://naif.jpl.nasa.gov/naif/toolkit.html.

[2] J. P. Berrut and L. N. Trefethen. Barycentric lagrange interpolation. resreport, Society for Industrial and Applied Mathematics, 2004.

[3] J. T. Betts. A survey of numerical methods for trajectory optimization, Aug. 1998.

[4] J. T. Betts. *Practical Methods for Optimal Control Using Nonlinear Programming.* Society for Industrial and Applied Mathematics, 2001.

[5] N. E. Bradley. *Initial Guess and Optimization Strategies for Multi-Body Space Trajectories with Application to Free Return Trajectories to Near-Earth Asteroids.* PhD thesis, The University of Texas at Austin, Aug. 2014.

[6] L. Bucci. Coupled orbital-attitude dynamics of large structures in non-keplerian orbits. Master's thesis, Politecnico di Milano, 2015.

[7] J. B. Caillau, B. Daoud, and J. Gergaud. Minimum fuel control of the planar circular restricted three-body problem. *Celestial Mechanics and Dynamical Astronomy*, Volume 114, Issue 1-2, pp. 137-150, Oct. 2012.

[8] M. D. Canon, C. D. Cullum, and E. Polak. *Theory of Optimal Control and Mathematical Programming.* McGraw Hill, 1970.

[9] S. R. Carnà. Mission analysis for the ARDENT project. Technical report, Politecnico di Milano, 2016.

[10] A. Colagrossi. Coupled dynamics around irregular-shaped bodies with enhanced gravity field modelling. Master's thesis, Politecnico di Milano, 2014.

[11] H. D. Curtis. *Orbital Mechanics for Engineering Students*. Butterworth-Heinemann, 2013.

[12] D. A. Dei Tos. Automated trajectory refinement of three-body orbits in the real solar system model. Master's thesis, Politecnico di Milano, 2014.

[13] J. Demeyer and P. Gulfil. Tranfer to distant retrograde orbits using manifold theory. *Journal of Guidance, Control and Dynamics*, Volume 30, No. 5, 2007.

[14] D. H. Ellison. Automated planetary satellite tour planning with a novel low-thrust direct transcription method. Master's thesis, University of Illinois at Urbana-Champaign, 2013.

[15] D. H. Ellison, J. A. Englander, M. T. Ozimek, and B. A. Conway. Analytical partial derivative calculation of the Sims-Flanagan transcription match point constraints. In *AAS 14-310*, 2014.

[16] J. A. Englander, M. A. Vavrina, and D. Hinckley. Global optimization of low-thrust interplanetary trajectories subject to operational constraints. In *ASS 16-239*, 2016.

[17] E. S. Gawlik, P. C. Du Toit, J. E. Marsden, and S. Campagnola. Lagrangian coherent structures in the elliptic restricted three-body problem. resreport, Caltech, 2008.

[18] D. J. Grebow, M. T. Ozimek, K. C. Howell, and D. C. Folta. Multi-body orbit architectures for lunar south pole coverage. In *AAS 06-179*, 2006.

[19] D. Guzzetti. *Coupled Orbit-Attitude Mission Design in the CIrcular Restricted Three-Body Problem*. PhD thesis, Purdue University, May 2016.

[20] D. Guzzetti, E. M. Zimovani, K. C. Howell, and D. C. Davis. Station-keeping analysis for spacecraft in lunar near rectilinear halo orbits. In *AAS 17-395*, 2017.

[21] G. Haller. Lagrangian Coherent Structures, 2015.

[22] G. K. Harden. Automated patch point placement for autonomous spacecraft trajectory targeting. Master's thesis, Purdue University, Aug. 2013.

[23] G. W. Hill. *Collected Mathematical Works of G. W. Hill.* Carnegie Institution of Washington, 1905.

[24] K. C. Howell and J. V. Breakwell. Almost rectilinear halo orbits. *Celestial Mechanics and Dynamical Astronomy*, Volume 32, Issue 1, pp 29-52, 1984.

[25] D. Izzo. Lambert's problem for exponential sinusoids. Technical report, Advanced Concepts Team, ESA/ESTEC, 2005.

[26] D. Izzo. Advances in global optimisation for space technology and science. In *25th International Symposium on Space Technology and Science*, 2006.

[27] M. P. Kelly. Transciption methods for trajectory optimization. resreport, Cornell University, 2015.

[28] W. S. Koon, M. W. Lo, J. E. Marsden, and S. D. Ross. *Dynamical Systems, the Three-Body Problem and Space Mission Design.* Interdisciplinary Applied Mathematics, 2006.

[29] S. M. Marsh and K. C. Howell. Double lunar swingby trajectory design. Technical report, Purdue University, 1988.

[30] G. Mengali and A. A. Quarta. *Fondamenti di meccanica del volo spaziale.* Pisa University Press, 2014.

[31] X. Ming and X. Shijie. Exploration of distant retrograde orbits around moon. *Acta Astronautica*, 2009.

[32] C. Moore. Technology development for nasa‘s asteroid redirect mission. National Aeronautics and Space Administration.

[33] NASA. Asteroid redirect mission (ARM) formulation assessment and support team (FAST) final report. techreport, NASA/TM-2016-219011, 2016.

[34] NASA. Asteroid redirect robotic mission (ARRM), July 2016. Mission Design Description.

[35] I. Newton. *Philosophiae Naturalis Principia Mathematica.* University of California Press, 1999.

[36] M. T. Ozimek. *Low-Thrust Trajectory Design and Optimization of Lunar South Pole Coverage Mission.* PhD thesis, Purdue University, May 2010.

[37] T. A. Pavlak. Mission design applications in the earth-moon system: Transfer trajectories and stationkeeping. Master's thesis, Purdue University, May 2010.

[38] T. A. Pavlak. *Trajectory Design and Orbit Maintenance Strategies in Multi-Body Dynamical Regimes.* PhD thesis, Purdue University, May 2013.

[39] T. A. Pavlak and K. C. Howell. Strategy for optimal, long-term stationkeeping of libration point orbits in the earth-moon system. Technical report, American Institute of Aeronautics and Astronautics, 2012.

[40] A. E. Petropoulos and J. M. Longuski. Automated design of low-thrust gravity-assist trajectories. In *AIAA-2000-4033*, 2000.

[41] H. Poincaré. *Les Methodes Nouvelles de la Mecanique Celeste.* Gauthier-Villars, 1893.

[42] P. J. Prince and J. R. Dormand. High order embedded Runge-Kutta formulae. *Journal of Computational and Applied Mathematics*, Volume 7, Issue 1, pp. 67-75, March 1981.

[43] R. E. Pritchett. Numerical methods for low-thrust trajectory optimization. Master's thesis, Purdue University, Aug. 2016.

[44] A. V. Rao. A survey of numerical methods for optimal control. In *AAS 09-334*, 2009.

[45] H. Schaub and J. L. Junkins. *Analytical Mechanics of Aerospace Systems.* AIAA Education Series, Jan. 2002.

[46] A. M. Schinder. Optimized low thrust trajectories compared to impulsive trajectories for interplanetary mission.

[47] C. J. Scott. *Transfer and Capture into Distant Retrograde Orbit.* PhD thesis, The Pennsylvania State University, 2010.

[48] C. R. Short and K. C. Howell. Lagrangian coherent structures in various map representations for application to multi-body gravitational regimes. *Acta Astronautica*, 2013.

[49] J. A. Sims, P. A. Finlayson, E. A. Rinderle, M. A. Vavrina, and T. D. Kowalkowski. Implementation of a low-thrust trajectory optimization algorithm for preliminary design. In *AIAA 2006-6746*, 2006.

[50] J. A. Sims and S. N. Flanagan. Preliminary design of low-thrust interplanetary missions.

[51] V. Szebehely. *Theory of Orbits*. Academic Press Inc., Aug. 1967.

[52] L. N. Trefethen. *Approximation Theory and Approximation Practice*. University of Oxford, 2011.

[53] D. A. Vallado. *Fundamentals of Astrodynamics and Applications*. Microcosm Press, 2013.

[54] M. A. Vavrina. A hybrid genetic algorithm approach to global low-thrust trajectory optimization. Master's thesis, Purdue University, Dec. 2008.

[55] M. A. Vavrina, J. A. Englander, and D. H. Ellison. Global optimization of n-maneuver, high thrust trajectories using direct multiple shooting. In *AAS 16-272*, 2016.

[56] G. V.N. Matds. A MATLAB-based program for dynamical system investigation.

[57] W. Whener. Analytic gradients in trajectory optimization. May 16, 2016.

[58] R. Whitley and R. Martinez. Options for staging orbits in cis-lunar space. resreport, IEEE, Oct. 2015.

[59] R. Whitley, R. Martinez, G. Condon, J. Williams, D. Lee, D. Davis, G. Barton, S. Bhatt, J. W. Jang, F. Clark, and H. Hinkel. Cislunar near rectilinear halo orbits for human space exploration.

[60] C. H. Yam, D. Izzo, and F. Biscani. Towards a high fidelity direct transcription method for optimisation of low-thrust trajectories. Technical report, Advanced Concepts Tea, ESA, 2010.

[61] C. Zhang, F. Topputo, F. Bernelli-Zazzera, and Y.-S. Zhao. Low-thrust minimum fuel optimization in the circular restricted three-body problem.